Investigating the role of dynamic histone modification in the mechanism of action of lysine deacetylase inhibitor (KDACi)

A thesis submitted to the Board of the Medical Science Division, University of Oxford,

in partial fulfillment of the requirements for the degree of Doctor of Philosophy

Li-Yao Huang

University College

Michaelmas Term 2019

Acknowledgment

This thesis is made possible thanks to so many people. The most important person is my supervisor and mentor, Catherine Pears, who gives me advice on scientific questions, encourages me when I was down and cares about my personal feeling and development. I enjoyed my DPhil time thanks to her support.

As this journey ends, I would like to also thank Prof. Hao-Jen Huang and his wife, Shao-Yen Chen. My experience as a master student under Prof. Huang's supervision has laid a strong foundation on my scientific career. I also received enormous mental support from the two of them.

My sincere thanks to colleagues who I have worked with. You provide a dynamic and friendly working environment. Thank you, Julien Brustel, Khairul Ramlee, Alastair Gunn, George Ronson, Ellie Warren, Iza Bombik, Eric Liang, Antoine Verslype, Monika Papayova, Anna Moteneko, Guifeng Wei, Seiji Ura,Jagoda Rokicka, Yuntao Wang, and Huajiang Xiong.

Friends are key during my DPhil study as they made my life outside the lab so enjoyable and memorable. I will definitely miss all the laughter, chat and good memories we created

together, especially those with Fu-sheng Chang, Jeff Lin and Andre Liu, thank you all.

A special thanks to my girlfriend Di Yang who has become a very important part of my life. Thank you for your support, understanding and encouragement. I am simply grateful for your existence.

Finally, I would like to thank my family, who I owe a lot for not being able to company them for so long. My sincere and deep gratitude to my mother, Min-Feng Li, who gave me everything she can provide to support me; my father Jia-he Huang, who believes in me and is always there to help; my elder bother Fan Huang, who has carried all the burden and responsibilities for so long. This thesis is dedicated to you.

Abstract

Methylation and acetylation of histones are tightly connected to the control of gene expression. Changes in patterns of methylation and acetylation of histones are associated with changes in gene expression during growth and development. It has become widely accepted that misregulation of histone modifications, including histone methylation and acetylation, can play a critical role in cancer cells. Consequently, inhibitors targeting histone-modifying enzymes, such as lysine deacetylase inhibitors (KDACis), have shown therapeutic potential against a number of different types of cancer. Multiple hydroxamate-based KDACis have been approved for clinical use. However, the exact mechanism of action of these compounds remains uncertain as do the mechanisms of resistance that are either intrinsic or acquired on KDACi treatment.

Hydroxamate-based KDACis such as Trichostatin A (TSA) induces rapid initial acetylation of histone 3 (H3) proteins which are already modified by *tri*-methylation on lysine 4 (H3K4me3) while acetylation of bulk histones happens later. In this thesis, I reveal the role of dynamic acetylation in the mechanism of action of hydroxamates using the eukaryotic social amoeba *Dictyostelium discoideum* as a model. Loss of H3K4me3 in strains with mutations in the gene encoding the methylating enzyme or the histone molecules themselves confers resistance to KDACi-induced inhibition of development

and slows the accumulation of histone acetylation. Furthermore, the dynamic rapid acetylation of H3K4me3 requires the *Dictyostelium* orthologue of Sgf29 which recognizes the H3K4me3 mark via its tandem Tudor domain. Disruption of the gene encoding Sgf29 abolished rapid dynamic acetylation of H3K4me3 and led to developmental resistance to TSA.

However, loss of rapid acetylation of H3K4me3 did not provide resistance to growth inhibition caused by TSA. Aiming to identify genes involved in the process, a genome-wide screen was performed using a newly established technology REMI-seq (REMI-seq.org). This allows parallel phenotyping of thousands of insertional mutants in a population to identify strains with growth advantage under TSA treatment. The screen identified genes encoding proteins such as ABC transporters, transcription factors and protein kinases and a number were demonstrated to be resistant to TSA during growth as single clones but not resistant during development. The results of this thesis provide a previously unidentified role of dynamic acetylation of H3K4me3 in the mode of action of hydroxamates and prove that REMI-seq is a powerful tool in *Dictyostelium* to identify resistance-related genes when studying drug mechanisms.

Abbreviations

cAMP — Cyclic AMP

CDK — Cyclin-dependent kinases

CTCL — Cutaneous T-cell lymphoma

GNATs — Gcn5 N-acetyltransferases

H3 — Histone 3

H3K4me3 — Histone H3 with *tri*-methylated on lysine 4

HAT — Histone acetyltransferase module

KAT — Lysine acetyltransferase

KDAC — Lysine deacetylase

KDACi — Lysine deacetylase inhibitor

MTA2 — Metastasis-associated protein-2

MYST — Morf, Ybf2, Sas2 and Tip60

NAD^+ — Nicotinamide adenine dinucleotide

PCR — Polymerase chain reaction

PTMs — Post-translational modifications

SAGA — Spt-Ada-Gcn5-acetyltransferase

SAHA — Suberoylanilide hydroxamic acid

siRNA — Small interfering RNA

TNF — Tumor necrosis factor

TRAIL — TNF-related apoptosis-inducing ligand

TSA — Trichostatin A

U.S. FDA — U.S. Food and Drug Administration

VPA — Valproic acid

Table of contents

1. Introduction

Growth and development of organisms occurs through division and differentiation of living cells and cells must be able to determine the appropriate time and place to start or stop these processes. This is often achieved by signaling pathways triggered by external or internal environmental changes, leading to an appropriate response. One fundamental mechanism of a rapid response to environmental cues is post-translational modifications (PTMs) by enzymes which modify proteins by addition of different functional groups. The chemical process is fast, thus allowing an immediate response, and is often reversible. The most common and best understood PTMs include ubiquitylation, phosphorylation, methylation and acetylation. Among these PTMs, methylation and acetylation are of importance because they are particularly implicated in regulating gene expression by modification of histones. In eukaryotes, 147 base pairs of DNA is coiled around a nucleosome consisting of two copies of histones H2A, H2B, H3 and H4 (Fig. 1A) (Zhou et al., 2019). Nucleosomes are further packaged to form chromatin which is found to have open and condensed forms. Genes in the open regions (euchromatin) can be transcribed while genes in condensed regions (heterochromatin) are typically silenced. Acetylation on histone H3 and H4 are enriched in euchromatin while the nucleosomes associated with the promoters of active transcription regions are marked by *tri-*

methylation of histone H3 on lysine 4 (H3K4me3), and acetylation of a number of lysine residues including H3K9 and K14 (H3K9ac and H3K14ac) (Fig. 1B) (Butler and Dent, 2013; Schübeler et al., 2004).

While methylation of different residues on histone H3 can be associated with either active (H3K4 or H3K36) or repressed (H3K9 or K3K27) genes, acetylation of lysine residues of histones is correlated with active gene expression (Wang et al., 2008). This process neutralizes the positive charges on histones and has been proposed to lead to a less compact chromatin structure thus allowing access of transcription factors and RNA polymerase to negatively charged DNA. Alternatively, the acetylated lysine residues on H3 serve as binding sites for proteins carrying acetyllysine-binding domains such as bromodomains. For example, in budding yeast the bromodomain of Gcn5 was shown to be necessary to anchor Gcn5 and its interacting protein complex SAGA (Spt-Ada-Gcn5-acetyltransferase), a cofactor for RNA polymerase II, to acetylated nucleosomes (Baptista et al., 2017; Hassan et al., 2002).

The sequence and structure of the nucleosome core histones (H2A, H2B, H3 and H4) are highly conserved in eukaryotes (Mariño-Ramírez et al., 2011). Histones are predominantly acetylated on lysine residues of the amino terminal tails which extend

from the nucleosome core and so are available to interact with both DNA and other proteins (Fig. 1A and C). Though acetylation has been found on all four histone proteins, the positions of the modified lysine residues vary on histone H2A and H2B in different species while that of H3 is highly conserved (Fig. 1C) (Zhao and Garcia, 2015). Studies on H3 acetylation (H3ac) have revealed that almost all discovered H3ac marks are correlated with transcription activation (Zhao and Garcia, 2015). Acetylation of the lysine residues is catalyzed by enzymes with lysine acetyltransferase (KAT) activity and can be reversed by lysine deacetylases (KDACs) (Fig. 1D).

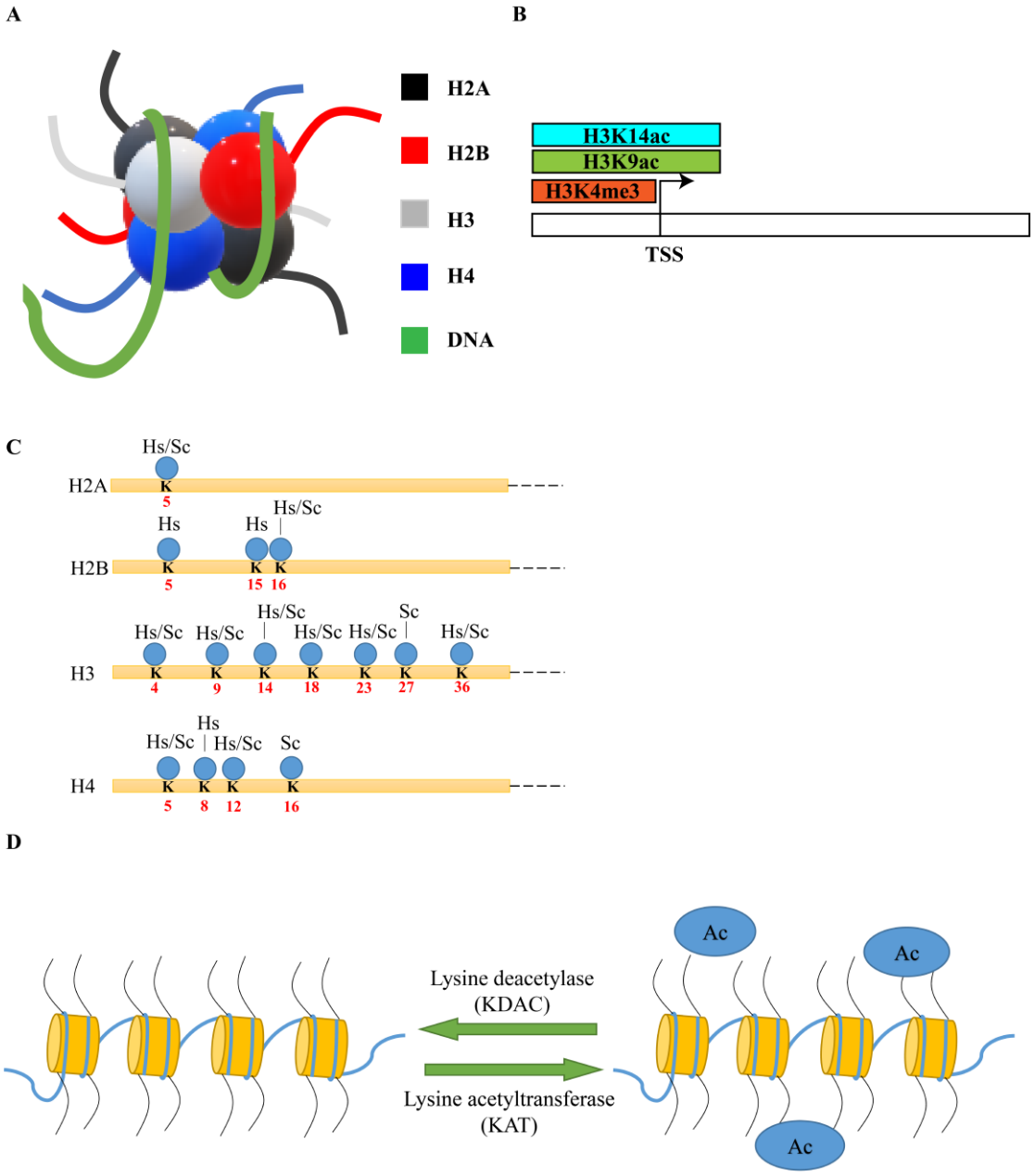

Fig. 1 Acetylation of nucleosome components

(A.) Schematic diagram showing histone H2A, H2B, H3 and H4 in a nucleosome. **(B.)** Commonly enriched histone modifications of active genes around the transcription start site (TSS). **(C.)** Schematic diagram showing conserved acetylation on lysine residues of histone H2A, H2B, H3 and H4 in *Saccharomyces cerevisiae* (Sc) and *Homo sapiens* (Hs). **(D.)** Schematic diagram illustrating the reversible reaction of lysine acetylation mediated by lysine acetyltransferases and deacetylases.

1.1 Lysine acetyltransferases

The two largest KAT families are conserved from yeast to humans. The two families are the Gcn5 *N*-acetyltransferases (GNATs) and MYST proteins, which are named after different members of the family, namely Morf, Ybf2, Sas2 and Tip60. These two types of acetyltransferases are classified based on the consensus domain structure within each family (Avvakumov and Côté, 2007; Neuwald and Landsman, 1997). Acetyltransferases that don't fall into either family are grouped as 'orphan class' (Fig. 2) (Cerbo and Schneider, 2013).

1.1.1 GNAT family

Acetyltransferases in the GNAT family are characterized by a KAT catalytic domain and often a *C*-terminal bromodomain (Fig. 2) (Sterner and Berger, 2000). Gcn5 is the founding member of the GNAT family firstly discovered in budding yeast as a transcription activator (Berger et al., 1992). Orthologues of yeast Gcn5 have since been discovered in *Drosophila* and humans (Smith et al., 1998; Wang et al., 1997). Other GNAT family enzymes include Hat1, Elp3 and Hpa2 found in yeast and PCAF found in humans.

Gcn5 forms a histone acetyltransferase module (HAT) consisting of Ada2, Ada3 and

Sgf29 as part of SAGA protein complex (Bian et al., 2011). Studies on *in vitro* HAT activity revealed that it catalyzes acetylation most effectively on H3K14, followed by K23, K9, K18, K27 and K36 while H4 is a weak substrate (Cieniewicz et al., 2014; Riss et al., 2015; Roth et al., 2001). Acetylation of these lysine resides have been shown to correlate with active transcription (Zhao and Garcia, 2015). In addition, correlation between the presence of these acetylated residues was also discovered. For example, the genome-wide distributions of H3K9ac and H3K14 are highly correlated and mostly found on active promoter regions in mouse embryonic stem cells (Karmodiya et al., 2012).

1.1.2 MYST family

MYST members are defined by a MYST KAT domain and often include a zinc finger motif or a chromodomain. In some cases, an additional domain such as a PHD finger is also present (Carrozza et al., 2003). Known MYST acetyltransferases include Esa1, Sas2/3 in *Saccharomyces cerevisiae*; HBO1 and MORF in *Homo sapiens,* and TIP60 and MOF in *Drosophila melanogaster*. Like GNATs, MYST enzymes also function as part of large protein complexes. Examples include Esa1 in the NuA4 complex in yeast and HBO1 in the HBO1 complex in humans (Lee and Workman, 2007).

Unlike GNATs, most members of the MYST family were found to acetylate the histone H4 tail. For example, TIP60 acetylates K5, K8, K12 and K16 of histone H4 while MOF activity is directed towards H4K16 (Sapountzi and Côté, 2011; Voss and Thomas, 2018). HBO1 also predominantly acetylates histone H4 though acetylation of H3K14 by HBO1 was also reported *in vitro* (Saksouk et al., 2009).

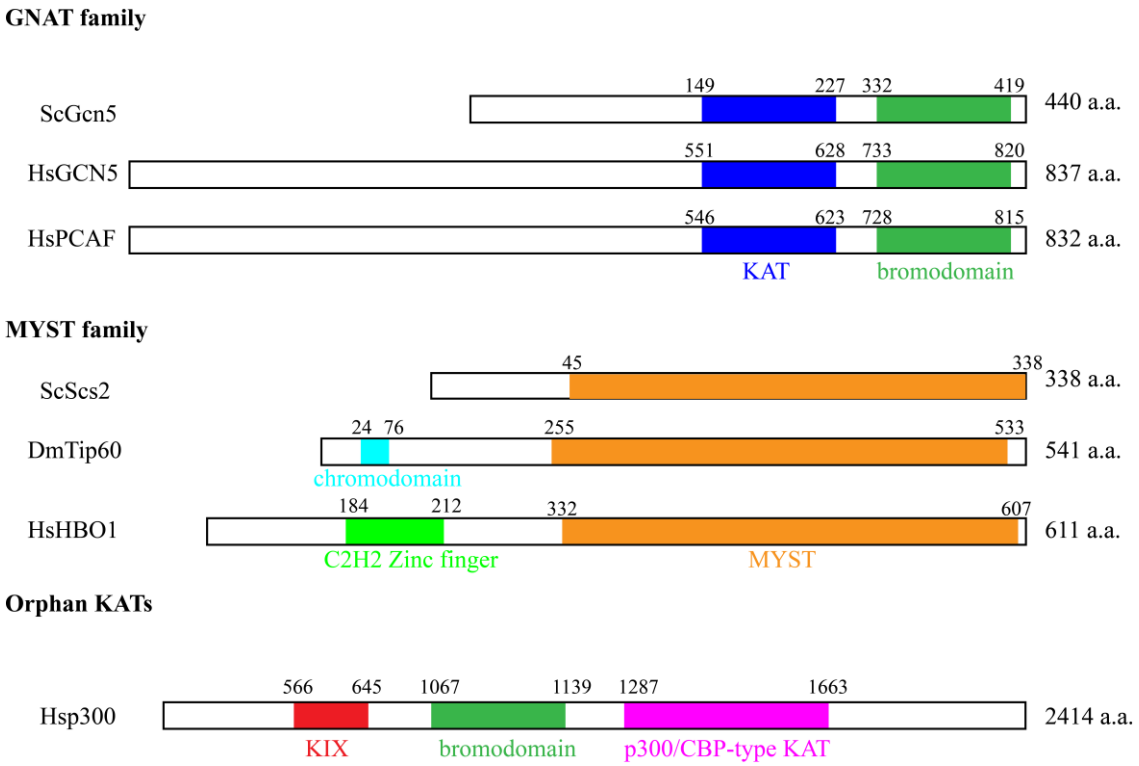

Fig. 2 The domain structure of different KAT families

The domain structure of examples of GNAT, MYST and orphan acetyltransferases are shown in blocks and the name of each functional domain is listed underneath the blocks. The total length of amino acids of each protein is indicated at the right hand side. On top of each functional domain the beginning and ending positions are indicated. Sc, *Saccharomyces cerevisiae*; Hs, *Homo sapiens*; Dm, *Drosophila melanogaster*.

1.1.3 Orphan KATs

Acetyltransferases that do not fall into either the GNAT or MYST families are considered orphan KATs. These include p300/CBP, nuclear receptor coactivators such as SRC1, and some subunits of transcription initiation factors such as TAF1. Unlike GNAT and MYST acetyltransferases, most of the orphan KATs are only found in metazoans (Escriva et al., 2004). p300/CBP is the most well-characterized member among orphan KATs. Functional domains in p300/CBP include a bromodomain, KAT domain and domains required for interaction with other KATs or transcription factors (Sterner and Berger, 2000). All four histones in nucleosomes are targets of p300/CBP (Ogryzko et al., 1996). Both p300 and CBP acetylate K9, K14, K18, K23 and K27 on H3; K5, K8, K12 and K16 on H4. Though p300 and CBP are highly similar in terms of the domain structure, the two enzymes target histone H3 and H4 tails with different specificity under different conditions (Henry et al., 2013).

1.2 Lysine deacetylases

Acetylation of histone lysine residues can be reversed by lysine deacetylases (KDACs) also referred to as HDACs in literatures. The 18 human lysine deacetylases are assigned to four different classes based on sequence similarities to yeast deacetylases (Table 1). The protein sequences of Class I lysine deacetylase are similar to yeast Rpd3 while Class

II lysine deacetylases are similar to yeast Hda1. KDAC6 and KDAC10 in Class II are subclassified to Class IIb because of a putative second catalytic domain. The Class III deacetylases (SIRT 1 - 7) are similar to yeast Sir2. There is only KDAC11 in Class IV, which shares sequence similarity with both Class I and II deacetylases. Class I, II and IV proteins are Zn^{2+}-dependent KDACs that contains Zn^{2+} in their catalytic pockets, while Class III proteins are NAD^{+}-dependent (Seto and Yoshida, 2014). The substrates of these deacetylases include both histones and non-histone proteins. KDAC1 has been shown to deacetylate the transcription factor and tumor suppressor protein p53 when in association with metastasis-associated protein-2 (MTA2) (Ito et al., 2002). KDAC6 has been shown to deacetylate non-histone substrates including tubulin and heat shock protein 90 (Li et al., 2013).

Table. 1 Lysine Deacetylases (Adapted from Wang et al., 2012)

	KDACs	Location	Substrate examples
Class I (Zn^{2+} dependent)	KDAC1	Nucleus	Histones, p53, BRAC1, NF-kB, DNMT1
	KDAC2	Nucleus	Histones, p53, BRAC1, NF-kB
	KDAC3	Nucleus/cytoplasm	Histones, KDAC4, 5, 7, 9
	KDAC8	Nucleus	HSP70
Class IIa (Zn^{2+} dependent)	KDAC4	Nucleus/cytoplasm	Histones, p53, p21KDAC3
	KDAC5	Nucleus/cytoplasm	Histones, KDAC3
	KDAC7	Nucleus/cytoplasm	Histones, KDAC3, PML
	KDAC9	Nucleus/cytoplasm	Histones, KDAC3, MEF2
Class IIb (Zn^{2+} dependent)	KDAC6	Nucleus/cytoplasm	α-tubulin, HSP90, KDAC11
	KDAC10	Nucleus/cytoplasm	LcoR, PP1
Class IV (Zn^{2+} dependent)	KDAC11	Nucleus	Histones, KDAC6, Cdt1
Class III (NAD^{+} dependent)	Sirtuin1	Nucleus/cytoplasm	Histones, p53, p73, p300, Ku70, TIP60
	Sirtuin2	Nucleus	Histones, α-tubulin,
	Sirtuin3	Mitochondria	Histones, Ku70, GDH
	Sirtuin4	Mitochondria	GDH
	Sirtuin5	Mitochondria	cytochrome c
	Sirtuin6	Nucleus	Histone H3, TNF-z
	Sirtuin7	Nucleus	p53

Surprisingly, little is known as to whether different KDACs selectively deacetylate specific lysine residues on histone H3/H4 as is the case of KATs or if functional differences are due to different mechanisms of recruitment or regulation of activity. However, the *in vivo* functions of some KDACs have been studied. Some KDACs have been found both in nucleus and cytoplasm. KDAC 1 and 2 are found primarily in the nucleus and deletion of genes encoding both in embryonic stem cells results in decreased

cell viability and mitotic defects (Jamaladdin et al., 2014). Downregulation of KDAC1 by siRNA reduces proliferation in ovarian cancer cells while targeting KDAC3 suppresses both proliferation and cell migration (Hayashi et al., 2010). KDAC6 is found mainly in the cytoplasm and is involved in biological processes such as protein degradation and cell motility (Li et al., 2013). Deletion of KDAC6 in mouse embryo fibroblasts impairs the formation of stress granules associated with translational suppression (Kwon et al., 2007).

1.3 Dysregulation of histone acetylation in cancer

It is generally agreed that many epigenetic modifications including histone acetylation are dysregulated in cancer cells. Altering the balance of histone acetylation is often achieved by mutations in KATs and KDACs. Increased expression of GCN5 is correlated to increased tumor size in patients with non-small cell lung cancer, and overexpression of GCN5 accelerates tumorigenesis in mice (Chen et al., 2013). Downregulation of MOF in kidney cancers has also been reported (Wang et al., 2013). Similarly, inactivation of p300/CBP KAT was discovered in numerous types of cancers including breast cancer, colorectal cancer, pancreatic cancer, and lymphoma (Cheng et al., 2017; Gayther et al., 2000; Kang-Decker et al., 2004; Muraoka et al., 1996).

During the last decade, many types of cancer have been identified carrying mutations in

one or multiple KDACs. Surprisingly, the majority of the identified mutations are up-regulation of different KDACs. Some of the examples include overexpression of KDAC2 in medulloblastoma, lung and pancreatic cancers; high expression of KDAC1, 2 and 3 in ovarian cancers; high expression of KDAC6 in hematological cancers including Acute Lymphoblastic Leukaemia and Adult Acute Myeloid Leukemia (reviewed in Li and Seto, 2016).

These discoveries have stimulated the idea that small molecule inhibitors targeting the mutated KATs or KDACs are potential therapeutic drugs against cancers. Some natural products such as curcumin and anacardic acid are found to have KAT inhibition activity. However, these natural KAT inhibitors are not selective and it is often difficult to determine the cause of the observed effects (Hemshekhar et al., 2012). This issue has been overcome by the use of synthetic KAT inhibitors mimicking both lysine and acetyl-CoA as the substrates of KAT (Lau et al., 2000). However, these synthetic inhibitors are not stable and often have low permeability due to their large molecular size. Recent advances utilized the power of structure simulation to screen for candidate compounds that bind to an input protein structure (Zeng et al., 2013). One of the most potent KAT inhibitors identified using this method is C646, which selectively inhibits p300 activity (Bowers et al., 2010). C646 has been used in pre-clinical studies to understand the

consequences of the inhibition of p300 in different cancer cell lines and in mice. For example, treating melanoma cells with C646 blocks the G1/S transition (Yan et al., 2013). A study using the MMTV-PyVT breast cancer mouse model discovered that administration of C646 to mice significantly reduced tumour weight (Li et al., 2019). However, the use of C646 is still limited to pre-clinical studies. Until today, not a single KAT inhibitor has been approved by U.S. Food and Drug Administration and deployed in clinics to treat patients with cancer.

1.4 Lysine deacetylase inhibitors

Currently most lysine deacetylase inhibitors target zinc-dependent Class I, II and IV lysine deacetylases. The structure of these inhibitors consists of a zinc-chelating group targeting the zinc ion inside the catalytic pocket of KDACs, an enzyme-interacting group and a spacer between the two groups (Finnin et al., 1999). KDACis are grouped into four classes based on their functional groups and chemical structure (Fig. 3).

The first class is the short-chain fatty acids including butyrate and valproic acid (VPA) (Fig. 3). VPA is used as a drug to treat epilepsy and has been found to have KDAC inhibition activity (Göttlicher et al., 2001). Short-chain fatty acids have been shown to inhibit both Class I and IIa KDACs (Bolden et al., 2006). However, the effective

concentration of VPA is at milli-molar level and it is known to target other non-KDAC proteins such as succinate semialdehyde dehydrogenase (El-Habr et al., 2016) and inositol metabolism (Eickholt et al., 2005; Williams et al., 2002; Xu et al., 2007).

The second class is the cyclic tetrapeptide compounds (Fig. 3). Members of this class are characterized by a ketone group that binds to the zinc ion (Kijima et al., 1993). Example compounds in this class include Romidepsin and Trapoxin. This group of KDACi targets Class I KDACs. Romidepsin has been shown to selectively induce apoptosis in cancer cells and also inhibit angiogenesis (Insinga et al., 2004; Kwon et al., 2002). In 2009, the FDA approved the use of Romidepsin to treat patients with cutaneous T-cell lymphoma (VanderMolen et al., 2011).

The third class are benzamides with members such as CI-994 and Entinostat (Fig. 3). This group of inhibitors are characterized by the bicyclic ring, which targets Class I KDACs (Bracker et al., 2009). Effects of Entinostat on hematological cancers include growth arrest, differentiation and apoptosis (Rosato et al., 2003). However, using Entinostat as a single agent therapy has been shown to have low efficacy in clinical trials treating solid tumors and hematologic malignancies (Knipstein and Gore, 2011).

The fourth class is the largest and most studied. Members in this class are hydroxamic acids including Trichostatin A (TSA), Suberoylanilide hydroxamic acid (SAHA), Belinostat and Panobinostat (Fig. 3). They are pan-KDACi that inhibit both Class I and II KDACs (Bolden et al., 2006). TSA was originally isolated as a metabolite with antifungal and antibiotic effects from *Streptomyces hygroscopicus* (Tsuji et al., 1976). Later, it was found to induce differentiation of murine erythroleukemia cells and inhibit cell proliferation, though its mechanism was unknown (Yoshida et al., 1987). The KDACi activity of TSA was later reported by the same group, suggesting that the observed effects of TSA may arise from its KDACi activity (Yoshida et al., 1990).

The discovery of SAHA was independent of TSA. It was originally reported that small, polar compounds induce differentiation of Murine-virus-infected erythroleukemia cells (Tanaka et al., 1975). Studies on this type of compound led to the development of a method to chemically synthesize SAHA, which is structurally similar toTSA (Richon et al., 1996). Studies have found that SAHA inhibits tumor growth and reduces tumor volume at a concentration higher than TSA (Butler et al., 2000; Cohen et al., 1999; Glick et al., 1999; Richon et al., 1998). Aiming to increase the potency and pharmacokinetics, syntheses of other hydroxamic acids were subsequently reported (Plumb et al., 2003). To date, three hydroxamic acid KDACis, namely SAHA, Belinostat and Panobinostat have

been approved by the U.S. FDA for treating cutaneous T-cell lymphoma (CTCL), peripheral T-Cell lymphoma and multiple myeloma respectively (Li and Seto, 2016).

Though the potential to utilize KDACis as anti-cancer reagents is strong, like all other anti-cancer drugs, the problem of intrinsic and acquired resistance to KDACis becomes evident during clinical trials. For example, the overall response rate of CTCL patients to SAHA is ~30% (Mann et al., 2007). A similar discovery in patients with CTCL was reported in a phase II trial of Romidepsin with an average response rate of 34% and a large variation of response duration between one month to over 4 years (Piekarz et al., 2009).

Some exploratory clinical studies have discovered increased efficacy of potential combinations of KDACis with different chemotherapeutic reagents in certain types of cancer. For instance, an exploratory study discovered that combining Tucidinostat, a benzamide KDACi targeting KDAC1, 2, 3 and 10, with exemestane, an FDA-approved antiestrogen for treating breast cancer, resulted in better response than exemestane alone in patients with advanced breast cancer (Zhang et al., 2018). The discovery was further transferred to a phase III trial involving 365 patients with hormone receptor-positive breast cancer. The report showed that the combination of both drugs increased median

progression-free survival from 3.8 months to 7.4 months, which is almost doubled (Jiang et al., 2019). Currently, more than 60 clinical trials are being conducted, investigating the potential of combining different KDACis with other interventions to target breast cancer (reviewed in Huang et al., 2019).

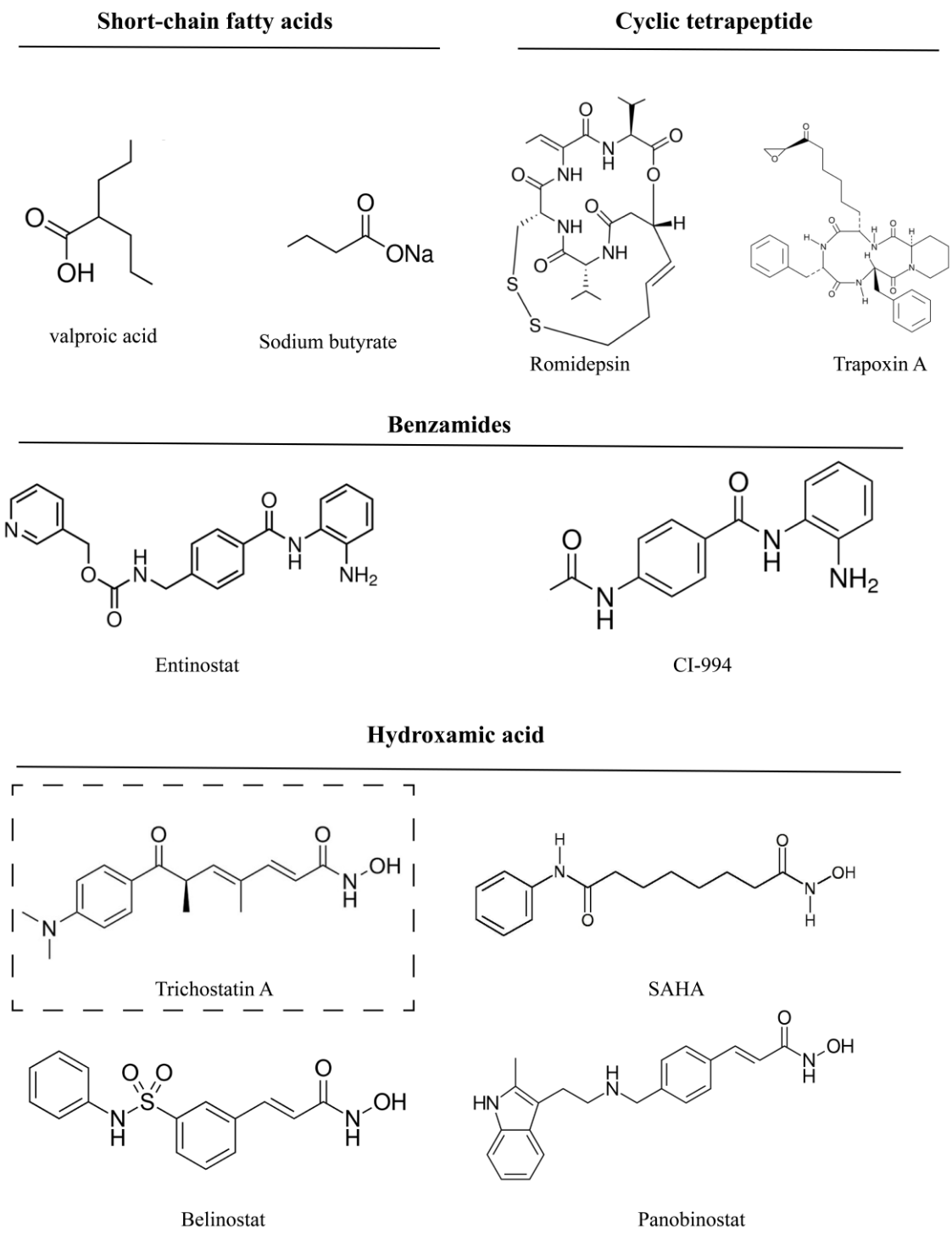

Fig. 3 Chemical structure of KDAC inhibitors with an emphasis on TSA that is used for most of the experiments in this thesis

1.5 Mechanisms of action of KDACi in cancer therapy.

KDACis are potent potential anti-cancer drugs because of their enhanced activity in cancer cells (Batova et al., 2002; Burgess et al., 2004; Insinga et al., 2004; Nebbioso et al., 2004). KDACi selectively induce growth arrest, cell death or differentiation in transformed cells at a concentration that is non-toxic to normal cells. Because KDACs target both histone and non-histone proteins, the effects of KDACis could be due to altered acetylation states of non-histone proteins or histone acetylation-related change in gene expression (West and Johnstone, 2014). Though the exact mechanism is unclear, studies have found that genes in pathways involved in these cellular processes are specifically upregulated by KDACi in cancer cells. Examples for genes involved in cell cycle arrest and apoptosis are described below.

1.5.1 Cell cycle arrest and Differentiation

Low concentrations of KDACi trigger G_1 arrest while high concentrations induce both G_1 and G_2/M arrest in cancer cells (Li and Wu, 2004; Richon et al., 2000). KDACis are known to induce cell cycle arrest by up-regulation of p21, an inhibitor of cyclin-dependent kinases (CDK) that regulate cell cycle progression (Archer et al., 1998; Li and Wu, 2004; Richon et al., 2000; Sasakawa et al., 2002). Progression through G_1 phase is controlled by CDK4/6, while the G_1/S transition is regulated by CDK2. In addition,

cdc2/CDK1 that regulates the G_2/M transition is also a target of p21 (Vidal and Koff, 2000). Repression of genes encoding for cyclins may also contribute to cell cycle arrest induced by KDACi (Sandor et al., 2000).

In many cases, arrested cell cycle caused by hydroxamate KDACis is accompanied by differentiation (Marks and Breslow, 2007). Early investigation on the effects of TSA on human urinary bladder carcinoma (T24) and cervix carcinoma cells *in vitro* revealed changes including cell cycle arrest (G1 or G2) and restoration of actin stress fibers (Hoshikawa et al., 1994). In addition, TSA, as well as a cyclic tetrapeptide Trapoxin A, are able to reverse the transformation of sis-transformed mouse fibroblast cells and restore the morphology (Sugita et al., 1992; Yoshida and Sugita, 1992). The TSA-induced morphology change was blocked by 1) actinomycin D, an RNA synthesis inhibitor, and 2) Cycloheximide, a protein synthesis inhibitor, suggesting *de novo* RNA synthesis and protein synthesis are required for the process (Hoshikawa et al., 1994; Sugita et al., 1992). The working hypothesis of the field is that changes in gene expression and subsequent protein expression, as well as modulation of non-histone proteins by KDACi, are responsible for the downstream phenotypes, but the exact mechanism could be cell-type specific (Marks et al., 2000). For example, the KDACi Romidepsin induces differentiation of chondrosarcoma cells with an increase in expression of several collagen

genes, a characteristic of differentiated chondrocytes (Sakimura et al., 2007). The group also correlates the increment of collagen gene expression with elevated histone H3 acetylation at enhancer and promoter regions.

1.5.2 Apoptosis

Apoptosis is a form of programmed cell death and can be triggered through extrinsic and intrinsic signals. Extrinsic activation of apoptosis can be achieved by binding of a death ligand such as TRAIL to death receptors (Ashkenazi, 2002). The binding activates caspase-8 and caspase-10 to initiate apoptosis. Expression of both death receptors and their ligands have been shown to be upregulated by KDACis *in vitro* and *in vivo*, and the induction is limited to transformed cells but not non-transformed cells (Insinga et al., 2004; Nakata et al., 2004). In addition to the extrinsic pathway, KDACis also alter expression of genes involved in intrinsic activation of apoptosis. Apoptosis can be triggered upon release of apoptosis-inducing factors such as cytochrome *c* from mitochondria. This process is mediated by Bcl-2 family proteins (Shamas-Din et al., 2013). KDACi has been shown to increase the expression of pro-apoptotic genes in the Bcl-2 family (Bolden et al., 2006).

1.6 Evidences of cross-talk between histone methylation and acetylation in the presence of KDACi

It is believed that KDACis could exert their effects by inducing hyperacetylation on histone H3 and H4, resulting in downstream changes in gene expression and subsequent phenotypes (Drogaris et al., 2012). Although acetylation is associated with upregulation of transcription of all genes, transcriptomic studies have found that KDACis only change the expression of a small portion of protein-coding genes (< 10%) with similar numbers of up- and down-regulated genes (Daly and Shirazi-Beechey, 2006; Halsall et al., 2012). The genes up-regulated by KDACi could be explained by histone hyperacetylation and enhanced transcription. Recently, up-regulation of BIM, a pro-apoptotic protein in the Bcl-2 family, by Panobinostat in triple negative breast cancer cell lines was found coupled with induced H3K27ac at two BIM enhancers (Huang and Ling, 2017). However, histone hyperacetylation induced by KDACi is not equally distributed across the whole genome. A study revealed that though KDACi induces global histone hyperacetylation, some genomic regions are not acetylated and that is related to down-regulated genes (Rada-Iglesias et al., 2007). Nevertheless, the exact mechanisms of how changes in histone acetylation caused by KDACis leads to increased or decreased gene expression is unclear.

There is another layer of complexity in terms of how KDACis induce histone hyperacetylation. By combining Chip-seq and RNA-seq data, it has been reported that that TSA and SAHA induced global H3K9/14Ac in human aortic endothelial cells is highly associated with up-regulated genes, and co-localizes with H3K4me3 (Rafehi et al., 2014). Moreover, biochemical evidence also suggests that KDACi-induced early hyperacetylation is targeted to histones that are already carrying the H3K4me3 modification (Hazzalin and Mahadevan, 2005). This reveals that histones with the H3K4me3 modification are subject to rapid turnover of acetylation and so are the first histones to become acetylated upon TSA treatment. The result was shown in mouse fibroblast cells by western blot of acid urea gels, in which the same histone carrying a modification (acetylation or phosphorylation) can be separated due to difference in net charge. Use of modification-specific antibodies showed that histone H3 carrying *tri*-methylation of lysine 4 was rapidly acetylated to saturation (i.e. all available lysine residues are acetylated) within 15 minutes of TSA treatment, while in the case of bulk histone H3 this saturation was only seen after 2 hours. This dynamic acetylation of H3K4me3 histones was later shown conserved in human, mouse and *Drosophila* cells (Crump et al., 2011). Furthermore, using a p300-specific inhibitor, the group demonstrated that the enzyme responsible for the dynamic acetylation is p300 in mouse and *Drosophila* cells. In addition, the acetylation added on H3K4me3 was targeted to

H3K9 and H3K14. However, it is unclear if the dynamic acetylation is important for the long term biological effects of KDACi on cell cycle arrest and cell differentiation, and if so what is the mechanism?

To understand the role of this pool of histones showing dynamic acetylation, one can interfere with enzymes catalyzing acetylation or deacetylation. However, the large number of genes coding for acetyltransferases in mammals makes this difficult. The second method is to manipulate genes encoding methyltransferases. However, there are five methyltransferases in humans known to catalyze H3K4 trimethylation (Hyun et al., 2017), and their functional redundancy makes genetic studies complicated. Furthermore, it has been reported that in *Drosophila*, mutation of dSet1, a methyltransferase responsible for global H3K4 *tri*-methylation, is lethal at an early larval stage (Hallson et al., 2012). Yeast has a single, non-essential, Set1 gene required for all H3K4 methylation (Schneider et al., 2005) but dynamic acetylation of H3K4me3 has not been detected in this organism (L. Mahadevan, personal communication). Therefore, to study the role of dynamic acetylation in the mode of action of KDACi, an alternative model organism should be considered.

1.7 *Dictyostelium discoideum* as a model organism

1.7.1 Life cycle of *Dictyostelium discoideum*

Dictyostelium discoideum is a haploid, eukaryotic organism with an unusual life cycle in that the growth and development stages are separated. *Dictyostelium* feeds on bacteria and under nutritious conditions exists as single cells (Muñoz-Braceras et al., 2013). When the nutrition is depleted the developmental cycle is triggered. This starts with secretion of cyclic AMP (cAMP) as a signal by some cells and attracts surrounding cells to move toward the source of the signal by chemotaxis. The process results in a multicellular aggregate structure which goes through different stages of development and eventually forms a fruiting body consisting of spore and stalk cells (Fig. 4). This unique life cycle makes *Dictyostelium* a good model to separate the effects of KDACis on growth and development.

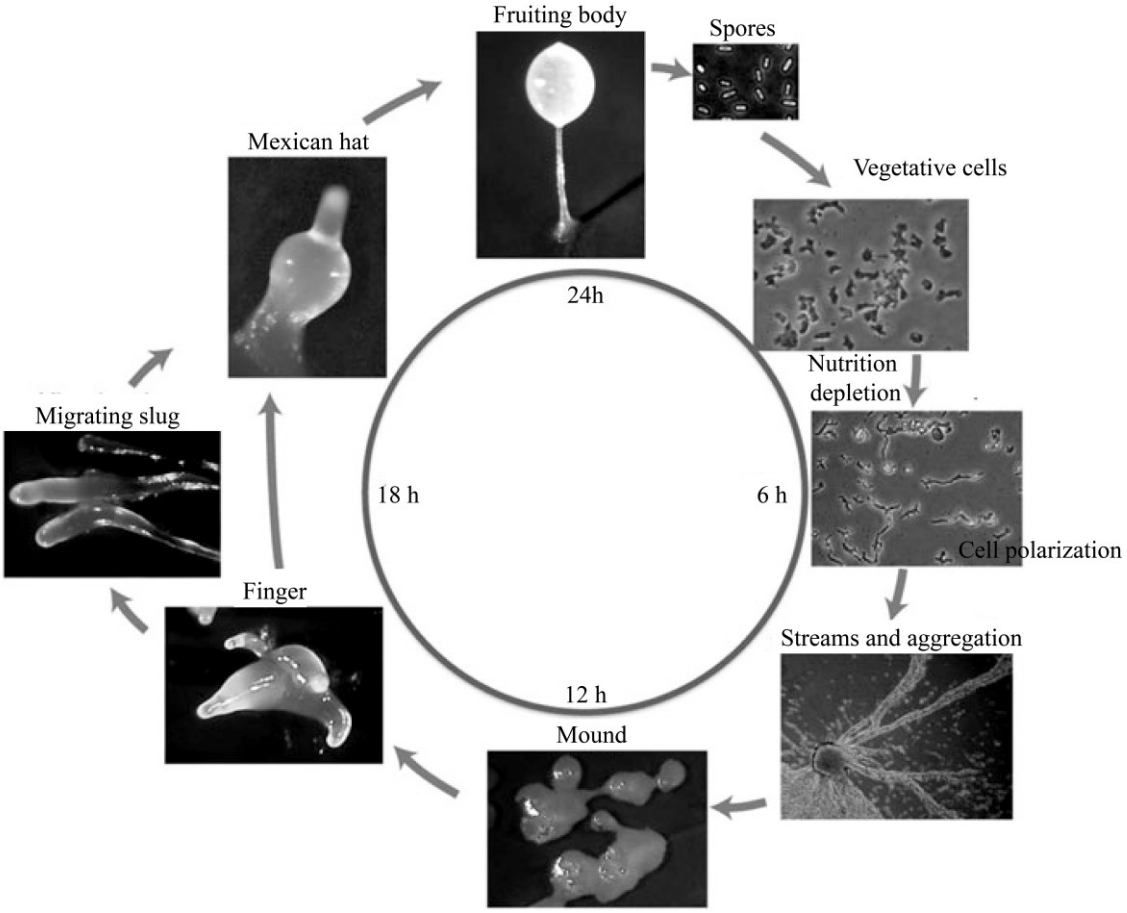

Fig. 4 Life cycle of *Dictyostelium* cells

Upon depletion of nutrients, cells aggregate, forming a stream of migrating cells (Lower right corner). After aggregation, cells form a mound which develops a tip which elongates to form a finger structure. After an optional migratory slug stage, this structure goes through a number of morphological changes. Within 24 hours the final structural fruiting body forms, which consists of a stalk supporting a spore head containing spore cells. Modified from (Muñoz-Braceras et al., 2013)

1.7.2 Histones and its modifying proteins in *Dictyostelium*

Besides its life cycle, *Dictyostelium* is also a good model organism to study the role of dynamic acetylation in the mode of action of KDACis for the following reasons.

- The amino acid sequences of histones and corresponding acetylation sites are mostly conserved when compared to humans.

- In comparison to human, the organism has a reduced number of single copy genes encoding acetyltransferases and deacetylases while the haploid genome provides ease of genetic manipulation.
- Dynamic acetylation of histone H3 trimethylated on lysine 4 is conserved in *Dictyostelium*.

The details of the above advantages are illustrated below.

1.7.2.1 Histone proteins in *Dictyostelium*

The four core histone proteins H2A, H2B, H3 and H4 as well as the linker histone H1 are found in *Dictyostelium* with an expanded number of variants compared to budding yeast. Importantly however, most of these are encoded by single copy genes (there are two genes encoding identical H4 proteins) to facilitate genetic manipulation which is impossible in human cells as they contain up to 16 copies of genes encoding a single variant (Table 2).

Table 2 Number of histone variants and histone-coding genes

Histone	*H. sapiens*	*D. discoideum*	*S. cerevisiae*
H1	**10**/*12*[a]	**1**/*1*	**1**/*1*
H2A	**7**/*38*	**5**/*5*	**2**/*3*
H2B	**4**/*29*	**3**/*3*	**1**/*2*
H3	**8**/*21*	**5**/*5*	**2**/*3*
H4	**1**/*16*	**1**/*2*[b]	**1**/*2*

[a] The number of histone variants is marked in **bold** while the number of encoding genes is marked in *italic.*

[b] Two genes encode identical products

By using mass spectrometry, it was reported that the major histone variants expressed in vegetatively growing *Dictyostelium* are H2Bv3, H2AX, H3a, H3b, H4, with traces of H2AZ (Hsu et al., 20012). H3a is about 2-fold more abundant than the slightly smaller H3b. Furthermore, the mass spectrometry data revealed that many histone modifications found in higher eukaryotes are conserved in *Dictyostelium* (Stevense et al., 2011). Examples include modifications related to active transcription such as H3K4me3, and acetylation on K9, K14, K18, K23, K27 of both histones H3a and b (Fig. 5). Western blot analysis using modification specific antisera suggest that H3b is more abundantly acetylated on H3K9 than H3a (Hsu et al., 2012). The histone modification profile in *Dictyostelium* is more complex than budding yeast, where for example, *di-* and *tri-* methylation of H3K9 is observed in *Dictyostelium* while absent in budding yeast (Klose et al., 2007). Therefore, histones in *Dictyostelium* are more diverse than in other lower eukaryotes and possess conserved modifications found in higher eukaryotes.

H3a

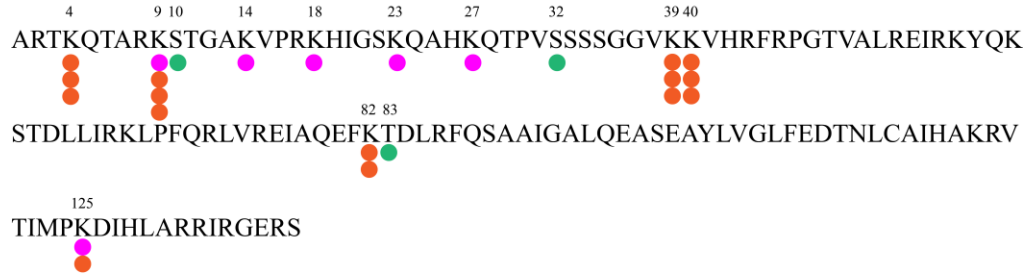

H3b

Fig. 5 Identified methylation, acetylation and phosphorylation sites on histone H3 in *Dictyostelium*

Coloured dots represent different post-translational modifications as indicated in the grey box. *Mono-*, *di-* and *tri*-methylation is represented by the number of orange dots. Modified from (Stevense et al., 2011).

1.7.2.2 Lysine acetyltransferases and deacetylases in *Dictyostelium*

Genes encoding for both GNAT and MYST acetyltransferases are found in the genome of *Dictyostelium* (Fig. 6) (Ludwig et al., 2006; DictyBase (http://dictybase.org/) and Uniport (http://uniprot.org/)). These include four GNAT acetyltransferases and two MYST acetyltransferases. However, no functional research has been reported on the protein products of these genes yet.

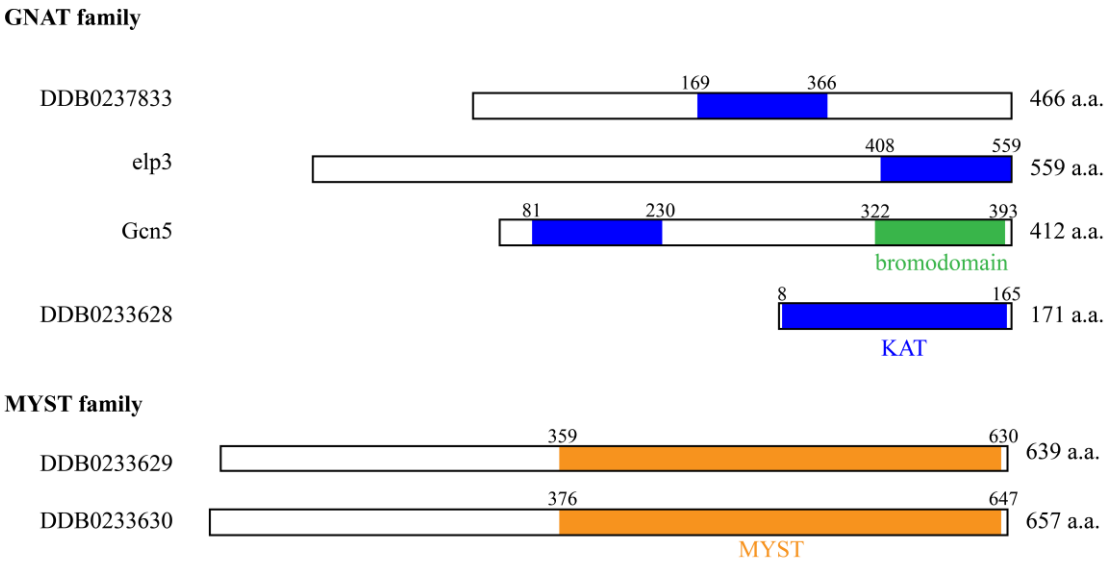

GNAT	Description
DDB0237833	probable ortholog of *H. sapiens* and *S. cerevisiae* HAT1, a subunit of the HAT1/HAT2 histone acetyltransferase complex
eip3	similar to ELP3, the histone acetyltransferase subunit of the subunit of the RNA polymerase II elongator complex
Gcn5	ortholog of *S. cereviciae* GCN5
DDB0233628	putative histone acetyltransferase; highly similar to bacterial GCN5-related N-acetyltransferase (GNAT)
MYST	
DDB0233629	contains a MOZ/SAS-like domain (Monocytic leukemia Zinc finger/Something About Silencing) predicted to have histone acetyltransferase activity
DDB0233630	contains a MOZ/SAS-like domain (Monocytic leukemia Zinc finger and Something About Silencing) predicted to have histone acetyltransferase activity

Fig. 6 Predicted acetyltransferases in *Dictyostelium*

The domain structure of predicted GNAT and MYST acetyltransferases in *Dictyostelium* are shown in blocks and the name of each functional domain is listed underneath the blocks. The total length of amino acids of each protein is indicated at the right hand side. On top of each functional domain the beginning and ending positions are indicated. The description of the listed genes is included in the bottom panel (http://dictybase.org/).

In the contrast, members of families of lysine deacetylases have been reported and studied in *Dictyostelium* (Sawarkar et al., 2009). Four genes encoding for Class I and II lysine deacetylases were identified, namely *hdaA*, *hdaB*, *hdac* and *hdaD*. Based on the

result of phylogenetic analysis, *hdaA* and *hdaB* are grouped as class I KDACs while *hdac* and *hdaD* are Class II KDACs. During development, the expression of *hdaA* and *hdaB* was reduced while expression of *hdac* was induced. Furthermore, KDAC activity from both cytosolic and nuclear extracts were inhibited by TSA. In addition, the nuclear KDAC activity in *hdaB* null cells was reduced when compared to parental cells. The *hdaB* null cells grew and developed normally, though they showed a sporulation defect when developed in chimaeras. In addition, class III KDACs *Sir2A* and *Sir2D* have been reported in *Dictyostelium* (Lohia et al., 2018; Shrivastava et al., 2016). Deletion of *sir2A* or *Sir2D* resulted in growth and developmental defects and reduced autophagic reactivity. Therefore, Class I, II and III lysine deacetylases exist in *Dictyostelium* and TSA can inhibit cellular KDAC activity in *Dictyostelium*.

1.7.2.3 Histone methyltransferase in *Dictyostelium*

In *Dictyostelium*, several genes encoding for methyltransferases have been reported. Dot1 has been found responsible for the *di*-methylation of H3K79 and deletion of its coding gene causes negative effects on growth and development (Müller-Taubenberger et al., 2011). Another methyltransferase Set1was reported by Chubb and his colleagues (2006). In the report, they demonstrated that Set1 is required for *mono*- *di*- and *tri*-

methylation of H3K4 such that signal of methylated H3K4 was undetectable in *set1*$^{-}$ cells. Deletion of *set1* also alters global transcription profile. Further ChIP analysis on selected altered genes showed that *di*- and *tri*- methylation of both up- and down- regulated genes are more abundant in parental cells compared to the background signal in *set1*$^{-}$ cells. Loss of *set1* results in minor growth defects when cells are cultured together with parental cells, while during development *set1*$^{-}$ cells finishes aggregation two hours earlier than parental cells.

1.7.3 Dynamic acetylation of H3K4me3 in *Dictyostelium*

The effects of TSA on *Dictyostelium* have been reported by two groups (Hsu et al., 2012; Sawarkar et al., 2009). TSA delays the development of *Dictyostelium* for 4 hours at 500 nM. At the histone modification level, TSA induces accumulation of acetylation at H3K9 within 4 hours. Most importantly, TSA causes saturated acetylation of H3K4me3 histones within 2 hours while for bulk histones it was observed after 4 hours of treatment. As mentioned previously, dynamic acetylation of H3K4me3 histones by TSA is conserved in mouse, fly and human but not observed in budding yeast. In the contrast, the dynamic acetylation of H3K4me3 is conserved in *Dictyostelium*.

Taken together, *Dictyostelium* possesses diverse histone machinery, conserved histone modifications, a simple-to-manipulate genome and conserved dynamic acetylation of H3K4me3, all of which makes it a good model organism to study the role of dynamic acetylation in the mode of action of KDACis.

1.8 Aims

The major aim of this thesis is to understand the role of dynamic acetylation in the mode of action of KDACis with an emphasis on hydroxamates. The major aim can be further broken down to the following aims.

- Determine the effects of different KDACis on the growth and development of *Dictyostelium.*
- Utilize strains with altered H3K4 methylation to determine if the cellular response of the strains to KDACis is affected. This includes inhibition of both growth and development in response to KDACi treatment, and changes in the histone acetylation profile.
- If changes in H3K4 methylation alter the cellular responses to KDACis, investigate the candidate proteins mediating the process.

In addition, I aim to utilize a recently available technology to identify *Dictyostelium* mutants that are resistant to KDACis during growth in an unbiased screen to better understand the mechanism of action of these compounds.

2. Materials and Methods

2.1 Materials

All reagents are prepared at room temperature (22℃) using double distilled water (MQ water). All reagents are either autoclaved or filtered through 0.2 μM filter (Nalgene) for sterile purpose. All chemicals are purchased from Sigma unless otherwise addressed.

2xSDS gel loading buffer
50 mM Tris pH 6.8
4% SDS
20% glycerol
0.2% bromophenol blue
100 mM dithiothreitol

KK2
19 mM KH_2PO_4
3.6 mM K_2HPO_4
Autoclaved

SDS-PAGE Running buffer
25 mM Tris
250 mM Glycine
0.1% SDS

SDS-PAGE Transfer buffer
25 mM Tris
250 mM Glycine
20% methanol

HL5 (Formedium)
53 mM maltose
1.4% bactopeptone
0.7% yeast extract
4 mM Na_2HPO_4
3.5 mM KH_2PO_4
340 μM dihydrostreptomycin sulphate
74 μM vitamin B12
82 μM biotin
532 μM riboflavin
Adjusted to pH 6.5
Autoclaved

SM agar
1% bactopeptone
56 mM glucose
0.1% yeast extract
16 mM KH_2PO_4
5.5 mM K_2HPO_4
4 mM $MgSO_4$
1.7% agar
Autoclaved

Elution buffer
10 mM Tris
1 mM EDTA
pH 8.0

KA suspension
Use half of a SM agar plate covered by KA. Resuspend the bacteria in 5 ml of KK2.

Nuclei buffer
40 mM Tris, pH 7.8
1.5% Sucrose
0.1 mM EDTA
6 mM MgCl2
40 mM KCl
0.4% NP40 substitute
5 mM DTT

AE lysis buffer
50 mM Tris pH 8.0
20 mM NaCl
3 mM $MgCl_2$
3 mM $CaCl_2$
0.5 M Sorbital
0.6% Triton X-100
10 mM Sodium butyrate
In 5 ml of the above mix add
25 µl Phosphatase inhibitor cocktail 2
25 µl Phosphatase inhibitor cocktail 3
1 tablet of EDTA-free proteinase inhibitor cocktail

AE wash buffer
The same as AE lysis buffer but for every 5 ml buffer add
50 µl β-mechaptolethanol
5 ml of 8M Urea

AU gel loading buffer
8M Urea
12.5 mg/ml protamine sulfate
5% Acetic acid

TBST
20 mM Tris
150 mM NaCl
pH 7.6
1X TBS solution
0.02% Tween-20

Blocking solution
5% skimmed milk powder in TBST

2.2 Methods

2.2.1 *Dictyostelium* techniques

2.2.1.1 Axenic culture

Dictyostelium discoideum axenic strains Ax2 or Ax4 were used for individual experiments. Cells from frozen stocks were firstly cultured on SM agar plates in association with *Klebsiella aerogenes* (KA). Cell from leading edge were subsequently grown axenically in HL5 media in Petri dishes at 22℃. Confluent cells from Petri dishes were transferred to 100 ml or 500 ml flasks and cultured in shaking suspension at 220 rpm at 22℃. Exponentially growing cells were used for all experiments.

2.2.1.2 Genetically modified cell lines

Plasmids containing a Blasticidin-resistant (bsR) or neomycin-resistant cassette (neoR) were used for transformation of Ax2 cells to confer blasticidin S (BS) or neomycin (G418) resistance. Resistant strains were selected and maintained in HL5 medium containing 10 μg/ml BS or 50 μg/ml G418.

2.2.1.3 Transformation

Exponentially growing cells were collected and washed twice with cold H-50 buffer.

Cells were resuspended to a density of 5 x 10^7 cells/ml in cold H-50 buffer. A volume of 90 µl cells were added to a chilled 1-mm gap electroporation cuvette (Bio-Rad) and 10 µl plasmid (2 - 4 µg for overexpression and 4 - 8 µg for gene replacement) were mixed with cells. After 5 minutes incubation on ice, cells were electroporated for twice at 5 second interval using the following condition: 0.65kV and 25µF. Cells were then incubated on ice for another 5 min before transferred to 90 mm Petri dishes containing 10 ml of HL5. Selection drugs were added the next day.

2.2.1.4 Permanent stocks of *Dictyostelium discoideum*

Exponentially growing cells were collected and resuspended in HL5 supplemented with 10% DMSO to a final density of 1 - 5 x 10^7 cells/ml. Cryovials (Thermo Fisher Scientific) were used to store cells. Vials were immediately transferred into Mr. Frosty™ (Thermo Fisher Scientific) and kept at -80°C O.N. For long-term storage, vials were kept in liquid nitrogen.

2.2.1.5 Growth assay

Exponentially growing cells were collected and resuspended at 1 x 10^4 cells/ml in HL5 media. In a 24-well plate, 500 µl cells were seeded in each individual well. Twenty microliter TSA was added to reach the indicated concentration while DMSO was used as a control. After 48 hours of incubation at 22°C, HL5 media was removed by aspiration. Cells were then resuspended in 500 µl KK2 and allowed to reattach to the plate surface. Pictures of each well were taken using a camera (Hamamatsu, model ORCA-05G) attached to a dissection microscope (Leica, model MZFLLIII) under 8X magnification. Cell number was then manually counted using the pictures taken.

2.2.1.6 Development assay on agar

Development assays were carried out in a 24-well plate format. Plates were prepared by pouring 0.5 ml melted 1.5% agar (Formedium) in KK2 into each well and allowed to set and dry in a laminar flow hood using maximum air flow for 2h with lid open. DMSO or TSA was applied on top of the agar to reach desired concentration and the plates dried as described in the previous step. Exponentially growing cells were collected and washed three times with KK2. Cells were then resuspended to 1.4 x 10^8 cells/ml in KK2 and 20 µl of the cells were applied on agar and dried in the hood using maximum air flow for 30

mins with lid open. Cells were allowed to develop on agar for 24 hours. Pictures of each well were taken using a camera (Hamamatsu, model ORCA-05G) attached to a dissection microscope (Leica, model MZFLLIII). The number of fruiting bodies was manually counted using pictures taken.

2.2.1.7 REMI-seq screen

The initial mutant pool was kindly provided by Chris Thompson in UCL (Gruenheit et al., 2019). Upon receiving the pool of mutants, the pool was expanded by growth in HL5 in Petri dishes and multiple vials were frozen immediately when cells were confluent using 50% FBS/7.5% DMSO/42.5% HL5. A total number of 2×10^7 cells are within each stored vial. At the start of a screening, one copy of frozen pool was thawed into a Petri dish in 10 ml HL5 containing folic acid (453 μM) and vitamin B12 (440 nM). The cells were confluent next day and resuspended in pure HL5 at a cell density of 2.3×10^5 cells/ml. A total number of 2.3×10^6 cells were subjected to DMSO or 6 μM TSA treatment in HL5 in a Petri dish. The media was replaced every 24 hours with fresh DMSO or TSA until cells in the DMSO-treated sample were confluent. The doubling time was calculated and both DMSO and TSA-treated cells resuspended to the starting cell density 2.3×10^5 cells/ml and a total number of 2.3×10^6 cells were subjected to a

second-round treatment. The screen continued for a total number of eight rounds. At the end of each round, 5×10^5 cells were spread on a 9-cm plate with 400 µl KA suspension and allowed to grow for 60 hours at 22°C to have a clear plate. All cells on the plate were then collected and washed 6 times in KK2, collected by spinning at 1,700 × g for 2 minutes at 4°C to remove KA. Next, cells were lysed in 10 ml of nuclei buffer followed by centrifugation at 4,000 × g for 20 minutes at 4°C. The lysis step was repeated once. The pellet was resuspended to a final volume of 150 µl in 100 mM EDTA, pH 8.0 and then mixed with 150 µl 10% SDS and incubated at 55°C for 20 minutes. Next, 375 µl 4M ammonium acetate was added to the sample and centrifuged at 16,000 × g for 15 minutes at 4°C. The supernatant (450 µl) was mixed with 900 µl pure ethanol and centrifuged at 16,000 × g for 15 minutes at 4°C. The genomic DNA pellet was washed with 1 ml of 70% ethanol and collected as in the previous step. The genomic DNA was resuspended in 98 µl elution buffer and 2 µl RNase (Invitrogen).

A total amount of 2 µg genomic DNA was digested with MmeI (10U, NEB) for 17 hours followed by I-SceI (25U) digestion for 9 hours. The digested DNA was ethanol precipitated as described previously. The digested DNA was then ligated with D5 and different D7 adaptors, after processing the adaptors. The adaptors consist of two strands a and b. The two strands were annealed first before being ligated to digested genomic

DNA by mixing equal molar amounts of a and b strands and incubating at 85℃ for 10 minutes in a heat block. After incubation, the heat block was set to room temperature and allowed to cool down gradually. Ligation of digested genomic DNA to annealed adaptors was performed in the following reaction O.N. at 16℃. In this reaction, the amount of D5 used is more than D7 because the ligation of D5 to Mme-I digested sites relies on two nucleotides in random combination (NN, 16 possibilities). Due to short overhangs, the increased amount also aims to increase the chance of ligation. The sequences of both strands of D5 and D7 adaptors used in this study are listed in Appendix 1.

Reagent	**Volume**
Digested DNA	50 µl
Adaptor D7 (200 pg/µl)	10 µl
Adaptor D5 (20 ng/µl)	10 µl
10X ligase buffer	18 µl
H_2O	111 µl
T4 DNA ligase (400 U/µl)	1 µl
Total	200 µl

A quarter of the ligated product was subjected to PshAI (10U, NEB) digestion for 4 hours to reduce mitochondrial DNA contamination. Next, the library was amplified using the following recipe and PCR program.

Reagent	Volume
Sample post PshAI digestion	1.0 µl
Different D7_a (10 µM)	2.5 µl
P5 (10 µM)	2.5 µl
5x flexi buffer	10 µl
MgCl2	2.0 µl
dNTPs (40 mM)	1.0 µl
H_2O	30.75 µl
GoTag G2 (Promega)	0.25 µl
Total	50 µl

Step	Temp.	Time	Note
1	95°C	2 min	
2	95°C	30 sec	
3	66°C	5 sec	
4	68°C	1 min	Return to step 2 for 34 times
5	68°C	10 min	
6	12°C	infinity	

The PCR products (15 µl) were resolved on a 2.5% agarose gel (VWR) to confirm the presence of desired product (183 bp). Next, the remaining PCR product was resolved in 3.5% GTG agarose gel (LONZA) and visualized by staining with Midori green (NIPPON). The desired product (183 bp) was gel purified using Zymoclean Gel DNA Recovery kit (ZYMO). The size selection was carried out for a second time on the purified products. Samples post size-selection were then mixed in equal molar ratio to from a pooled library. In this study, a total number of 8 samples were mixed. The quality of the pooled library was checked by cloning into sequencing vector pJET1.2 (Thermo Fisher Scientific) and Sanger sequencing to confirm the mitochondrial DNA

contamination was at an acceptable level (~25%). Finally, the library was sent to WHG Oxford Genomics Centre for Illumina sequencing using NextSeq 550 System High-Output Kit (maximum reads are 400 million). The requested sequencing length was single read 50 bp. After sequencing, the data was analyzed using a Perl script and an R script provided by Chris Thompson Lab, which will be available on the main website of REMI-seq (https://remi-seq.org/).

2.2.2 Biochemical and molecular techniques

2.2.2.1 General cloning techniques

Polymerase chain reaction (PCR), restriction enzyme digestion, phosphatase reaction, agarose gel electrophoresis, ligation, and transformation of DNA into *Escherichia coli* were performed as described in "Molecular Cloning" (Green and Sambrook, 2012). The *E.coli* strain used for plasmid amplification was DH5α (NEB), and for protein expression the strain used was Rosetta-gami™2(DE3) (Novagen). All fragments amplified by PCR were cloned into pJET1.2 vector (Thermo Fisher Scientific) for sequencing before subcloning unless otherwise described.

2.2.2.2 Preparation of *Dictyostelium* genomic DNA and cDNA

Genomic DNA of exponentially growing cells (5×10^6 cells in total) was prepared using Quick-DNA Miniprep Kit (Zymo) according to the manufacturer's instructions. Total RNA was isolated from 5×10^6 cells using the TRIzol® Reagent (Life Technologies) and 10 µg total RNA was subjected to TURBO DNA-free™ Kit (Life Technologies) to remove residual genomic DNA. cDNA was generated using 2 µg DNA-free RNA by SuperScript™ IV First-Strand Synthesis System (Invitrogen) following the manufacturer's manual.

2.2.2.3 RT-PCR

RT-PCR was performed using cDNA samples and MyTaq™ Red Mix. Specific primers are listed in Appendix 1. The PCR program was set as following: 95°C, 3 minutes → 34 × (95°C, 30 second; 55°C, 30 second; 68°C, 1 minute) → 68°C, 5 minute.

2.2.2.3 Cloning of *Gcn5* disruption vector

The 5' homology arm targeting -1515 to -563 upstream the first nucleotide of the coding sequence of *Gcn5* was cloned into pJET1.2 vector using primers Gcn5KO_LR_F and Gcn5KO_LR_R, generating pJET_Gcn5KO_LR. The 3' homology arm spanning 1162 to 2171 downstream of the *Gcn5* start codon was cloned into pJET1.2 vector using

primers Gcn5KO_RR_F and Gcn5KO_RR_R, generating pJET_Gcn5KO_RR. Next, pJET_Gcn5KO_RR was digested by XhoI and MluI to release the 3' arm. The 3'arm was inserted into the XbaI site of pJET_Gcn5KO_LR. The desired orientation was confirmed by restriction enzyme digestion, generating pJET_Gcn5KO_LRRR. Next, the blasticidin-resistance (bsR) cassette was obtained from the pLPBLP vector by SmaI digestion and subsequently inserted at an Eco53KI site in pJET_Gcn5KO_LRRR, generating the final disruption vector pJET_Gcn5KO. Sequences of primers used are listed in Appendix 1.

2.2.2. 4 Cloning and expression of GST-Tudor fusion proteins in *E. coli*

The sequence coding for the tandem Tudor domain (S277 - K411) in *Dd*Sgf29 (411 a.a.) was amplified from genomic DNA using primers Tudor-F and Tudor-R, which carried EcoRI and XhoI recognition sites respectively. A fragment to express a mutant Tudor domain with two amino acids of the binding site mutated was amplified by two stages of PCR. First, primers Tudor-F and Tudor-N-R were used to amplify the N-terminal sequence of the Tudor domain with the first binding residue mutated (F359A) by Tudor-N-R; primers Tudor-C-F and Tudor-R were used to amplify the C-terminal sequence of Tudor domain with the second binding residue mutated (Y366A) by Tudor-C-F. Second, the two fragments had overlapping sequences and were used as templates for a second-

round of PCR using primers Tudor-F and Tudor-R. Wildtype or mutant Tudor domain was then subcloned into the pGEX-KG vector using EcoRI (5') and XhoI (3') sites. This generated an expression cassette with GST fused to the N-terminus of the Tudor domain and the expression in *E. coli* was driven by an IPTG-inducible (Isopropyl β- d-1-thiogalactopyranoside) promoter.

Expression and purification of wildtype and mutant GST-protein in transformed *E.coli* was carried out using the following steps. First, transformed *E.coli* was inoculated into 50 ml LB containing 100 mg/ml ampicillin (LB-Amp) and cultured at 37℃ O.N. The starting culture was diluted into 600 ml LB-Amp the next day at 37℃ until O.D 600 reached 0.55. One milliliter of the culture was stored before IPTG was added to a final concentration of 0.1 mM. The culture was then incubated at 16℃ O.N. for maximum protein expression. One milliliter of the O.N. culture was stored before cells were collected and lysed by sonication (10 watts, 10s intervals with 1-minute cooling in between) in 15 ml lysis buffer (50 mM Tris, 50 mM NaCl and 1X protease inhibitor cocktail from Roche) at 4℃. Cell lysates were centrifuged at 48,000 × g for 20 min at 4℃ to separate soluble protein in supernatant from inclusion bodies in the precipitates, both of which were stored for SDS-PAGE analysis. The GST-Tudor fusion protein was purified using Glutathione sepharose 4B (GE Healthcare) following the manufacturer's

manual. Samples collected from various stages mentioned above, including flow through sample and purified GST-Tudor fusion protein, were resolved by 10% SDS-PAGE to examine the purification process and the purity of the final product. Sequences of primers used are listed in Appendix 1.

2.2.2.5 Cloning and expression of full-length *DdSgf29* in *Dictyostelium*.

Full length wildtype and mutant DdSgf29 were cloned by two steps. First, the coding sequence of 1 to 854 (relative to first nucleotide of the start codon) of *Sgf29* was amplified from cDNA by primers DdSgf29_1-854_F and DdSgf29_1-854_R. The N-terminal end of the amplicon carried a BamHI cutting site introduced by the forward primer while the C-terminal end of the fragment overlapped with the previously cloned wildtype and mutant Tudor domains. Within the overlapping region sits an unique endogenous NcoI cutting site. In the second step, the N-terminal fragment was cloned into pGEX-KG carrying wildtype or mutant Tudor domain using BamHI and NcoI sites, thus generating full-length wildtype or mutant *Dd*Sgf29 in the vector. The full-length *Dd*Sgf29 cassette also carries BglII and SpeI sites at 5' and 3' ends respectively. These sites are introduced by DdSgf29_1-854_F and Tudor-R primers respectively. The two sites allowed subcloning of the full-length *Dd*Sgf29 cassette into the pDM series of vectors, which

drive protein expression in *Dictyostelium* using an actin15 promoter and provide numerous options for N- and C- terminal tags including a FLAG tag (Veltman et al., 2009). Sequences of primers used are listed in Appendix 1.

2.2.2.6 *Sgf29* disruption vector

The methodology was the same as described for generating the *Gcn5* disruption vector. The 5' homology arm spanning 1 to 1084 relative to the first nucleotide of the start codon of *Sgf29* was cloned into pJET1.2 vector using primers DdSgf29_1-854_F and Sgf29KO_LR_R, generating pJET_Sgf29KO_LR. The 3' homology arm targeting 1943 to 2877 downstream of the start codon of *Sgf29* was cloned into pJET1.2 vector using primers Sgf29KO_RR_F and Sgf29KO_RR_R, generating pJET_Sgf29KO_RR. Next, pJET_Sgf29KO_RR was digested by XhoI, which cut both ends of the 3'arm and released it. The 3'arm was then inserted at the XhoI site of pJET_Sgf29KO_LR. The desired orientation was confirmed by restriction enzyme digestion, generating pJET_Sgf29KO_LRRR. Next, the bsR cassette was obtained from the pLPBLP vector by SmaI digestion and subsequently inserted at the HincII site in pJET_Sgf29KO_LRRR, generating the final disruption vector pJET_Sgf29KO. Sequences of primers used are listed in Appendix 1.

2.2.2.7 Acid extraction for histone-enriched samples

A total of 2 × 10^8 exponentially growing cells were pelleted at 1,700 × g for 3 min, washed in 25 ml of cold KK2 twice and lysed by 2 ml of AE lysis buffer to isolated nuclei. Nuclei were collected by centrifugation at 2,500 × g at 4℃ and washed twice by 1 ml of AE wash buffer at 4℃. Nuclei were then subjected to acid extraction using 250 µl 0.4M HCl for 1h at 4℃. Thee sample was centrifuged at 16, 000 × g for 15 min to separate supernatant and insoluble proteins. The supernatant was transferred to a new 2 ml tube and the proteins were precipitated by adding 6.2X volume of cold acetone. Samples for SDS-PAGE and AU gel were separated at this step with one fourth (SDS-PAGE) of the total sample transferred into one Eppendorf and the rest sample (AU gel) remained in the original tube. Proteins are allowed to precipitate O.N. at 4℃. Samples were washed twice with 1 ml cold acetone after O.N. precipitation. For SDS-PAGE analysis, samples were resuspended in 50 µl 1X SDS gel loading buffer. For Acid-Urea gel analysis, sample was resuspended in 110 µl AU gel loading buffer.

2.2.2.7 SDS-PAGE electrophoresis and western blot

The preparation of different percentages of SDS-PAGE and performing of electrophoresis were carried out as described in “Molecular Cloning” (Green and

Sambrook, 2012). Acid extracts were resolved by 18% SDS-PAGE then transferred to a PVDF membrane at 60 mA O.N. at 4°C. The membrane was blocked by blocking solution for 3h at room temperature followed by incubation with specific first antibodies at 4°C O.N. After incubation with the first antibody, the membrane was washed for three times using TBST for 15 min each. The membrane was incubated with a corresponding secondary antibody for 1h at room temperature to detect the signal of the first antibody. The same wash steps were repeated and the membrane was incubated with 400 µl SuperSignal™ West Femto Maximum Sensitivity Substrate (Thermo Fisher Scientific) for 2 min at room temperature. The Western blot signal was detected using LICOR ODYSSEY. Antibodies (first and secondary) used and their dilutions are listed in Appendix 2.

2.2.2.9 Acid-Urea gel electrophoresis

The methods to cast Acid-Urea gel and perform electrophoresis was modified from a previous study (Crump et al., 2011). Briefly, 20% acid-urea gels are made using the following recipe.

Gel type	Resolving	Stacking
Percentage	20%	7.50%
40 % acrylamide	10 ml	0.95 ml
2 % bis-acrylamide	2 ml	0.25 ml
urea	4.8 g	2.4 g
acetic acid	1 ml	0.25 ml
TEMED	80 µl	40 µl
10 % APS	400 µl	200 µl
ddH_2O (up to)	20 ml	5 ml

Sixteen milliliter of resolving gel was poured into a 0.75 mm wide glass cassette after adding TEMED and APS. The gel was then layered with 400 µl isopropanol and allowed to set for 30 minutes at room temperature. The stacking gel was poured on top of resolving gel after isopropanol removal and allowed to set for 30 minutes. For each well, 40 µl of 4 M urea/10 % PEG-8000/12.5 mg/ml^{-1} protamine sulfate solution was loaded, and a pre-run performed at 150V for 8 hours at 4℃ with reversed electrodes so protein migrates from positive to negative charge. The running buffer used was 5% acetic acid. After the pre-run, the wells were washed twice with running buffer and samples in AU gel loading buffer were loaded into wells. The electrophoresis was performed firstly at 200V for 2.5 hours at 4℃ then increased to 600V/30mA for 12 hours at 4℃. After electrophoresis, proteins were transferred to a PVDF membrane, again with electrodes reversed. The subsequent Western blot procedures were the same as described above in the SDS-PAGE electrophoresis section.

3. Cross-talk between H3K4me3 and acetylation of H3 in the mode of action of KDACi

3.1 Introduction

Analysis of histones extracted from cells treated with TSA has revealed two populations of acetylated histone H3. Histone H3 containing the H3K4me3 modification is subject to rapid acetylation consistent with dynamic turnover of acetylation of these histones. The remainder of the histone H3 is much more slowly acetylated, consistent with slower turnover. This phenomenon was originally reported in mammalian cells at the promoters of the rapidly inducible immediate early genes (Crump et al., 2011) and has since been found to be conserved in *Drosophila* and *Dictyostelium* (Hsu et al., 2012). It is not known if the effects of KDACi such as TSA are specifically due to increased acetylation of histones and, if so, whether the rapid increase in acetylation of the H3K4me3 pool is involved in the response to TSA and *Dictyostelium* offers an excellent system to examine this.

3.1.1 Enzymes catalyzing methylation of H3K4 and the homologue in *Dictyostelium*

It is known that methylation of H3K4 is a hallmark of active transcription and the modification is conserved from yeast to humans (reviewed by Hyun et al., 2017). H3K4me1 is particularly associated with enhancer regions, H3K4me2 is enriched at the

5’ end of transcribing genes, and H3K4me3 is found enriched at the promoters of poised and actively transcribing genes (Heintzman et al., 2007). In *S. cerevisiae*, there is only one methyltransferase Set1 that catalyzes *mono, di-* and *tri-* methylation of H3K4 (Briggs et al., 2001). The number of Set1 homologues expands in higher eukaryotes. There are two and six family members in *Drosophila melanogaster* and *Homo sapiens* respectively. Among them, SET1 in *Drosophila* and SET1A, SET1B, MLL1 and MLL2 in humans can carry out *mono, di-* and *tri-* methylation of H3K4 while others harbour only *mono-* to *di*-methylation ability (reviewed in Hyun et al., 2017).

The homolog of SET1 in *Dictyostelium* has been identified and studied by Chubb and his colleagues (2006). They reported that Set1 in *Dictyostelium* not only harbours a conserved catalytic SET domain, but also insertion of a blasticidin-resistance cassette (bsR) in the coding sequence upstream of the SET domain, leads to loss of all detectable *mono-*, *di-* and *tri*-methylation on H3K4, similar to the situation in *S. cerevisiae*. The morphology of *Dictyostelium set1*$^{-}$ cells is similar to parental Ax2 cells. However, *set1*$^{-}$ cells were found to have a mild growth disadvantage and a developmental advantage in that the early stages of development were more rapid than in parental cells, though the resulting fruiting bodies were apparently normal.

***Dictyostelium* strains with mutations at histone H3K4.**

As Set1 could have other substrates than H3K4, two *Dictyostelium* strains are available in which the endogenous gene encoding for one of the two major H3 variants, H3a and H3b, has been replaced with a version in which K4 is mutated to alanine and so cannot be methylated (Hsu et al., 2012). This leads to strains with a different pattern of methylation on K4. Methylation (*mono*, *di* and *tri*) of both H3a and H3b on lysine K4 is absent in *set1*$^{-}$ cells, while in H3aK4A cells *mono*-, and *di*- methylation is detectable on H3b but not *tri*-methylation. H3bK4A cells show no detectable methylation on H3bK4 but all methylation on H3aK4 is not affected (Table 3.1) (Hsu et al., 2012).

Table 3.1 Strains with abnormal H3K4 methylation in *Dictyostelium*

Strain	Loss of H3K4 methylation						Reference
	mono-		***di-***		***tri-***		
	H3a	H3b	H3a	H3b	H3a	H3b	
set1^{-}	X*	X	X	X	X	X	(Chubb et al., 2006; Hsu et al., 2012)
H3aK4A	X		X		X	X	(Hsu et al., 2012)
H3bK4A		X		X		X	(Hsu et al., 2012)

*Undetectable modification is marked with an X

3.1.2 Conserved acetyltransferases in eukaryotes

GNAT and MYST are two families of acetyltransferases conserved in yeast, flies and humans (Lee and Workman, 2007). These acetyltransferases form large protein complexes that function in chromatin remodeling and regulation of transcription. In *Dictyostelium*, protein sequences with high homology to GNAT or MYST have been identified, including homologues of yeast GCN5 and Sas2 (Ludwig et al., 2006). Despite the sequence homology, functional data for the activities of the predicted GNAT or MYST proteins is absent.

Apart from the two well-conserved acetyltransferase families, some transcription coactivators also harbor HAT activity but are not classified as members of the GNAT or MYST family due to lack of conservation of consensus residues in the active site of the HAT domain (Yuan and Marmorstein, 2013). One example is p300/CBP that is found only in metazoa but not in lower eukaryotes like yeast (Eckner, 1996). There is no evidence suggesting the existence of a p300/CBP-like protein in *Dictyostelium.*

3.2 Aims

This chapter aims to understand if dynamic acetylation (i.e. rapid acetylation) of lysine-4-trimethylated histone H3 is important for the mode of action of hydroxamic acid, the

most common form of KDACi used in clinics at the time of writing. And if so, which acetyltransferase is responsible for the acetylation induced by KDACi. The first aim is to analyze inhibition of *Dictyostelium* growth and development by two hydroxamic acids, namely TSA and SAHA, using parental Ax2 cells and *set1*$^{-}$ strain which is predicted to have impaired dynamic acetylation due to loss of methylation on H3K4. To understand if a similar mechanism exists for another structurally distinct KDACi, VPA which belongs to short chain fatty acids, was also included in this study. Strains with mutations of K4 in the endogenous H3 proteins are used to determine if the effects of loss of Set1 are due to modification of histone H3 or other potential targets. The second aim is to examine if strains with altered H3K4 methylation exhibit an altered H3 acetylation profile in comparison to parental cells upon TSA treatment. The final aim is to understand whether the Gcn5 acetyltransferase is responsible for basal and/or TSA-induced histone hyperacetylation in *Dictyostelium* and if it is involved in the mode of action of TSA.

3.3 Results

3.3.1 Effects of TSA, SAHA and VPA on the growth and development of Ax2 cells

To understand the effect of KDACis on the growth and development of *Dictyostelium discoideum*, a range of concentration of TSA, SAHA or VPA was used to treat Ax2 cells. Vegetative cells were exposed to KDACi in HL5 in 24-well plates with a starting cell number of 5×10^3 cells/well, and the relative cell density compared to vehicle-treated sample was calculated after 48 hours treatment. Both TSA and VPA showed dose-dependent growth inhibition in *Dictyostelium* (Fig. 3.1A). By 4 μM, the cell density of TSA-treated sample was inhibited to 69% of DMSO-treated sample, while inhibition by 1 mM VPA was 59% compared to water-treated sample. In contrast, there was little effect of SAHA on cell growth. Even at the highest concentration used (20 μM), the cell density of SAHA-treated sample was only reduced to 85% of DMSO-treated sample.

To determine the effect of KDACis on development, cells were developed on agar containing different concentrations of KDACi. The final structures were imaged after 24h. All three KDACi nhibitors showed a dose-dependent inhibition of *Dictyostelium* development (Fig. 3.1B). At 2 μM TSA, 15 μM SAHA or 0.5 mM VPA, the majority of Ax2 cells were at mound stage after 24h while vehicle-treated cells formed fruiting bodies.

A

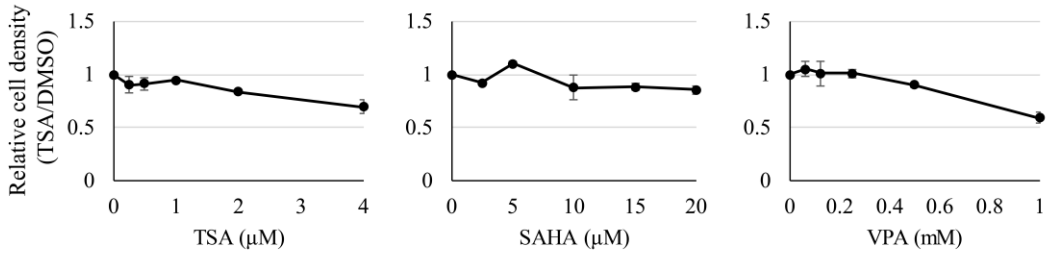

B

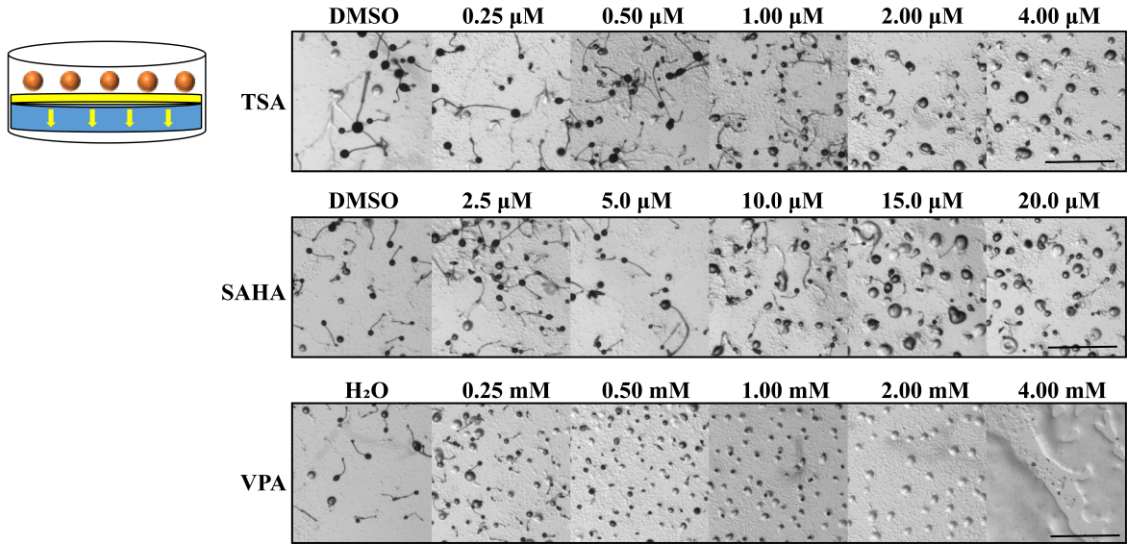

Figure 3.1 Dose-dependent inhibition of *Dictyostelium* growth and development by TSA, SAHA or VPA.

(A.) Ax2 cells were cultured in HL5 in a 24-well plate (5×10^3 cells/well starting density) with increasing concentrations of TSA, SAHA or VPA in individual wells. Relative cell density (inhibitor/vehicle) was calculated after 48 hours of growth and data shown as mean ± SD from three independent experiments. **(B.)** KDACi (yellow) was applied on top of 1.5% agar (w/v, blue) in a 24-well plate and allowed to dry for 2 hours at 22°C. Exponentially growing cells (orange) were collected by centrifugation and washed twice with KK2 before spreading on agar (2.8×10^6 cells/well). After 24 hours development in the presence of different concentrations of KDACi at 22 °C, images were taken using a dissection microscope. Scale bar represents 1 mm.

3.3.2 Growth and development inhibition by TSA, SAHA or VPA in cells with abnormal H3K4 methylation

To understand if rapid acetylation of H3K4me3 histones is important for the mode of action of KDACi, the above effective concentrations were used to determine whether available mutants with alterations in histone 3 modification potential showed altered sensitivity to KDACi during growth and/or development. These strains include loss of methylation on H3K4 due to loss of a methyltransferase, namely Set1 (Chubb et al., 2006); loss of all modification on variants of H3 at K4, namely H3aK4A and H3bK4A cells (Table 3.1 and Fig 3.2A).

If dynamic acetylation of H3K4me3 is important for the mode of action of TSA, the sensitivity of the cell lines listed in Table 3.1 with altered methylation patterns may differ from parental cells. Therefore, they were subjected to a 48 hours growth assay. Parental Ax2 cells were used as a control for *set1*$^{-}$cells. For H3aK4A and H3bK4A cells, a strain harbouring an H3aK4K gene replacement was used as a control as described by Hsu *et al*. (2012).

The growth assay showed *set1*$^{-}$ cells were more sensitive to TSA and SAHA compared to Ax2 cells. In *set1*$^{-}$ cells, the cell density dropped to 28% and 66% of DMSO-treated

cells by TSA and SAHA, respectively, while Ax2 cells were at 40% and 82% (Fig. 3.2B and C, $p < 0.05$). However, sensitivity to VPA was similar between Ax2 and *set1*$^{-}$ cells consistent with VPA acting independently of H3K4me3(Fig. 3.2D). H3aK4A cells were more sensitive to TSA and SAHA while H3bK4A cell were only significantly more sensitive to TSA when compared to H3aK4K cells, although the variability of the SAHA data may mask a small effect. These data indicate that methylation on H3K4 is important for growth under TSA (Fig. 3.2E and F).

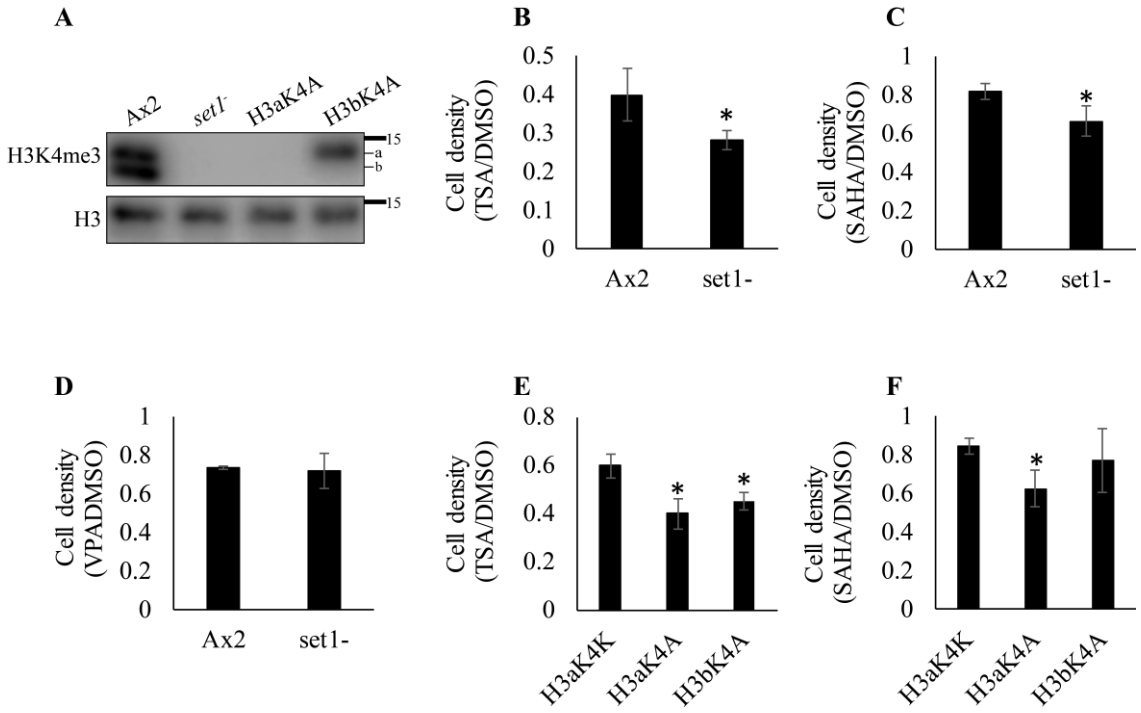

Figure 3.2 Growth of strains with altered H3K4 methylation in the presence of TSA, SAHA or VPA.

(A.) Western blot confirming the absence of H3K4me3 in *set1*$^{-}$, H3aK4A and H3bK4A cells. Exponentially growing cells were subjected to acid extraction to enrich for histones. Extracts were resolved by 18% SDS-PAGE. Levels of H3 and H3K4me3 were detected using specific antibodies. **(B-F.)** Growth assay of *set1*$^{-}$, H3aK4A and H3bK4A cells in the presence of KDACi. Exponentially growing cells were cultured in HL5 in a 24-well plate (5×10^3 cells/well) with 4 μM TSA, 20 μM SAHA or 1 mM VPA. Relative cell density (inhibitor/vehicle) was calculated after 48 hours of growth and data was shown as mean ± SD from three independent experiments. Statistical significance was assessed using T-Test (*, $p < 0.05$)

To further understand the role of dynamic acetylation in KDACi-caused developmental inhibition, the same cell lines listed in Table 3.1 were subjected to a developmental assay in the presence of 2 μM TSA, 15 μM SAHA or 0.5 mM VPA, concentrations known to inhibit control cell development. The result revealed a strong developmental resistance phenotype for *set1*$^{-}$ cells in the presence of TSA or SAHA (Fig. 3.3A). *set1*$^{-}$ cells

successfully formed fruiting bodies while Ax2 cells were still at aggregate or slug stage under 2 μM TSA or 15 μM SAHA treatment, respectively. However, the resistance was not found in *set1*$^{-}$ cells in the presence of VPA (Fig. 3.3A). To understand if these phenotypes are due to loss of methylation on H3K4, H3aK4A and H3bK4A cells were also examined (Fig. 3.3B). Both types of cells had more advanced developmental structures compared to H3aK4K cells, though mature fruiting bodies were not found after 24 hours of development under 2 μM TSA or 15 μM SAHA treatment. In response to 0.5 mM VPA, development of H3aK4K and H3aK4A cells were markedly inhibited with only a few loose aggregates after 24 hours of development, but H3bK4A cells exhibited more complex structures such as tight aggregates and slugs. The result strongly suggests that methylation of H3K4 is important for TSA- and SAHA-induced developmental inhibition.

The results revealed that impaired methylation of H3K4, which is the common feature among *set1*$^{-}$, H3aK4A and H3bK4A cells, may play a crucial role in the mode of action of hydroxamic acid (TSA and SAHA)-induced developmental inhibition. In order to confirm the resistance phenotypes, *set1*$^{-}$, H3aK4A and H3bK4A cells should be subjected to a wider range of TSA or SAHA and monitored at different timepoints to examine the dynamics of their resistance during the development cycle.

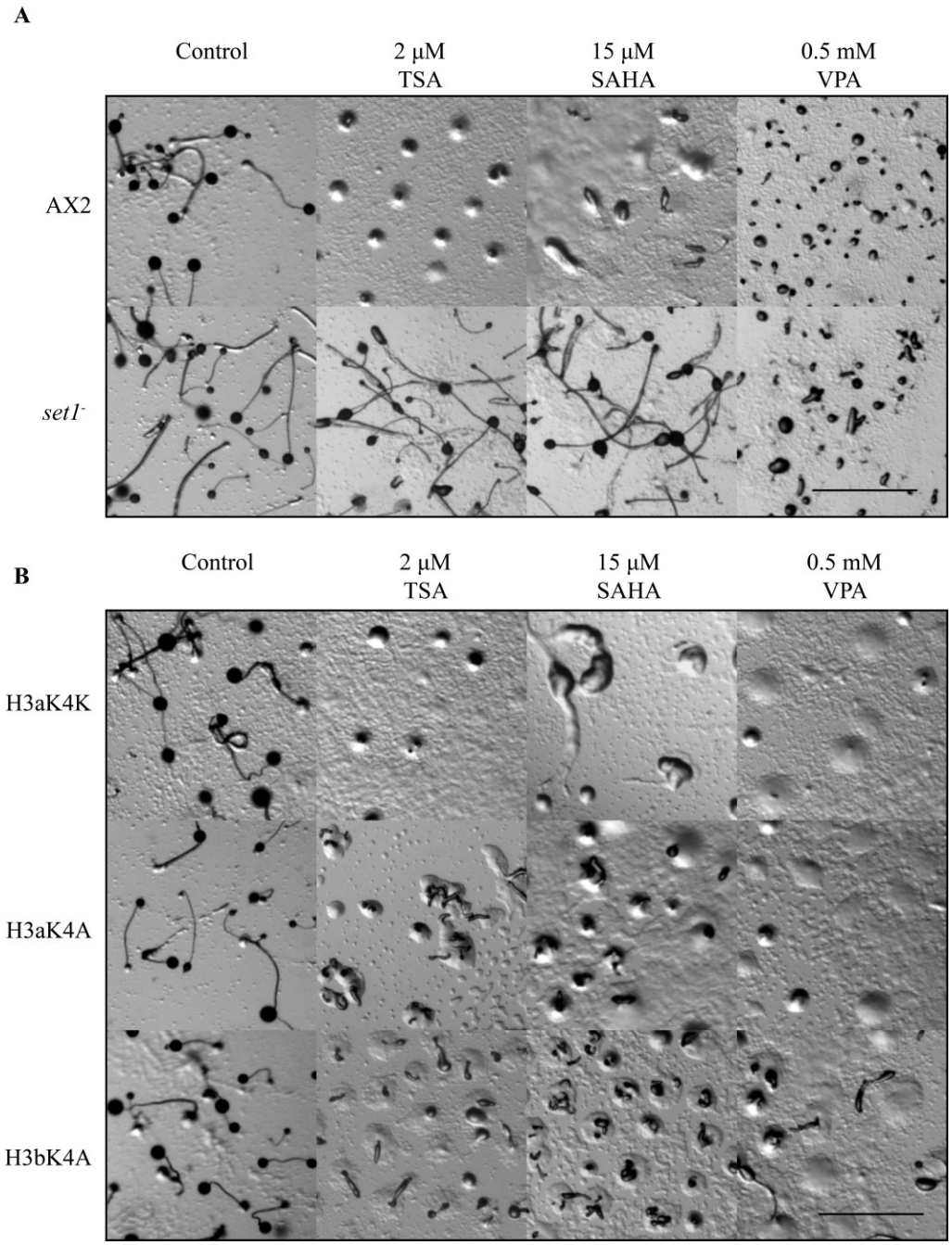

Figure 3.3 Development of strains with altered H3K4 methylation in the presence of TSA, SAHA or VPA.

Development assay of **(A)** Ax2 and *set1*$^{-}$ cells; **(B.)** H3aK4K, H3aK4A and H3bK4A cells. KDACi was applied on top of 1.5% agar in a 24-well plate and allowed to dry for 2 hours at 22°C. Exponentially growing cells were collected by centrifugation and washed twice with KK2 before spreading on agar (2.8×10^6 cells/well). After 24 hours development in the presence of 2 µM TSA, 15 µM SAHA or 0.5 mM VPA at 22 °C, images were taken using a dissection microscope. Scale bar represents 1 mm.

3.3.3 Effects of TSA, SAHA and VPA on Ax2 and *set1*$^-$ cells during the development cycle

In order to confirm that *set1*$^-$ mutant strains showed altered sensitivity to the presence of KDACi during development, and to reveal the stage of development most affected, the cells were developed on agar in the presence of a range of concentrations (Figure 3.4). Images of different developmental stages were collected from 9 timepoints, namely 0, 4, 6, 8, 12, 14, 16, 20 and 24 hours.

All three KDACis markedly inhibited the formation of slugs of Ax2 cells, at concentrations as low as 1 μM TSA, 10 μM SAHA or 0.5 mM VPA at 16h timepoint. At higher concentrations, the development of Ax2 cells was blocked at the mound stage by all three KDACis at 24h. In contrast, *set1*$^-$ cells successfully formed slugs by 16 hours even at the highest concentrations of TSA and SAHA tested and continued to form fruiting bodies at 24h, confirming that *set1*$^-$ cells are resistant to TSA and SAHA-induced developmental inhibition. In response to VPA, *set1*$^-$ cells showed subtle resistance compared to Ax2 cells. At 0.25 mM, formation of fruiting bodies of Ax2 cells was affected at 24 hours with some aggregates failing to proceed, which was not observed in *set1*$^-$ cells. At 0.5 mM, the majority of *set1*$^-$ cells were at slug stage at 24 hours while Ax2 cells were still at aggregate stage.

The result suggests that loss of *Set1* in *Dictyostelium* confers resistance to developmental inhibition caused by hydroxamic acid (e.g. TSA and SAHA) and partial resistance to short-chain aliphatic acid (e.g. VPA). However, it is unclear if the resistance is caused by loss of methylation on histone H3 lysine 4 or from mismethylation of other downstream targets of Set1.

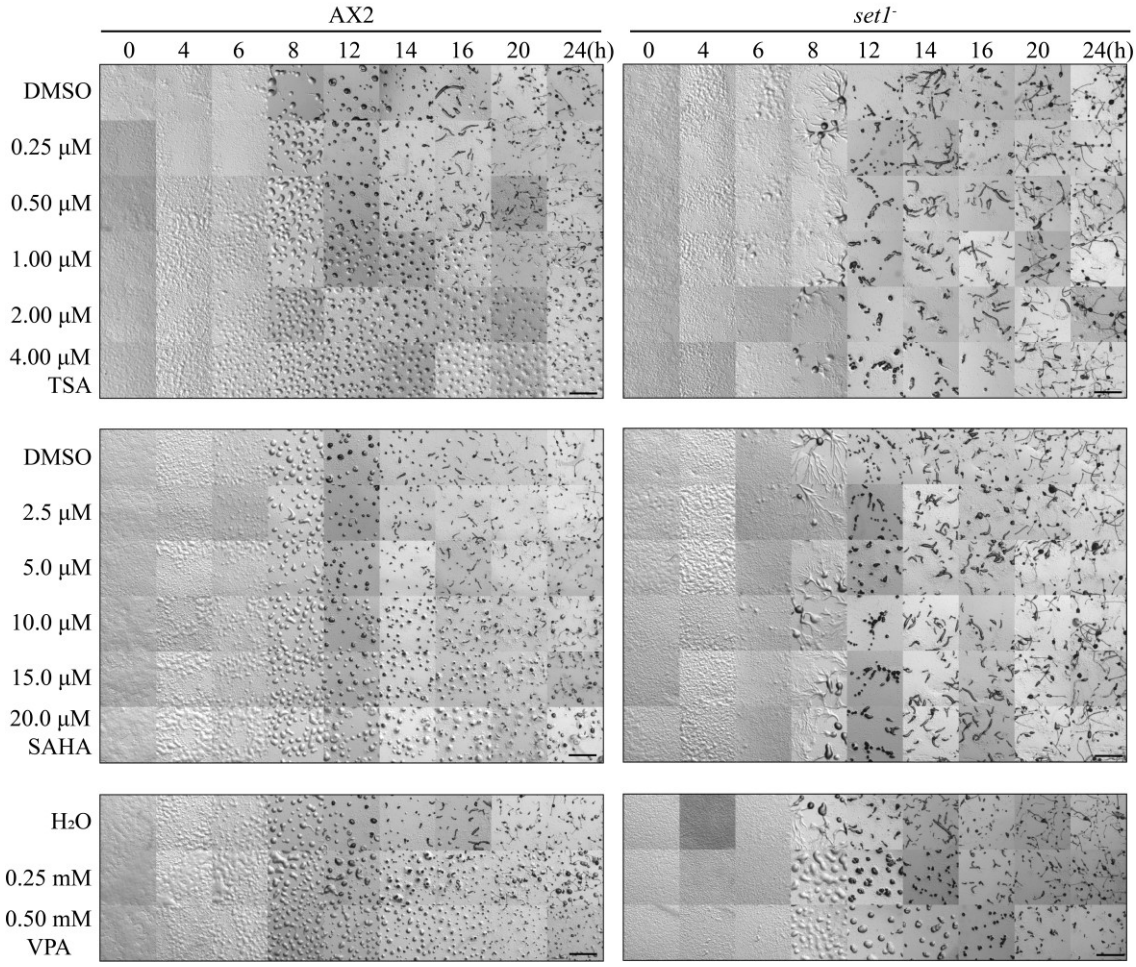

Figure 3.4 *set1*$^{-}$ cells are resistant to TSA, SAHA and VPA induced developmental inhibition

KDACi was applied on top of 1.5% agar (w/v) in a 24-well plate and allowed to dry for 2 hours at 22℃. Exponential Ax2 and *set1*$^{-}$ cells were collected and washed twice with KK2. Cells were then transferred to agar (2.8×10^6 cells/well) containing increasing concentration of TSA, SAHA or VPA. Images of different developmental stages were taken after 0, 4, 6, 8, 12, 14, 16, 20 and 24 hours of development Scale bar represents 1 mm.

3.3.4 Resistance to TSA during development by loss of methylation on H3K4

If the resistance phenotype of *set1*$^{-}$ cells is only due to loss of H3K4 methylation then H3ak4A cells should show a similar dose response to inhibition of development by TSA.

To address this question, a range of concentrations of TSA were tested for their ability to

inhibit development of H3aK4A and H3bK4A cells.

Development of control H3aK4K cells were inhibited by TSA from the lowest concentration used. At concentrations above 2 μM TSA, H3aK4K cells were marked inhibited with few loose aggregates at 26 h. In contrast, H3aK4A and H3bK4A cells were able to develop many tipped mounds and some slugs at 26 h (Fig. 3.5A). However, unlike *set1*$^{-}$ cells which formed mature fruiting bodies at concentrations of up to 4 uM TSA within 24 hours (Fig. 3.4), H3aK4A and H3bK4A failed to form mature fruiting bodies after 26h hours of TSA treatment (Fig. 3.5B). To determine whether TSA delays or stops the development of H3aK4A and H3bK4A cells, both cell lines were exposed to up to 4 μM TSA for 48 hours.

Even after 48h, the majority of H3aK4K cells treated with 2 or 4 μM TSA failed to complete the development cycle (Fig. 3.5B). However, H3aK4A and H3bK4A cells successfully formed fruiting bodies at 48 h under 4 μM TSA treatment (Fig. 3.5B).

Loss of K4 methylation in one of the two histone H3 variant in *Dictyostelium* is sufficient to confer developmental resistance in response to TSA (Fig. 3.5), suggesting that loss of methylation on H3K4 in *set1*$^{-}$ cells is the major contributor of its resistance phenotype.

Furthermore, H3aK4A and H3bK4A cells both lost *tri*-methylation of lysine 4 on H3b (Fig. 3.2A), which indicates loss of H3K4me3 on H3b alone is sufficient to confer TSA resistance during development. However, *set1*$^{-}$ cells form fruiting bodies in 24h under 4 μM TSA while H3aK4A and H3bK4A cells needed 48 hours, suggesting that *mono*- and *di*- methylation of H3K4 may also be involved in the mode of action of TSA. Thus, methylation of H3K4 plays an important role in the mode of action of TSA in *Dictyostelium* during development.

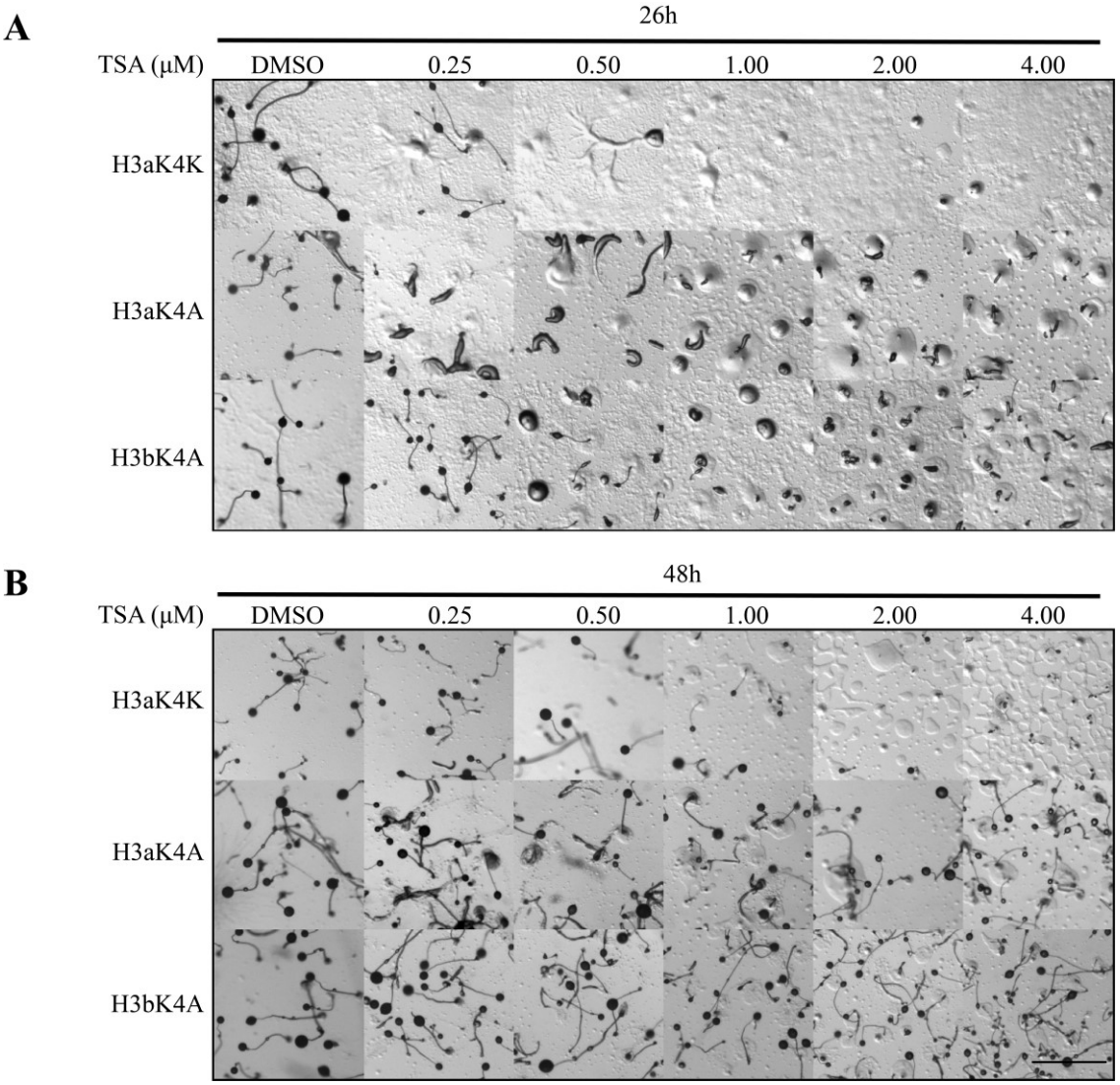

Figure 3.5 Loss of methylation on H3K4 confers resistance to TSA-induced developmental inhibition.

Cells were collected and washed twice with KK2. Cells were then transferred to 1.5% agar (2.8×10^6 cells/well) containing increasing concentrations of TSA. Images were taken after **(A.)** 26 and **(B.)** 48 hours of development. Scale bar represents 1 mm.

3.3.5 Early exposure-dependent development inhibition by TSA

At concentrations of TSA above 2 uM development is stalled at mound stage, which normally happens at 8 – 10 hours in the *Dictyostelium* development cycle (Fig. 3.4). This raises the question whether TSA is still effective after *Dictyostelium* cells have entered

mound stage. To address the question and gain further insight of the effects of TSA on different developmental stages, DMSO or TSA was added on top of developing cells at different timepoints. (Fig. 3.6A). The number of fruiting bodies were calculated and normalized to DMSO-treated samples.

All DMSO-treated samples, despite different hours of DMSO treatment, formed fruiting bodies as the untreated at the 24 h timepoint (data not shown). TSA-induced developmental inhibition was observed in samples where TSA was added after 0, 2 and 4 hours of development but not in samples exposed to TSA after 6 hours development (Fig 3.6B, upper panel). When exposed to 4 μM TSA during the first four hours of development, the formation of fruiting bodies dropped to ~10% of DMSO-treated sample. However, if the exposure happened after cells have developed for 6 hours, the number increased to ~60% of the control ($p < 0.01$) and further up to 80% for 8 and 10 h (Fig. 3.6B, lower panel).

Exposing cells to TSA in the first four hours of development is necessary for effective developmental inhibition, but it is still unclear if the first four hours only is sufficient. Also, it is unclear if *set1*$^-$ cells are resistant to short-term exposure of TSA. To answer the questions, exponential Ax2 or *set1*$^-$ cells were treated with 4 μM TSA or DMSO for 4h in KK2 in shaking suspension. Cells were then washed again to remove TSA and

transferred onto agar without TSA or DMSO to develop for another 20 h before pictures were taken. The number of fruiting bodies were calculated and normalized to DMSO-treated samples (Fig 3.6C). Treating Ax2 cells with 4 μM TSA for 4 h in KK2 led to a reduction in the number of fruiting bodies to 40% compared to DMSO-pretreatment, while in *set1*$^{-}$ cells the number is significantly higher at 88% ($p < 0.01$) (Fig. 3.6D).

These results confirm that treating developing cells with TSA for the first four hours of development is sufficient to reduce the number of fruiting bodies in Ax2 cells by 60% but that *set1*$^{-}$ cells are resistant at this early stage of development. The result suggests that the molecular event(s) that makes *set1*$^{-}$ cells resistant to TSA is likely to happen during the first fours of development.

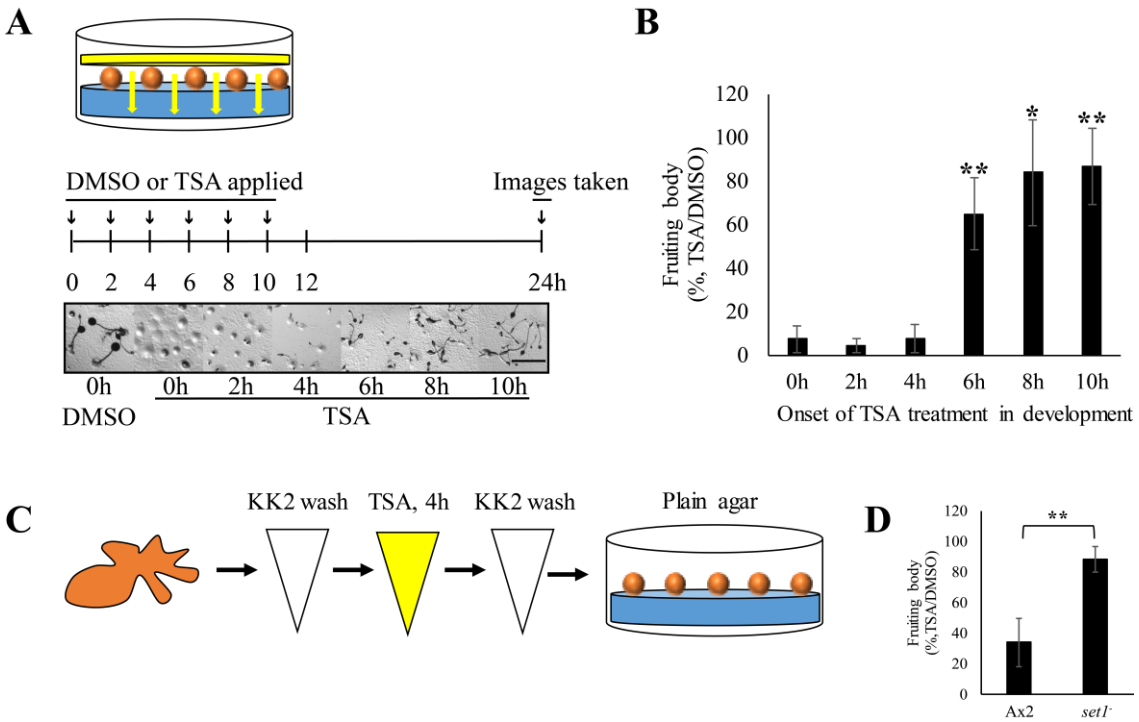

Figure 3.6 TSA-induced developmental inhibition is dependent on the early exposure of cells to TSA onset of development.

(A.) Schematic illustration of the development assay used. Cells (orange) were applied on 1.5 % agar (blue, 2.8 × 10^6 cells/well) and TSA (yellow, final concentration: 4 µM) was added on top of cells after 0, 2, 4, 6, 8 or 10 hours of development. Images were taken after 24 hours of development. **(B.)** Upper panel, representative images of cells after 24 hours of development. Lower panel, percentage of fruiting bodies (TSA/DMSO) after 24 hours of development. Data from three biological repeats was presented as mean ± SD. Statistical significance was obtained using T-Test by comparing samples to 0h (*, $p < 0.05$; **, $p < 0.01$). Scale bar represents 1 mm. **(C.)** Schematic illustration of the development assay used. Cells (orange) were washed by KK2, treated with 4 µM TSA (yellow) or DMSO in shaking suspension in KK2 for 4 hours (2 – 6 × 10^6 cells/ml) and then washed again with KK2 before allowed to develop on plain agar (blue, 2.8 × 10^6 cells/well). **(D.)** Percentage of fruiting bodies (TSA/DMSO) after 24 (4 + 20) hours of development. Data from three biological repeats was presented as mean ± SD. Statistical significance was obtained using T-Test by comparing *set1*$^-$ sample to Ax2 cells to 0h (**, $p < 0.01$).

3.3.6 Change in histone modification of *set1*$^-$ cells in response to TSA in early development

In mammalian cells it is known that TSA induces histone hyperacetylation and rapid dynamic acetylation of K4-trimethylated histone H3 happens predominantly on K9 and K14 on histone H3 (Crump et al, 2011). This dynamic acetylation of trimethylated histone has also been shown in exponentially growing Ax2 cells (Hsu et al., 2012). The loss of methylation on lysine 4 of histone H3 in *set1*$^-$ cells is predicted to lead to loss of dynamic acetylation and change in molecular response to TSA. To understand if the kinetics of histone H3 acetylation of *set1*$^-$ cells differs from Ax2 cells during the first four hours of development, exponentially growing cells were developed in the presence or absence of 4 μM TSA in KK2 for 0, 1, 2 or 4 hours. Acid extraction was performed at each timepoint to enrich for histones. Changes in H3K9ac, H3bK14ac and H3K4me3 across 4 hours of TSA treatment were detected by western blot and antibodies specific to H3K9ac, H3bK14ac and H3K4me3 (Figure 3.7).

Ax2 cells accumulated H3K9ac on both H3a and H3b in response to TSA present during the first four hours of development. H3bK14ac levels also increased. Both H3K9ac and H3bK14ac modifications start to increase after the first hour of development in the presence of TSA and by 4 hours, reach a significant 2.3 fold ($p < 0.01$) and 5.6 fold ($p <$

0.01) induction, respectively (Fig. 3.7). Accumulation of acetylation on H3K9 happens majorly on H3b as previously reported in our laboratory (Hsu et al., 2012). In contrast to rapid accumulation of H3K9ac and H3bK14ac in Ax2 cells, *set1*$^{-}$ cells failed to accumulate H3K9ac and H3bK14ac upon TSA treatment during the first four hours of development. The level of both types of acetylation signal remained unchanged across the course of 4 hours development and TSA treatment apart from a slight increase on H3aK9ac after 4 hours although the level remains much lower than on H3b. The H3K4me3 level does not change significantly in Ax2 cells. There was no H3K4me3 detectable in *set1*$^{-}$ cells as expected (Fig. 3.7).

The result confirmed that *set1*$^{-}$ cells have lost the ability to increase acetylation on H3K9 and H3bK14 within 4 hours of development in the presence of TSA. However, whether this is a consequence of loss of methylation on lysine 4 of histone H3 is still unclear.

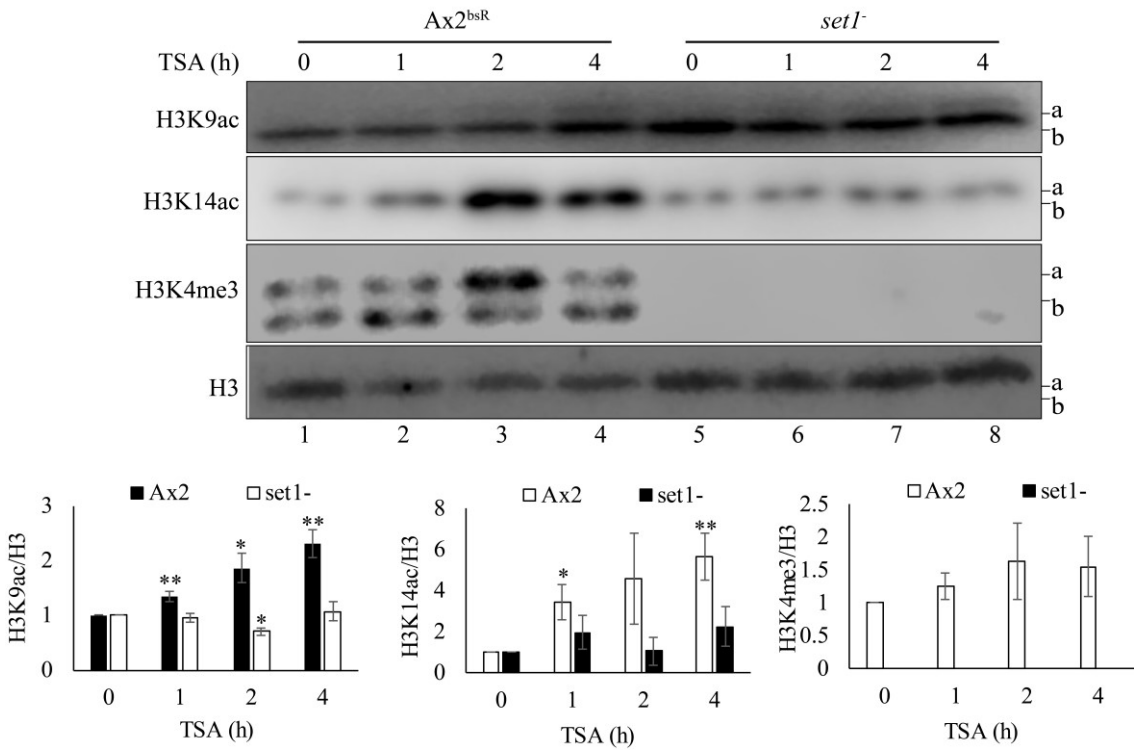

Figure 3.7 *set1*⁻ cells failed to accumulate H3K9ac and H3K14ac upon TSA treatment.

Histone-enriched acid extracts from TSA (4 μM) treated developing Ax2 and *set1*⁻ cells were prepared after 0, 1, 2 or 4 hours. Samples were resolved by 18% SDS-PAGE electrophoresis and western blots were performed using anti-H3K9ac, anti-H3bK14ac, anti-H3K4me3 and anti-H3 polyclonal antibodies. Position of histone H3a and H3b are shown on the right of each blot. Western blot results from three biological repeats were quantified using Image Studio Lite. Data of each timepoints was normalized to the level of total H3. The starting signal (0h) is denoted as 1. Data is presented as mean ± SD. Statistical significance was obtained using T-Test by comparing samples to 0h timepoint (*, $p < 0.05$; **, $p < 0.01$).

3.3.7 Change in histone modification of H3bK4A cells in response to TSA in early development

To determine if the loss of accumulation on histone H3bK9 and H3bK14 acetylation in developing *set1*$^{-}$ cells in the presence of TSA is due to loss of methylation on histone H3 or some other effect of *set1* loss, H3bK4A cells were treated with 4 μM TSA in KK2 for 0, 1, 2 or 4 hours and acid extraction was performed at each timepoint to collect samples enriched for histones. Changes in H3K9ac, H3bK14ac and H3K4me3 across 4 hours of TSA treatment was detected by western blot using antibodies specific to H3K9ac, H3bK14ac and H3K4me3 (Figure 3.8).

H3aK4K cells started to accumulate H3K9ac after 1h of development in the presence of TSA treatment (3.2 fold, $p < 0.05$), and reached 3.6 fold at 4h. In contrast, H3bK4A cells lost accumulation of H3K9ac on H3b. However, on H3a there was an increase of H3K9ac signal at the 4h timepoint as previously found in *set1*$^{-}$ cells (Fig. 3.7 and 3.8). In both H3aK4K and H3bK4A cells, a similar pattern of H3bK14ac accumulation during development in the presence of TSA was observed. However, the overall signal was markedly weaker in H3bK4A cells compared to H3aK4K cells, so although the fold increase in acetylation is similar, the total amount remains very low. There is no significant change in H3K4me3 levels in H3aK4K or H3bK4A cells, although the level

of H3K4me3 in the latter seemed elevated at 2 and 4 hours timepoints (Fig. 3.8).

The data revealed that loss of modification on H3bK4 resulted in loss of rapid induction of H3bK9ac in the presence of TSA during the first four hours of development. The basal level of H3bK14ac was reduced in H3bK4A cells but its induction by development and TSA remained. In *Dictyostelium*, the only known modification on H3K4 is methylation (Stevense et al., 2011). This suggests that methylation of H3K4 is necessary for developmental TSA-induced accumulation of H3bK9ac and the link between H3K4 methylation and H3 acetylation plays an important role in the mode of action of TSA.

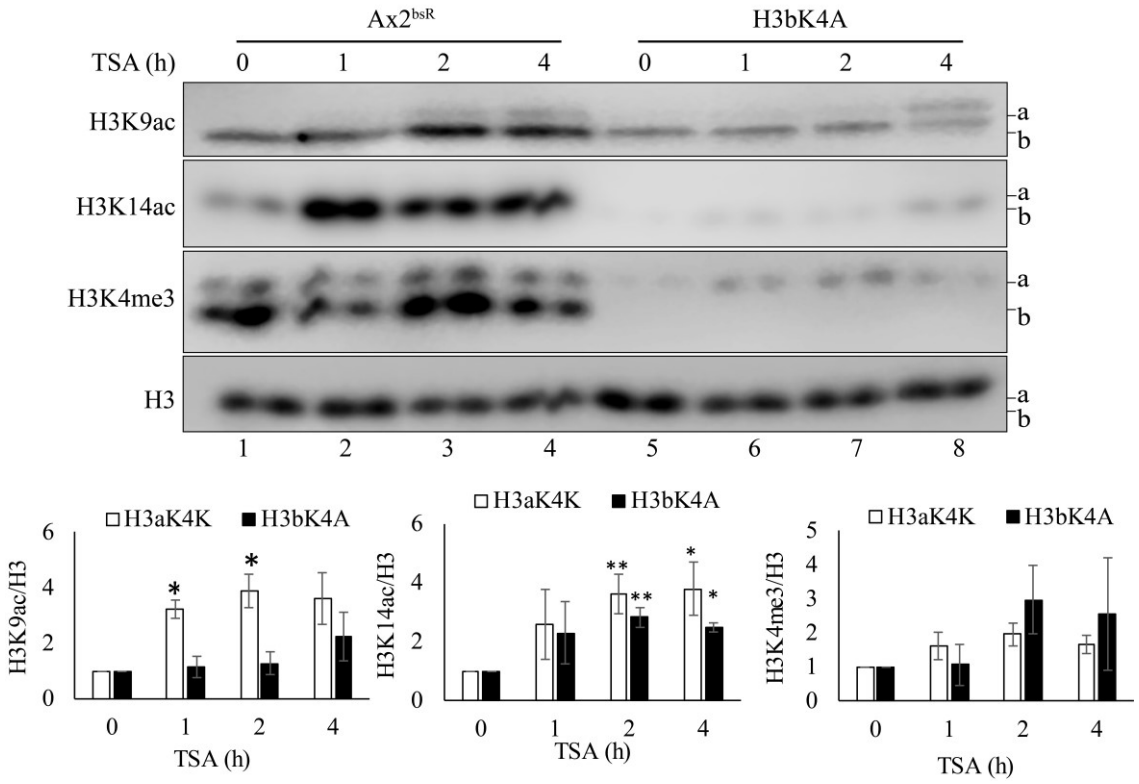

Figure 3.8 H3bK4A cells failed to accumulate H3bK9ac upon TSA treatment.
Histone-enriched acid extracts from TSA (4 μM) treated developing H3aK4K and H3bK4A cells were prepared after 0, 1, 2 or 4 hours. Samples were resolved by 18% SDS-PAGE electrophoresis and western blots were performed using anti-H3K9ac, anti-H3bK14ac, anti-H3K4me3 and anti-H3 polyclonal antibodies. Position of histone H3a and H3b are shown on the right of each blot. Western blot results from three biological repeats were quantified using Image Studio Lite. Data of each timepoints was normalized to the level of total H3. The starting signal (0h) is denoted as 1. Data is presented as mean ± SD. Statistical significance was obtained using T-Test by comparing samples to 0h timepoint (*, $p < 0.05$; **, $p < 0.01$).

3.3.8 An attempt to generate *gcn5*- cells

It is determined that methylation of H3bK4 is important for TSA-induced rapid accumulation of acetylation on H3bK9 and H3bK14 as well as developmental inhibition in *Dictyostelium*. The results provide direct evidence that methylation of H3K4 plays a role in the mode of action of TSA. However, to further support the hypothesis that dynamic acetylation is involved in the mode of action of TSA, it is necessary to determine the role of the rapid accumulated acetylation on H3K9 and H3K14 upon TSA treatment.

Acetylation of H3K9 is predominantly carried out by GNAT acetyltransferases (Berndsen and nu, 2008). Upon deletion of two redundant GNATs, namely GCN5 and PCAF, H3K9ac signal was not detectable in mouse embryonic fibroblasts by western blot (Jin et al., 2011). In addition, Gcn5 has been found to acetylate both H3K9 and H3K14 *in vitro* and *in vivo* (Bonnet et al., 2014; Cieniewicz et al., 2014; Kuo and Andrews, 2013). Moreover, Gcn5 is well conserved across multiple species and forms a HAT module with other protein subunits. The module is able to recognize H3K4me2/3 histones via a Tudor domain in one of the subunits, Sgf29, and deposit acetyl group on different lysine residues with varying specificity *in vitro* (Bian et al., 2011; Riss et al., 2015). To understand if Gcn5 is responsible for the rapid accumulation of H3K9ac and H3K14ac upon TSA treatment in *Dictyostelium*, I attempted to create a *gcn5* null strain utilizing

homologous recombination.

A potential Gcn5 homologue (DDB_G0283459) in *Dictyostelium* has been reported (Ludwig et al., 2006). To ensure the predicted protein shares the sequence homology in important domains with Gcn5 from other species, protein sequence alignment was performed using protein sequences of Gcn5 from *Dictyostelium discoideum*, *Homo sapiens*, *Saccharomyces cerevisiae* and *Schizosaccharomyces pombe* (Fig. 3.9A). The Gcn5 homologue in *Dictyostelium* contains an acetyltransferase and a bromodomain as found in the other three species. The catalytic domain shares more than 50% identity while the bromodomain shares more than 40% sequence identity with the other three species.

To replace the endogenous *gcn5* gene with a blasticidin resistance cassette (bsR), two genomic DNA (gDNA) fragments flanking the endogenous *gcn5* coding sequence were amplified using PCR and cloned into the pJET1.2 vector sequentially. Next, the bsR cassette flanked by loxP sites was inserted between the two fragments at an Eco53KI site (Fig. 3.9B and C). The final construct was then linearized by SwaI and BspHI, which generated a ~3kb fragment containing the bsR cassette flanked by two homology arms (Fig. 3.9C). The digested product was purified and used for subsequent transfection of

Ax2 cells. Transfected cells were resuspended in serial dilutions in HL5 and selected against blasticidin in 96-well plates until colonies formed. To identify successful replacement of the *gcn5* gene with bsR, colonies were screened via PCR using three sets of primers. Two sets of primers (Fig. 3.9B, P1 & P2; P3 & P4) were used to identify the insertion of both 5' and 3' arms at the correct sites, while a third primer set (P1 & P4) was used to confirm complete removal of endogenous *gcn5* gene sequences (Fig. 3.9B and D). In the event of complete replacement of the endogenous *gcn5*, it is expected to have a 5' amplicon of 1135 bp and a 3' amplicon of 979 bp and a single band at 3543 bp from the third primer set. If the parental *gcn5* is still is present, the size of the third PCR product will be 3727 bp. In some cases, insertion of only one arm was found (e.g. clone 2C9, Fig. 3.9D). After screening 100 colonies, a single colony 3F10 was found to have the correct PCR product for recombination events at both sides of the gene and the full length desired insertion but with parental signal contamination, which could either come from the well not being clonal or the result of a gene duplication and insertion at one copy. However, the signal persisted even after clonal isolation on bacterial lawn, which was consistent with the second interpretation. The same situation of parental gene contamination was found in subsequently identified clones harbouring the desired insertion (data not shown).

The attempt to generate *gcn5* null cells was unsuccessful. Deletion of *gcn5* or mutation of its catalytic domain has been found to be lethal in mice (Bu et al., 2007; Xu et al., 2000; Yamauchi et al., 2000). It is possible that complete deletion of *gcn5* is also lethal in *Dictyostelium*. Therefore, an alternative way to study the role of *gcn5* in the mode of action of TSA is needed.

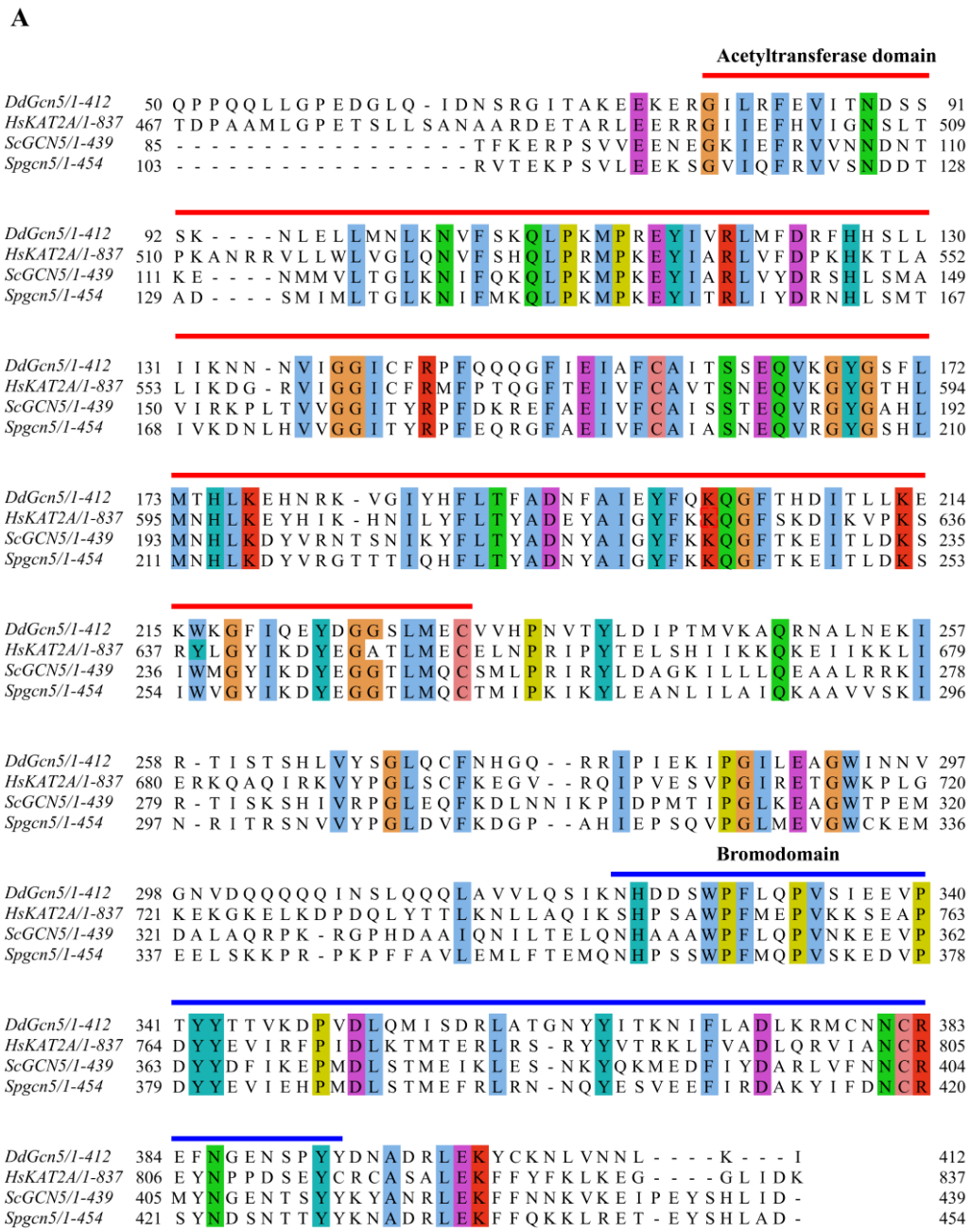

Figure 3.9. PCR screening of potential *gcn5*$^{-}$ clones

(A.) Protein sequence alignment of Gcn5 from *Dictyostelium discoideum*, *Homo sapiens*, *Saccharomyces cerevisiae* and *Schizosaccharomyces pombe*. Full length protein sequence of each protein is aligned using T-Coffee (https://www.ebi.ac.uk/Tools/msa/tcoffee/) and visualized by Jalview (https://www.jalview.org/). Acetyltransferase domain (marked by red line) and Bromodomain (marked by blue line) are shown.

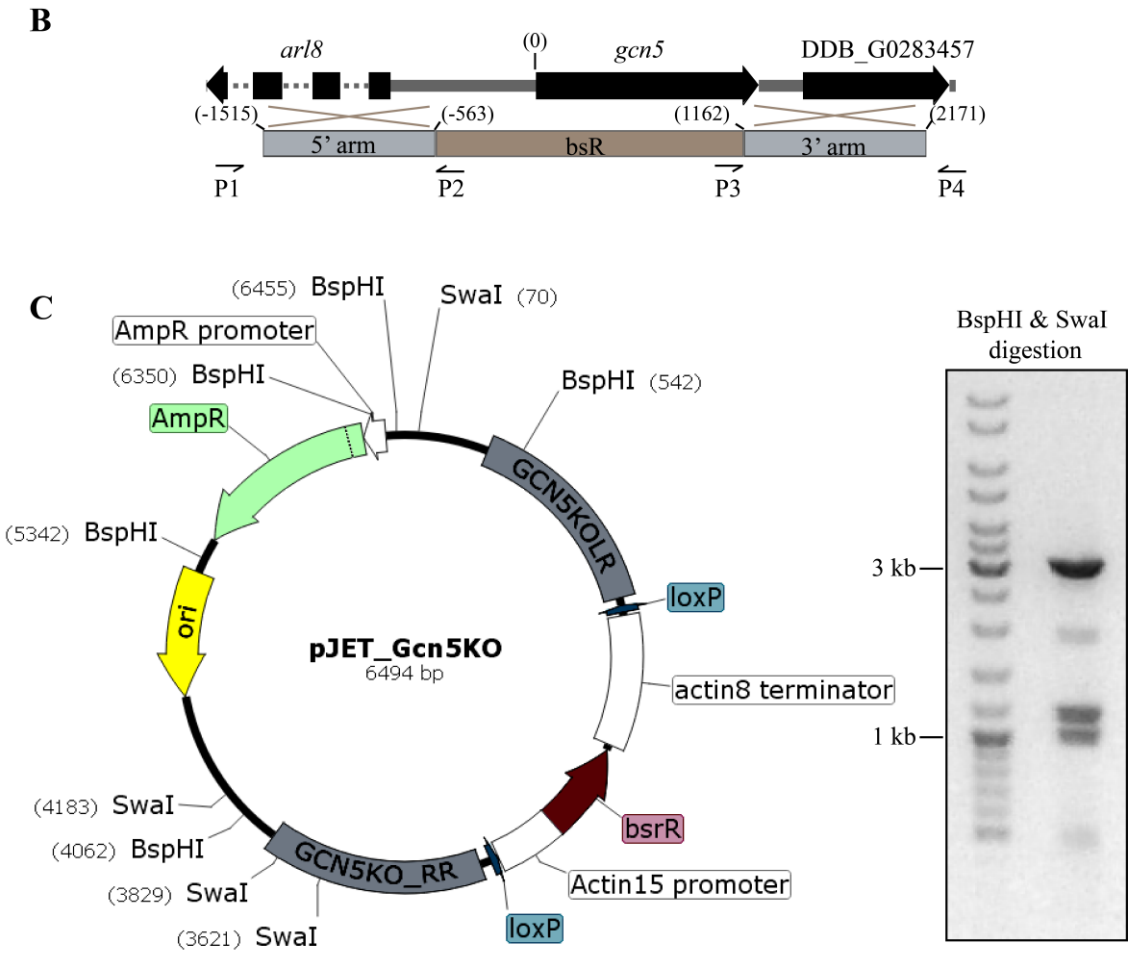

Figure 3.9 continued. PCR screening of potential *gcn5*$^{-}$ clones

(B.) Schematic representation of the homologous recombination event. A 953 bp fragment from -1515 to -563 upstream the *gcn5* coding sequence was cloned as 5' arm for gene replacement while 3' arm was from 1162 to 2171 downstream of start codon. **(C.)** DNA map of the Gcn5 disruption vector (left panel) and its linearized product by SwaI and BspHI (right panel). AmpR, β-lactamase. Ori, high-copy-number ColE1/pMB1/pBR322/pUC origin of replication. loxP, recognition site of Cre enzyme for Cre-lox recombination.

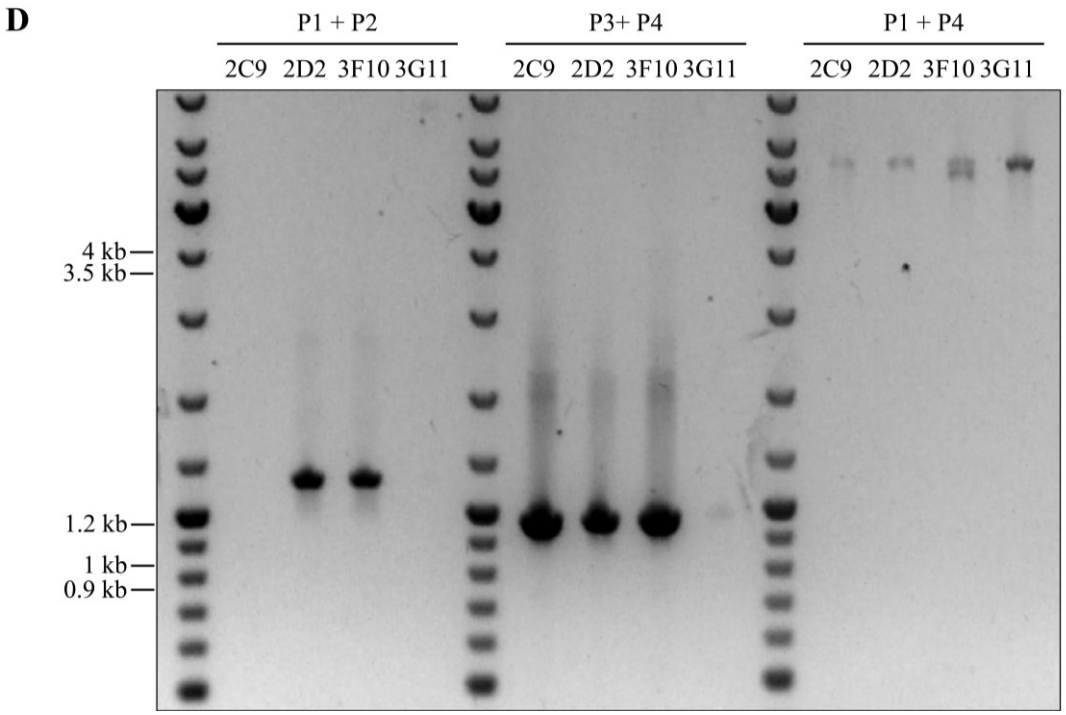

Figure 3.9 continued. PCR screening of potential *gcn5*$^{-}$ clones

(D.) gDNA was prepared from each colony and used in a diagnostic PCR screen to confirm integration of the bsR cassette at the *gcn5* locus. Two primer sets (P1 & P2 and P3 & P4) were used to check for targeted insertion of the bsR cassette at the 5' and 3' ends, respectively. PCR using P1 & P2 gives a band at 1135 bp while P3 & P4 gives a band at 979 bp if the desired recombination event has happened, but no band for random insertion of the cassette. A third primer set (P1 & P4) was used to confirm a change in overall fragment size of the *gcn5* gene region and detect parental contamination. Targeted insertion of both arms would produce a 3543 bp while a 3727 bp is expected from parental cells. Clone 3F10 has the correct insertion of both arms but parental *gcn5* is still present.

3.3.9 Genotyping of *gcn5⊿bromo* cells

It has been reported that the bromodomain of Gcn5 contributes to recruitment of the SAGA complex to chromatin and is important for substrate specificity, but it is dispensable for the catalytic function of Gcn5 (Barbaric et al., 2003; Candau et al., 1997; Cieniewicz et al., 2014; Hassan et al., 2002; Li and Shogren-Knaak, 2009; Sterner and Berger, 2000; Syntichaki et al., 2000). Mutation of an acetyl-lysine-binding residue in bromodomain has been reported to reduce acetylation of H3K9 (Cieniewicz et al., 2014). Given the above findings, deletion of Gcn5 bromodomain in *Dictyostelium* would be predicted to interfere with the proper function of Gcn5, providing a chance to understand the role of Gcn5 in the mode of action of TSA. One bromodomain mutant of Gcn5 (*gcn5⊿bromo)* in Ax4 background was kindly provided by Professor Chris Thompson in UCL, generated by restriction enzyme mediated integration (REMI) as part of the GWDI library (see Chapter 5).

The mutant was created by insertion of a bsR cassette at a DpnII site within the coding sequence of the bromodomain of Gcn5 (Fig. 3.10A). PCR verification of gDNA confirmed the insertion of the bsR cassette at the start of bromodomain sequence, causing an increase in product size of the predicted amount. There was no sign of parental contamination (Fig. 3.10B, lane 3 & 7). To understand if transcription of the

acetyltransferase domain and bromodomain was abolished by this insertion towards the 3' end of the gene, downstream of the acetyltransferase domain, RT-PCR was carried out. The expression of acetyltransferase domain remained unaffected (Fig. 3.10B, lane 11 & 16) but expression of bromodomain was greatly reduced (lane 12 & 17). The weak signal of bromodomain transcript in *gcn5⊿bromo* cells may be explained by mRNA readthrough from bsR cassette or part of 3' end of bsR cassette acts as a promoter (Fig. 3.10B, lane 17). To gain more insight into the expressional difference of acetyltransferase domain and bromodomain between parental and *gcn5⊿bromo* cells, RT-PCR was performed removing samples after different number of thermo cycles to prevent signal saturation (Fig. 3.10C). The result confirmed that the transcriptional level of acetyltransferase domain was comparable between parentalAx4bsR and *gcn5⊿bromo* cells while parental cells gave bromodomain signal five cycles earlier than *gcn5⊿bromo* cells.

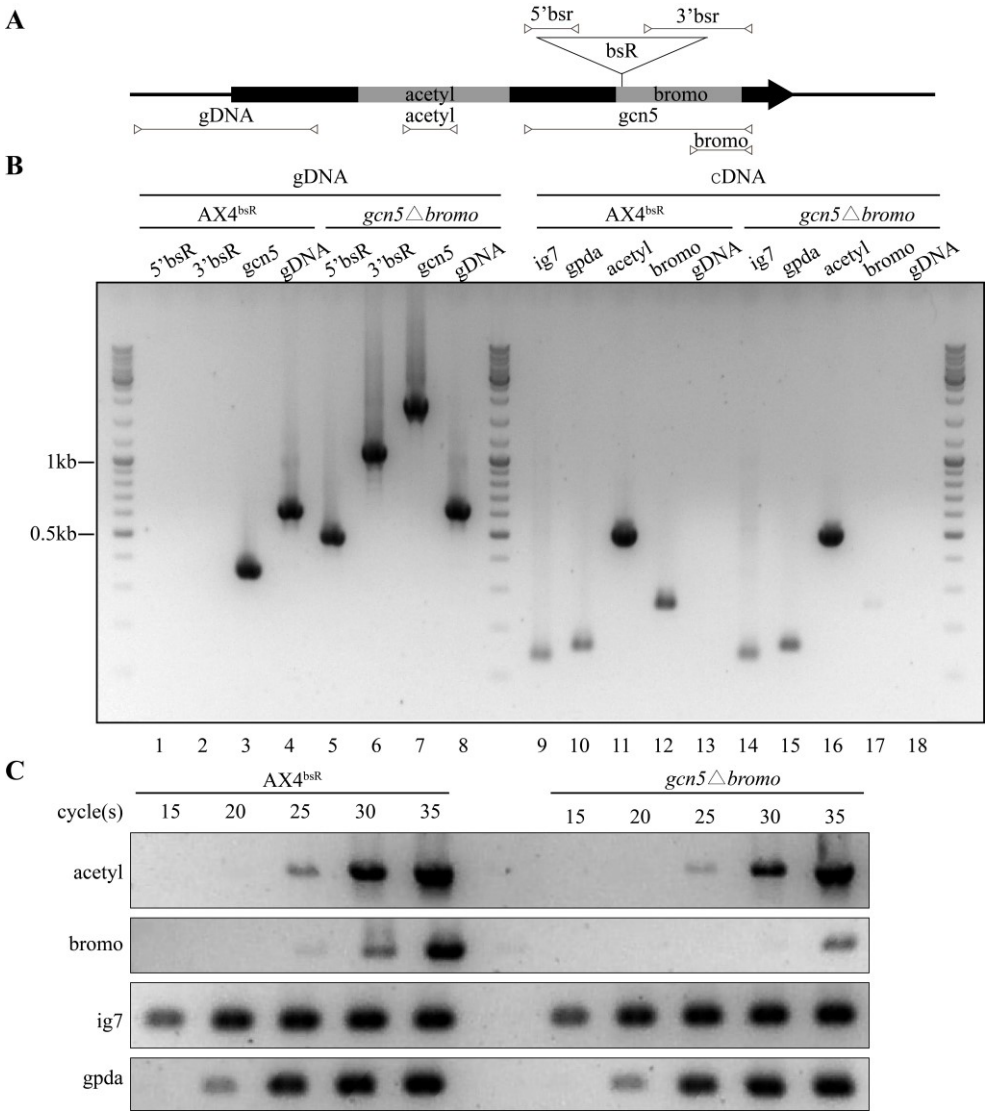

Figure 3.10. Genotyping of *gcn5⊿bromo* cells

(A.) Schematic representation of the insertion site of bsR cassette in the beginning of bromodomain. Primer sets were designed to detect bsR insertion (5'bsR & 3'bsR). A primer set amplifying the 3' region of *gcn5* is used to detect parental contamination. Primers to detect expression of acetyltransferase domain (acetyl) and bromodomain (bromo) were also used. Finally, gDNA contamination in cDNA is ruled out by the sixth primer set which amplifies the promoter region (gDNA). **(B.)** gDNA and cDNA were prepared from Ax4^{bsR} and *gcn5⊿bromo* cells. PCR was carried out using primer sets mentioned above. Insertion of bsR cassette in the beginning of bromodomain is confirmed without any residue parental signal, with a band at 1956 bp while the parental is at 367 bp. Expression of *ig7* and *gpda* serve as internal control for cDNA levels. **(C.)** cDNA was prepared from Ax4^{bsR} and *gcn5⊿bromo* cells. Expression of acetyltransferase domain and bromodomain were monitored at different number of thermocycles.

3.3.10 Histone H3 acetylation and developmental response of *gcn5⊿bromo* cells upon TSA treatment

The previous results revealed that expression of *gcn5* bromodomain in *gcn5⊿bromo* cells was markedly reduced. To understand if *gcn5⊿bromo* cells are able to rapidly accumulate histone acetylation in response to TSA, developing cells were treated with DMSO or TSA for 1 hour in shaking suspension and acid extraction was performed. Changes in H3K9ac and H3bK14ac levels were detected using western blot.

The result shows marked reduction of basal H3K9ac and H3bK14ac signals in *gcn5⊿bromo* cells compared to parental cells (Fig. 3.11A, lane 1-3 and 4-6). However, *gcn5⊿bromo* cells still accumulate acetylation on H3K9 and K14 after 1 hour of TSA treatment, though not to the same level as found in parental cells (Fig. 3.11A, lane 4-6 and 10-12).

Loss of bromodomain of *gcn5* resulted in reduced levels of H3K9ac and H3K14ac prior to and after 1 hours of TSA treatment. To investigate whether *gcn5⊿bromo* cells are resistant to TSA during development, cells were exposed to constant DMSO or different concentrations of TSA during development and images were taken at after 22 and 30 hours of development.

The development of *gcn5⊿bromo* cells was severely delayed (Fig. 3.11B). While parental cells finished development after 22 hours, *gcn5⊿bromo* cells were still at the aggregate stage. Even after 30 hours of development under normal conditions, *gcn5⊿bromo* cells failed to show visible terminal fruiting body structures. Interestingly, TSA did not further inhibit the development of *gcn5⊿bromo* cells. In contrast, the developmental defect was partially rescued by TSA (Fig. 3.11B). At 4 μM TSA, *gcn5⊿bromo* cells were able to form some fruiting bodies after 30 hours of development.

Previous results in *set1*$^{-}$ and H3bK4A cells revealed a connection between loss of methylation on H3K4 and inability to accumulate H3K9ac upon TSA treatment, and both types of cells were resistant to TSA-induced developmental inhibition. Here, the development result together with western blot data (Fig. 3.10) suggested that bromodomain of Gcn5 is required for maintaining acetylation levels and for development past the mound stage. Furthermore, *gcn5⊿bromo* cells are desensitized to TSA-induced developmental inhibition, suggesting proper function of Gcn5 is required in the mode of action of TSA. However, the fact that *gcn5⊿bromo* cells accumulate H3K9ac upon TSA treatment strongly suggests that the bromodomain of Gcn5 is not involved in the crosstalk between methylation of H3K4 and H3K9 acetylation.

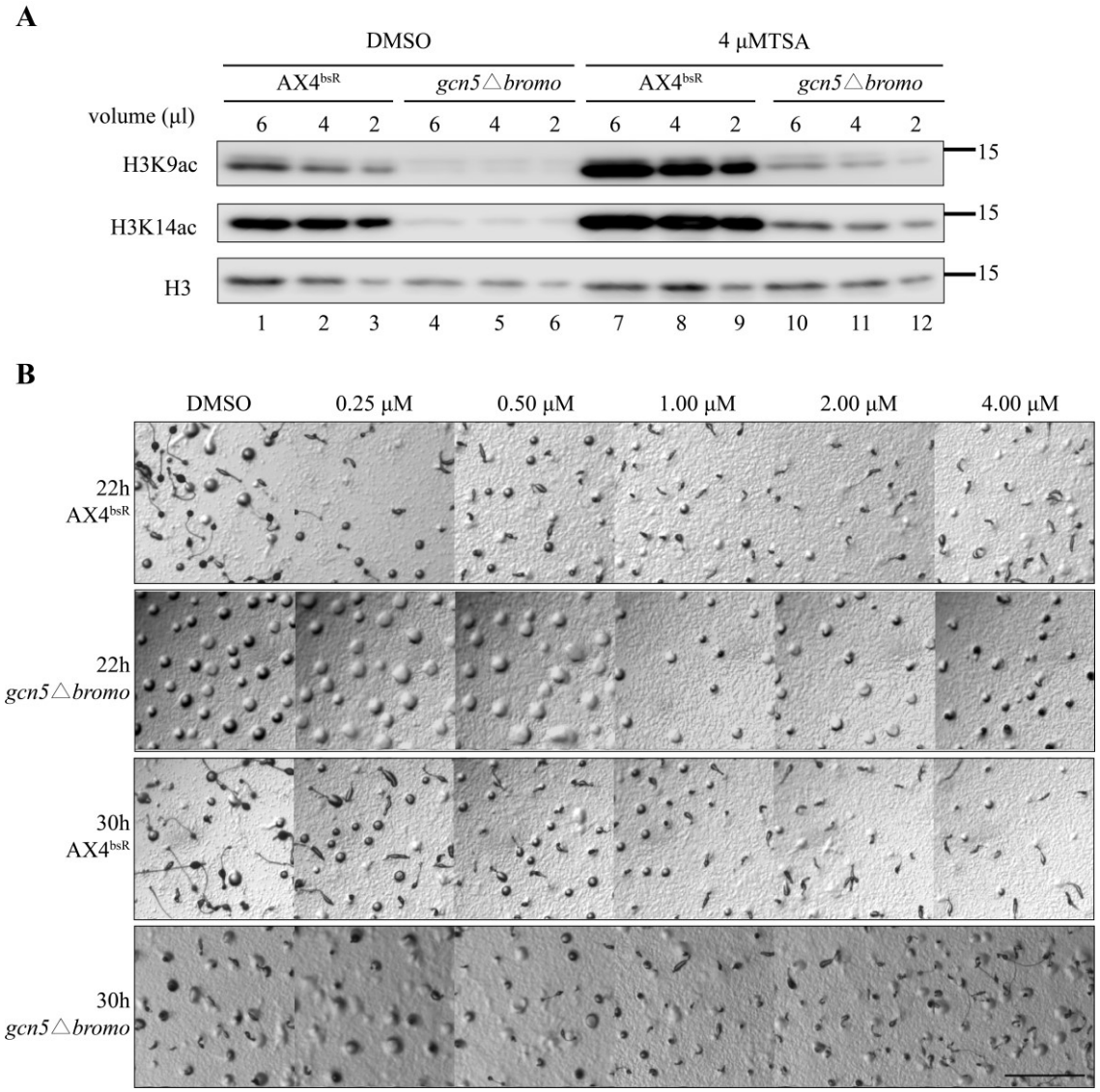

Figure 3.11. *gcn5⊿bromo* cells have reduced levels of H3 acetylation and delayed development but are not sensitive to TSA during development.

(A.) Representative western blot image of histone extracts from TSA (4 μM) treated developing Ax4bsR and *gcn5⊿bromo* cells. Histone-enriched acid extracts were prepared after 1 hour of TSA treatment. Different volumes of samples were resolved by 18% SDS-PAGE electrophoresis and western blots were performed using anti-H3K9ac, anti-H3bK14ac, and anti-H3 polyclonal antibodies. **(B.)** Cells were developed at a density of 2.8×10^6 cells/well on 1.5 % agar containing increasing concentration of TSA up to 4 μM. Images were taken after 22 and 30 hours of development. Scale bar represents 1 mm.

3.4 Discussion

In this chapter I provide evidence that the link between H3K4 methylation and dynamic histone acetylation is important for the mode of action of TSA in *Dictyostelium*.

I have shown that

- The KDACi TSA inhibits both growth and development of *Dictyostelium*. TSA exerts its effect on development during the first four hours.
- Cells lacking Set1 are more sensitive than parental cells to the presence of TSA during growth but resistant during development
- Cells with altered methylation of H3K4 are resistant to TSA to different extent, supporting H3K4 being the relevant target of Set1 for TSA affects.
- These cells also show reduced acetylation of H3K9 when cells are developed for four hours in the presence of TSA, similar to previous results reported for growing cells (Hsu et al 2012).
- Overall this suggests that the dynamic acetylation of H3K4 plays an important role in TSA-induced developmental inhibition.
- Cells with reduced expression of the bromo domain of Gcn5 show reduced overall levels of acetylation but still show increases in the presence of TSA. These cells show a developmental phenotype which is slightly improved by the presence of TSA.

In this chapter we examined the effect of different KDACis on the development and growth of *Dictyostelium* and focus on the mechanism of action of TSA. TSA causes adverse effects on development and growth (Fig. 3.1) as previously reported for TSA (Sawarkar et al., 2009). SAHA shows a similar effect on both growth and development, although the concentrations required are much higher. VPA has also been reported to have KDACi activity and also inhibits both growth and development as previously reported (Tilner et al., 1996). However, VPA is known to have many other targets and in *Dictyostelium* prolonged VPA treatment is known to attenuate inositol signaling (Williams et al., 2002; Eickholt et al., 2005). This may be a direct effect, rather than indirectly the result in changes in gene expression due to altered histone acetylation, as the acute effect of VPA on chemotaxis has been also shown to be predominantly via changes in inositol metabolism (Xu et al., 2007). Even so, the *set1*$^{-}$ and H3K4A strains showed some resistance to developmental inhibition by VPA. Further work is necessary to determine whether it is also acting as a KDACi in *Dictyostelium* development.

Interestingly, exposure of cells to TSA onset of the first four hours of development is necessary for TSA-induced developmental inhibition (Fig. 3.6). In addition, dose-response to TSA reveals that at low concentrations the formation of slugs is delayed while at high concentration cells are stalled at mound stage prior to slug stage. Of note, high

concentrations of KDACis inhibit the development at the tight mound (Fig. 3.4). It is known that cell sorting of prestalk and prespore cells happens at the mound stage before slug formation. The sorting results in a tipped mound with prestalk cells on the tip (reviewed in Strmecki et al., 2005). There are at least two possible mechanisms that KDACis could interfere with to generate the developmental phenotype. One is through interfering with cell fate decisions, which could involve expression of prestalk or prespore markers. Another one is to reduce the expression of developmental genes expressed in all cells. It has been shown that low concentrations of TSA delay the expression of genes such as *csaA*, which encodes an adhesion molecule needed for development as well as genes expressed later in development, though not inhibiting expression of early developmental genes such as *carA* and *acaA* (Ponte et al., 1998; Sawarkar et al., 2009). Taken together, TSA may alter the expression of important genes whose proper regulation at early developmental stages is required for subsequent developmental events, though what those genes are remains an interesting and open question.

It is interesting that the *set1*$^{-}$ and H3K4A cell lines investigated here show sensitivity to TSA during growth and resistance during development, which suggests that methylation of H3K4 have opposite roles in vegetative and developing cells in response to TSA.

Although the mechanism(s) is not known, this could have important implications for the use of KDACi in cancer therapy. KDACis can block tumour cell growth by distinct mechanism such as differentiation of tumour cells or through induction of apoptosis. These results suggest that mechanisms of resistance may be distinct for different phenotypes.

Developing Ax2 cells in the presence of TSA for 4 hours leads to an increase in the level of H3K9Ac and K14Ac. It is not possible to distinguish whether it is TSA or development which is causing this increase, or both. However, in Figure 3.11A Ax4bsr control cells developed in the presence of TSA for 1 hour showed an increase in acetylation relative to those developed in the absence of TSA, suggesting that TSA at least contributes to this increase.

Cells lacking *mono*-, *di*- and *tri*- methylation on H3K4 of both H3a/b variants due to loss of Set1 not only are resistant to TSA during development but also show no accumulation of H3bK9ac and H3bK14ac (Fig. 3.4 and 3.7) when developed in the presence of TSA. Supporting the hypothesis that the important target of Set1 is histone H3, cells without H3bK4me3 due to mutation of lysine 4 to alanine on H3a or b showed developmental resistance to TSA, though the cells require 48 hours to finish development under TSA

not 24 hours as found in *set1*$^{-}$ cells (Fig. 3.5). One interesting observation is that loss of methylation of H3b completely abolishes H3bK9ac accumulation in the first four hours of TSA treatment during development but in the meantime only reduces the overall level of H3K14ac but its accumulation is unaffected (Fig. 3.8). One possible explanation is that acetylation of H3bK9 and H3bK14ac are carried out by two different enzymes, and methylation on H3bK4 are required for the former while the modification improves acetylation of H3K14 by the latter but is not necessary for the reaction. The second possibility is that one enzyme acetylates both H3bK9 and H3bK14 with higher activity towards the latter and methylation on H3K4 facilitates its overall acetyltransferase activity. Several studies on Gcn5 in other systems support the second hypothesis. Gcn5 forms a HAT module together with Ada2, Ada3 and Sgf29. It acetylates multiple lysine residues including K9 and K14 on H3 with the highest specificity to K14, and overall acetylation of histone H3 by Gcn5 is enhanced in the presence of H3K4me3 *in vitro* (Cieniewicz et al., 2014; Kuo and Andrews, 2013; Ringel and Cieniewicz, 2015). Moreover, deletion of Sgf29, the subunit carrying a domain that recognizes H3K4me3, reduces overall acetylation on histone H3 in yeast (Bian et al., 2011). However, this does not explain why accumulation of H3bK14ac disappeared when Set1 is mutated, suggesting a more complicated mechanism (Fig. 3.7). A direct *in vitro* interaction of metazoan-specific HAT p300 with Set1 has been reported (Tang et al., 2013). Thus, the

possibility that Gcn5 or another acetyltransferase may interact with Set1 in *Dictyostelium* should be considered.

Speculating that Gcn5 may be involved in the mode of action of TSA, we tried to create a *gcn5* null strain, however we were unable to completely remove *gcn5* from the genome of *Dictyostelium* (Fig. 3.9). Deletion of *gcn5* has been reported in lower eukaryotes such as yeast, however deletion of *gcn5* in higher eukaryotes such as *Drosophila* resulted in a lethal phenotype in early development, and similar results was reported in mice embryos and worms (Bian et al., 2011; Ciurciu et al., 2006; *C. elegans* Consortium, 2012). Thus, deletion of *gcn5* in *Dictyostelium* may be lethal though more evidence is needed. Nevertheless, to investigate the function of Gcn5, an alternative approach other than complete disruption of *gcn5* was employed by using a *gcn5⊿bromo* strain which has a bsR cassette inserted upstream of the coding sequence of the bromodomain in *gcn5*. The strain exhibited greatly reduced basal levels of H3K9ac and H3K14ac, consistent with a previous *in vitro* study on yeast Gcn5 (Cieniewicz et al., 2014) and suggesting that Gcn5 is responsible for the majority of acetylation of H3K9 and H3K14 in *Dictyostelium* in cells developed for 1 hour. The level of both signals was elevated by TSA treatment but not to the level found in untreated parental cells (Fig. 3.11). In addition, developmental defects were observed in *gcn5⊿bromo* cells. Cellular development is tightly regulated

by activation of developmental genes and inactivation of growth-promoting genes (Loomis et al., 2015). In other organisms this process involves rapid changes of histone modification and Gcn5 has been reported to be involved in the regulation (Gao et al., 2017; Wang et al., 2018). In *Dictyostelium*, development is tightly regulated by a series of genes whose transcription is inactivated under normal growth condition. Upon depletion of surrounding nutrition, these genes are rapidly activated within 6 hours (Rosengarten et al., 2015). Thus, reduced levels of H3K9 and H3K14 acetylation may impair the activation of genes required for development, a process that can be partially rescued by TSA treatment. The developmental phenotype of the *gcn5⊿bromo* cells, make the effect of TSA difficult to interpret but the cells appear to be resistant.

In summary, we have identified a direct link between methylation of H3K4 and the effects of TSA, supporting one end of the hypothesis that dynamic acetylation is involved in the mode of action of TSA. Seeking to understand if rapid H3K9 and H3K14 acetylation by TSA, which is lost in strains with altered H3K4 methylation, is involved in the mode of action of TSA, we attempted to generate a *gcn5* null strain. However, we were unable to determine if Gcn5 is responsible for the rapid accumulation of both modifications. An alternative approach to investigate the function of *Gcn5* in the H3K4 methylation-associated events, is to manipulate the subunits that form HAT module together with *Gcn5*. The approach is investigated in Chapter 4.

4. Roles of a Tandem Tudor domain-containing protein in linking H3K4me3 and histone H3 acetylation in *Dictyostelium*

4.1 Introduction

4.1.1 Acetyltransferases implicated in acetylation of H3K4me3 histones

There is evidence for a number of acetyltransferase complexes playing a role in acetylation of H3K4me3. One targeting mechanism that has been proposed is that HAT complexes recognize methylated histones via binding domains in subunits of the complex.

4.1.1.1 HBO1 Complex

In the MYST family is the HBO1 acetyltransferase complex in humans, which consists of HBO1, ING4/5, EAF6, and JAD1/2/3 (Lee and Workman, 2007). Both ING4/5 and JAD1/2/3 in the HBO1 complex contain PHD domains that recognize K4-methylated histone H3. The PHD domain in ING4 binds specifically to methylated H3K4 peptides *in vitro* with strongest binding to the *tri*-methylated state and the binding facilitates acetylation of histone H3 by HBO1 (Hung et al., 2009). Moreover, it was shown that as well as ING4, PHD domains in ING5 and JAD1/2 also preferentially bind to K4-trimethylated H3 peptides (Saksouk et al., 2009). Similar results involving an ING4

homologue Yng1 in yeast NuA3 HAT complex have also been reported (Taverna et al., 2006).

4.1.1.2 p300/CBP

Unlike members of the GNAT and MYST families, p300/CBP itself contains a PHD domain (Xue et al., 2018). However, direct evidence for binding of p300/CBP to K4-methylated histone H3 via the PHD domain is lacking, though deletion of the PHD domain impairs the acetyltransferase activity (Rack et al., 2014). Despite this lack of evidence for direct interaction with H3K4me3 histones, the metazoan-specific p300/CBP was shown to be involved in dynamic acetylation of H3K4me3 upon TSA treatment in higher eukaryotes. Inhibition of enzyme activity through a p300/CBP-specific inhibitor results in loss of dynamic acetylation upon TSA treatment in fly and mouse cells (Crump et al., 2011) and RNAi-induced reduction in expression of CBP severely reduced TSA-induced hyperacetylation of H3K4me3 in *Drosophila* cells, whereas similar reduction in levels of other acetyltransferases including Gcn5 had no noticeable effect on the dynamic acetylation.

4.1.1.3 Gcn5 in the SAGA Complex

The SAGA (Spt-Ada-Gcn5-acetyltransferase) complex in the GNAT family consists of different modules with the catalytic activity carried out by the HAT module, which is formed by Gcn5, Ada2, Ada3 and Sgf29 (Lee et al., 2011). Among the subunits in this HAT module, Sgf29 was found to have a tandem Tudor domain. Sgf29 by itself preferentially binds to H3K4 *di*- and *tri*-methylated histone peptides *in vitro*. Deletion of yeast SGF29 reduces global acetylation levels of histone H3, including H3K9ac, H3K14ac and H3K18ac. The deletion also impairs the recruitment of SAGA complex to its substrate locus (Bian et al., 2011). At the nucleosome level, Sgf29 was found to be required for SAGA-mediated preferential acetylation of H3K4me3 nucleosomes *in vitro* (Ringel and Cieniewicz, 2015). This implicates the SAGA complex as the HAT involved in the rapid dynamic acetylation of H3K4me3, linked by Sgf29. However, rapid dynamic acetylation of H3K4me3 has not been reported in *S. cerevisiae* (Crump and Mahadevan personal communication) so this theory has not been directly tested.

My previous data suggests that the link between methylation of H3K4 and H3 acetylation is crucial for the mode of action of TSA (Chapter 3). If Gcn5 is the relevant HAT, the *Dictyostelium* orthologue of Sgf29 may be responsible for the link and is an important

target in understanding the action of TSA.

4.2 Aims

This chapter aims to identify the Sgf29 homologue in *Dictyostelium* and investigate if it is involved in linking histone H3 methylation on K4 to acetylation of K9 and K14 and the mode of action of TSA. The first aim is to search for Sgf29 homologue in *Dictyostelium* by sequence homology and determine if the predicted protein has a functional tandem Tudor domain. The second aim is to create *sgf29* null cells and use these to understand if Sgf29 is involved in rapid histone acetylation of H3K4me3 induced by TSA. The sensitivity of the developmental response to TSA of *sgf29* null cells and cells overexpressing Sgf29 is examined.

4.3 Results

4.3.1 Candidate Sgf29 homologue in *Dictyostelium*

It has been reported that protein sequences of Sgf29 from various species share low identity in the *N*-terminal region but have a relatively well-conserved tandem Tudor domain sequence at the C-terminus (Bian et al., 2011). To identify candidate genes encoding Sgf29 in *Dictyostelium* (*Dd*Sgf29), the protein sequence of the tandem Tudor domain from budding yeast, fission yeast and human were used in three independent

BLAST searches against the protein database in dictyBase (http://dictybase.org/). All three searches resulted in only one candidate protein of 411 amino acids encoded by the gene DDB_G0272054, whcih was found to have a tandem Tudor domain at the C-terminus of its protein sequence (Fig. 4.1B). In addition, protein sequence alignment showed conservation of three important binding residues (F359, Y366 and F387) in the tandem Tudor domain required for interaction with *tri*-methylated lysine in yeast (Bian et al., 2011), though in *Dictyostelium* the first aromatic residue is changed from tyrosine to phenylalanine. It has been shown that the tertiary structure of the tandem Tudor domain in different species is well conserved (Bian et al., 2011; Li et al., 2010). To verify if the tandem Tudor domain of the candidate *Dd*Sgf29 shares structural similarity with other species, a structure alignment was carried out using Chimera (https://www.cgl.ucsf.edu/chimera/). The result suggests that the tandem Tudor domain of *Dd*Sgf29 is structurally conserved with that of yeast and human (Fig. 4.1C). The bioinformatic analysis indicates the protein encoded by DDB_G0272054 may be the *Dictyostelium* Sgf29 homologue.

A

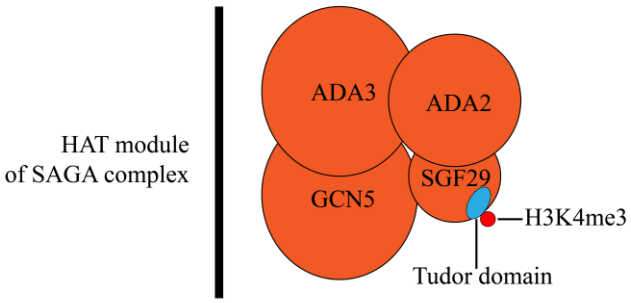

B

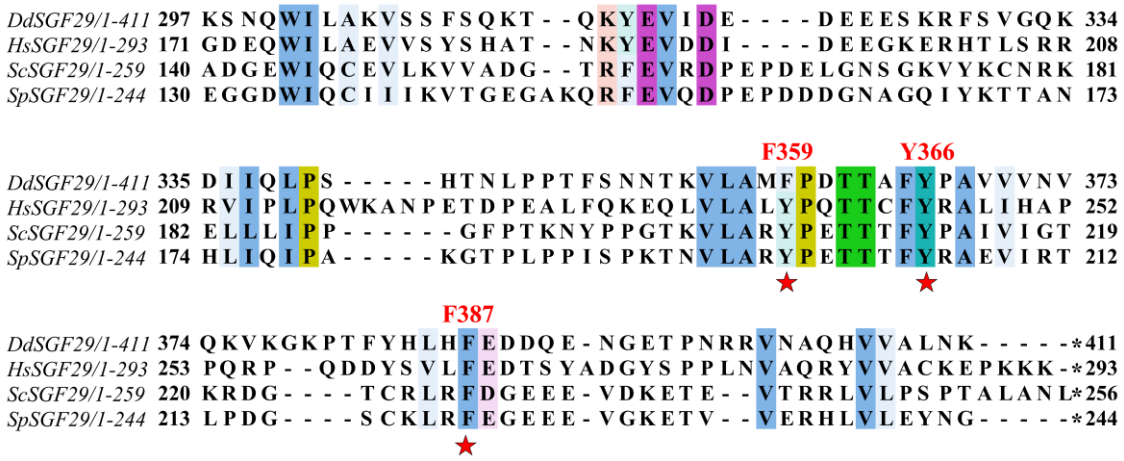

Figure 4.1 DDB_G0272054 encodes a protein with a structurally conserved tandem Tudor domain similar to Sgf29 in yeast and human.

(A.) Schematic illustration of the histone acetyltransferase (HAT) module consisting of Gcn5, Ada2, Ada3 and Sgf29. Sgf29 includes a tandem Tudor domain (blue) that recognizes K4-trimethylated H3 (red) *in vitro* (Bian et al., 2011). **(B.)** Protein sequence alignment of the tandem Tudor domains of Sgf29 from budding yeast, fission yeast and human together with the candidate Sgf29 homologue in *Dictyostelium* (*Dd*Sgf29) encoded by DDB_G0272054. Conserved binding residues targeting *tri*-methylated lysine are labeled with red asterisks and their positions relative to the first amino acid of *Dd*Sgf29 are shown. The stop codon is indicated by an asterisk. Protein sequences were obtained from NCBI (https://www.ncbi.nlm.nih.gov/) and aligned using T-Coffee (https://www.ebi.ac.uk/Tools/msa/tcoffee/). Visual representation was performed using Jalview (http://www.jalview.org/). Clustal X Colour Scheme is used to indicate the conservation of amino acid profile (http://www.jalview.org/help/html/colourSchemes/clustal.html) \

C

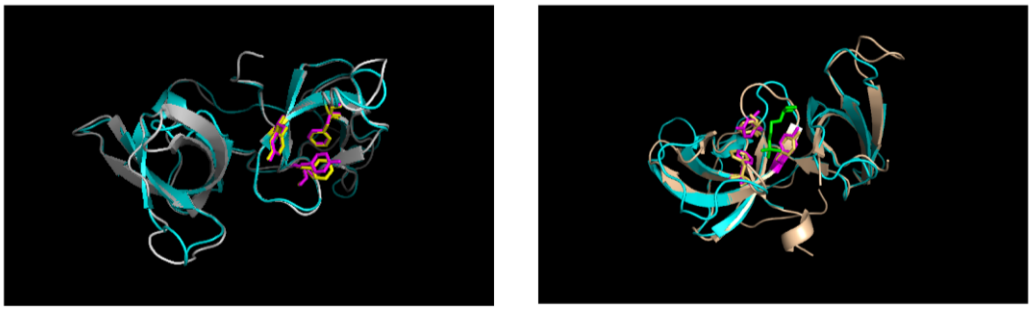

Tandem tudor domain
DdSgf29 V.S. HsSGF29

Tandem tudor domain
DdSgf29 V.S. ScSGF29

Figure 4.1 continued. DDB_G0272054 encodes a protein with a structurally conserved tandem Tudor domain similar to Sgf29 in yeast and human.
(C.) Predicted structure comparison of the tandem Tudor domain of *Dd*SGF29 with human Sgf29 (*Hs*SGF29) or budding yeast Sgf29 (*Sc*SGF29). The predicted tertiary structure of the tandem Tudor domain of *Dd*Sgf29 is shown by a blue ribbon while that of human or yeast is shown in grey. Conserved binding residues in *Dd*Sgf29 are shown by purple sticks. K4-trimethylated lysine is represented by a green stick. Structural prediction and comparison was done using Chimera (https://www.cgl.ucsf.edu/chimera/).

4.3.2 The tandem Tudor domain of Dd*Sgf29* binds H3K4me3 *in vitro*

A far-western blot strategy was designed to understand if the tandem Tudor domain of *Dd*Sgf29 binds to H3K4-trimethylated histones (Fig. 4.2B). The sequence encoding the tandem Tudor domain of *Dd*Sgf29 (S277 - K411) was amplified by PCR from cDNA and cloned in frame into the pGEXKG vector to allow expression of a GST-Tudor domain fusion protein in *E.coli.* To understand if the conserved binding residues are necessary for binding of tandem Tudor domain of *Dd*Sgf29 to K4-trimethylated histone H3, two point mutations were introduced by site directed mutagenesis targeting two conserved residues known to be important for binding methylated histone in yeast SGF29 (F359A

and Y366A) (Fig. 4.2B, upper panel). Both fusion proteins were expressed in *E. coli* and purified by binding and elution from glutathione sepharose (Fig. 4.2A). The amounts of purified wildtype and mutant fusion proteins were equalized (Fig. 4.2C) and then used to probe the blots of protein samples enriched for histones by acid extraction from *Dictyostelium* cells. The interaction between histone H3 and the GST-Tudor fusion protein was detected using α-GST antibody (Fig. 4.2B, lower panel).

The far-western blot shows that wildtype GST-Tudor protein interacts with a band of the predicted molecular weight of histone H3 from Ax2 and H3bK4A cells but not *set1*$^{-}$ or H3aK4A cells which lack the H3K4me3 modification (Fig 4.2D). In the contrast, mutated GST-Tudor protein failed to interact with histone H3 from Ax2 and H3bK4A cells. When GST protein alone was used in the assay, no signal was detected. Together this proves that the interaction seen with wildtype GST-Tudor protein was not due to interaction between GST and H3K4me3. Of note, the tandem Tudor domain by itself seemed to have higher affinity for H3bK4me3 than H3aK4me3 (Fig 4.2D, lane 1).

The result confirmed that the tandem Tudor domain of *Dd*Sgf29 binds to H3K4me3 *in vitro*. Also, the fact that the binding was only seen in histones isolated from Ax2 but not H3aK4A cells indicates that *in vitro* binding is H3K4me3 specific, because H3aK4A cells

still possess *mono*- and *di*- methylation on H3b (Hsu et al., 2012).

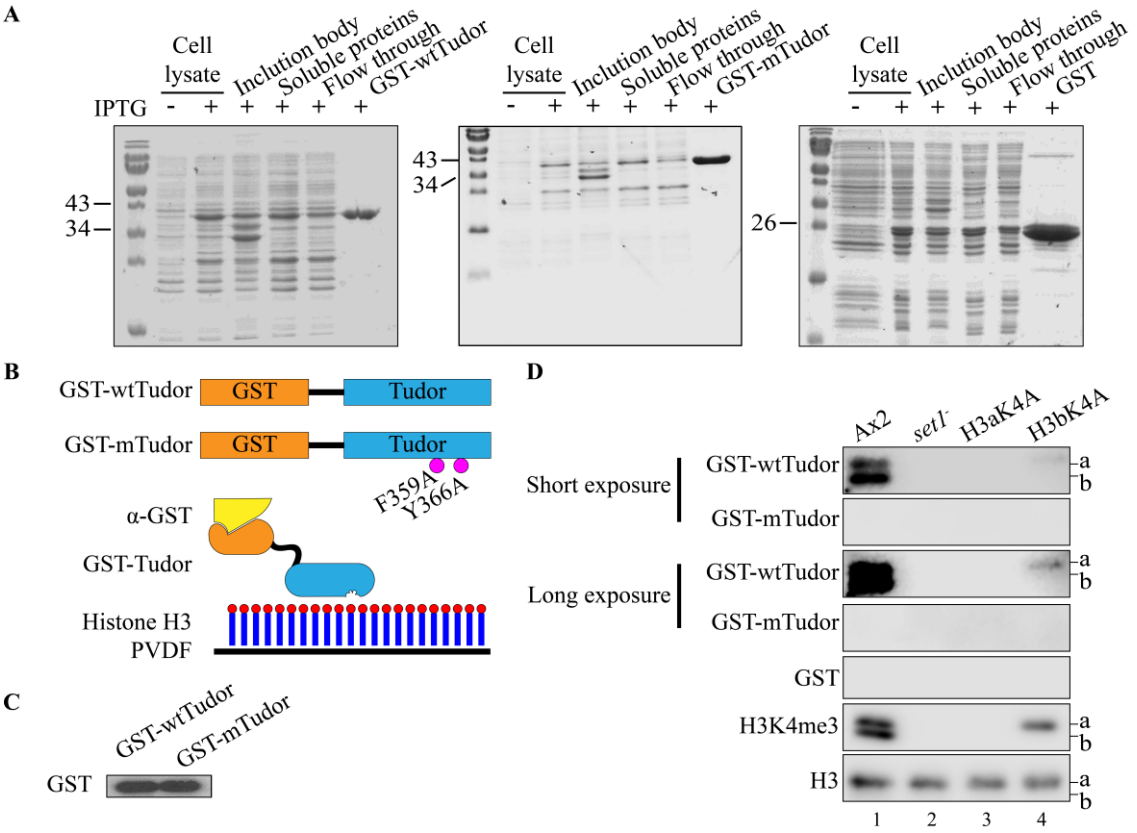

Figure 4.2 Tandem Tudor domain of *Dd*Sgf29 binds to histone H3 containing H3K4me3 *in vitro*.

(A.) GST and fusion proteins were purified glutathione sepharose. Samples from each purification steps were resolved by SDS-PAGE and proteins visualized by staining with Coomassie blue for GST-wtTudor, GST-mTudor and GST only on individual gel. **(B.)** Schematic illustration of *in vitro* binding assay using far-western blot. Wildtype or mutated (F359A and Y366A) tandem Tudor domain of *Dd*Sgf29 was expressed in *E.coli* and purified as a GST-fusion protein. Acid extract enriched for histones was resolved by SDS-PAGE and transferred to a PVDF membrane before incubation with one of the fusion proteins. Interaction between the GST-fusion protein and histone H3 was detected using anti-GST monoclonal antibody. **(C.)** Western blot result showing equalized amount of wildtype and mutant GST-Tudor fusion protein used in *in vitro* interaction assay. **(D.)** Interaction between GST-tandem Tudor domain fusion protein with acid extracts from parental Ax2 cells or strains that lack H3K4me3.Acid extracts from Ax2, *set1*$^{-}$, H3aK4A and H3bK4A cells were prepared and analyzed as mentioned above. Specific antibodies were used to detect H3K4me3, GST and histone H3. Predicted positions of histones H3a and H3b are shown on the right.

4.3.3 Creating *sgf29*$^{-}$ cells

4.3.3.1 Constructing a gene disruption vector for *sgf29*

A genetic approach was chosen to understand if *Dd*Sgf29 is involved in the mode of action of TSA, especially in the rapid accumulation of H3K9ac on H3K4 trimethylated histone. Two gDNA fragments of the *sgf29* gene were cloned into the pJET1.2 vector. The 5' arm spans from 1 to 1084 relative to the start codon while the 3'arm spans from 1943 to 2877 (Fig. 4.3A). Next, a bsR cassette flanked by two *loxP* sites was inserted between the two arms, resulting in the *Sgf29* disruption vector pJET_sgf29KO.

4.3.3.2 Generating and verifying *sgf29*$^{-}$ cells

To generate *sgf29* null cells, pJET_sgf29KO was linearized using BsrGI and BstZ17I restriction enzymes which generated a 3 kb fragment containing the disruption cassette (Fig. 4.3B). Linearized fragments were then introduced by electroporation into Ax2 cells. Cells were then resuspended in HL5 at three different dilutions and transferred to 96-well plates, aiming to obtain single colonies from one of the dilutions. Genomic DNA was extracted from single colonies surviving blasticidin selection and tested using PCR to identify the correct insertion of bsR cassette. Two primer sets (P2 & P5; P3 & P6) were used to identify colonies with the bsR cassette inserted correctly at the 5' and 3 sides,

while a third primer set (P5 & P6) was used to identify any parental contamination (Fig. 4.3A).

Among 100 colonies tested, four colonies (1D5, 3E1, 3E7 and 3H10) appeared to have the bsR cassette inserted at the correct sites. All four colonies have the correct PCR products for both 5' and 3' arms at 1368 and 1081 bp, respectively. However, only clones 1D5, 3E1 and 3H10 produced the correct PCR product at 3854 bp for primer set (P5 & P6) without any parental contamination (3121 bp). Colonies without insertion of either arm at the correct site but surviving blasticidin selection were due to a random insertion of the bsR cassette (5E8 and 6F3) (Fig. 4.3C). Therefore, colonies 1D5, 3E1, and 3H10 were subjected to clonal isolation on bacterial plates and were named *Sgf29*$^{-}$ clone 1- 3. Colony 5E8 will be referred to as Ax2^{bsR} and used as the control in subsequent experiments involving *Sgf29*$^{-}$ clones 1- 3.

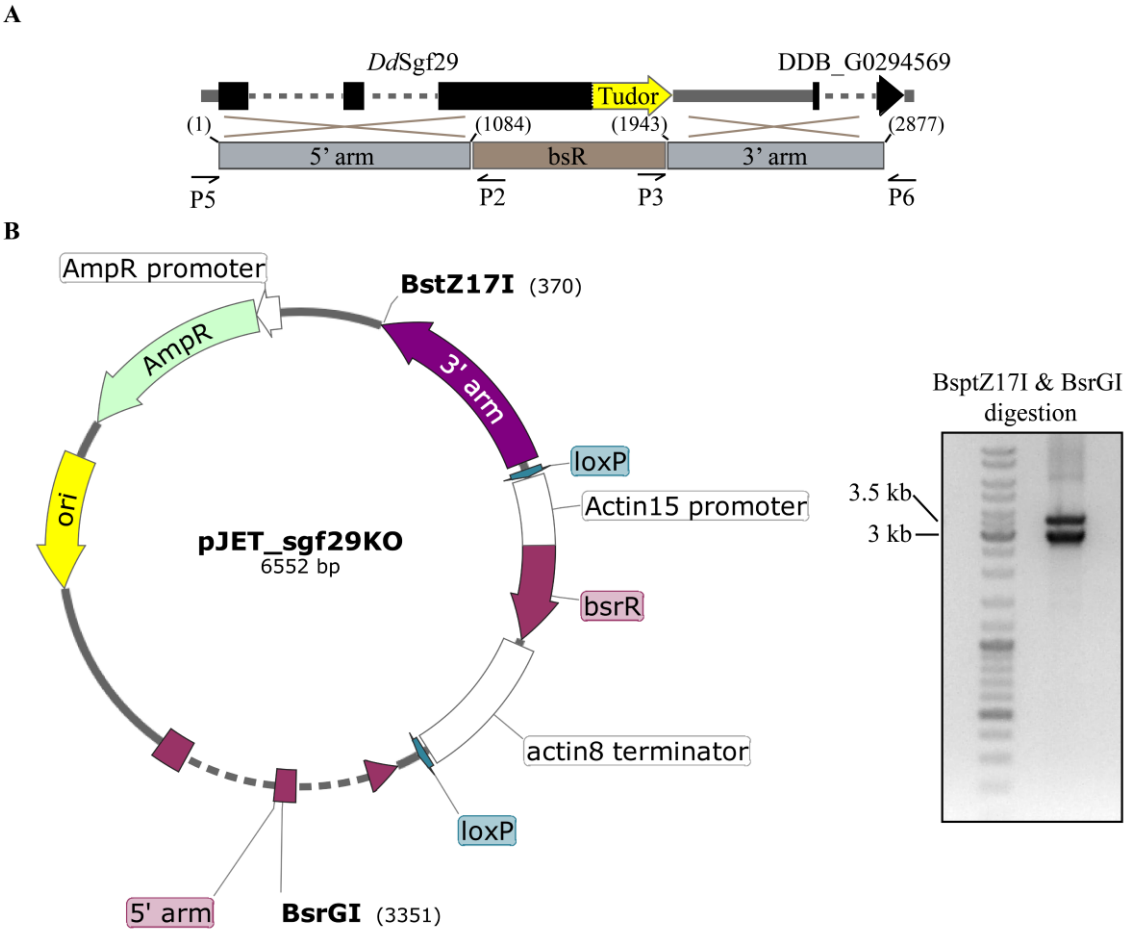

Figure 4.3. Genotyping of *sgf29*$^{-}$ cells

(A.) Schematic representation of the gene replacement event to generate *sgf29*$^{-}$ cells. Exon, intron and intergenic regions are represented by a thick black solid line, a dashed line and a solid grey line respectively. The tandem Tudor domain marked yellow is located at the 3'end of the coding region. The 5' arm spanning 1 to 1084 relative to the start codon, 3' arm (1943 to 2877) and the bsR cassette were cloned into pJET1.2 vector to generate pJET_sgf29KO disruption vector. Specific primer sets were designed to detect bsR insertion (P2 & P5; P3 & P6). A primer set (P5 & P6) flanking the linearized fragment was used to detect parental contamination. **(B.)** Map of the pJET_sgf29KO disruption vector. The vector was linearized using BsrGI and BstZ17I before transfected into parental Ax2 cells, as shown on the agarose gel

C

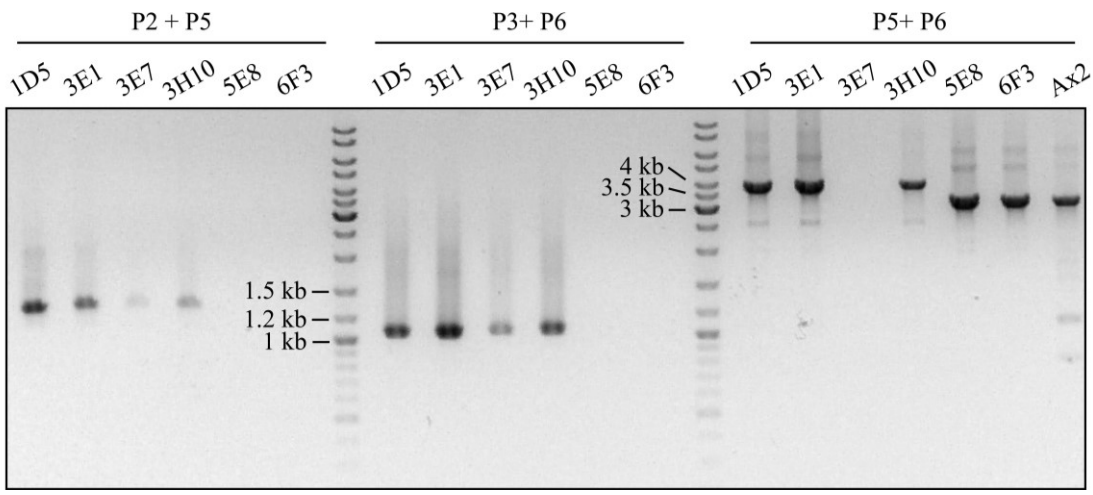

Figure 4.3 continued. Genotyping of *sgf29*⁻ cells

(C.) gDNA was prepared from surviving clones after blasticidin selection. PCR screening was carried out using primer sets mentioned above. Gene replacement at the correct sites were detected by primer P2 and P5 with the PCR product at 1368 bp while that of P3 and P6 was at 1091 bp. Parental signal was detected using primer set P5 and P6, with a band at 3121 bp while the size after gene replacement is 3854 bp.

4.3.4 Histone modification in *sgf29*⁻ cells in response to TSA

Due to the predicted function of the Sgf29 in the HAT module, the hypothesis is that deletion of its tandem Tudor domain will result in loss of binding to H3K4me3 and thus affect recruitment of the HAT module to its target. To understand if *sgf29*⁻ cells have a defect in accumulating acetylation on histone H3 upon TSA treatment, exponentially growing Ax2^{bsR} and *sgf29*⁻ cells were collected and washed twice with KK2 followed by incubation with 4 µM TSA in KK2 for up to 4h. Acid extraction was performed after 0, 1, 2 and 4 hours of TSA treatment and the samples were resolved by SDS-PAGE. Levels of H3K9ac, H3bK14ac and H3K4me3 were detected by western blot using modification-

specific antibodies.

Ax2^{bsR} cells accumulated H3K9ac and H3K14ac starting from 1 hour of TSA treatment and reached 2.9- and 3.0-fold after 4 hours of TSA treatment, respectively (Fig. 4.4, lane 1-4, $p < 0.05$). In contrast, accumulation of H3K9ac in *sgf29*$^{-}$ cells was only seen starting from 4 hours of TSA treatment, and a similar pattern was found for H3bK14ac (Fig. 4.4, lane 5-8). Ax2^{bsR} cells had a mild increase in H3K4me3 signal up to 1.5 fold by 4 hours of TSA treatment.

Thus, disruption of *sgf29* in *Dictyostelium* causes delay of accumulation of H3K9ac and H3K14ac under TSA treatment, supporting the idea that Sgf29 is involved in rapid histone acetylation induced by TSA.

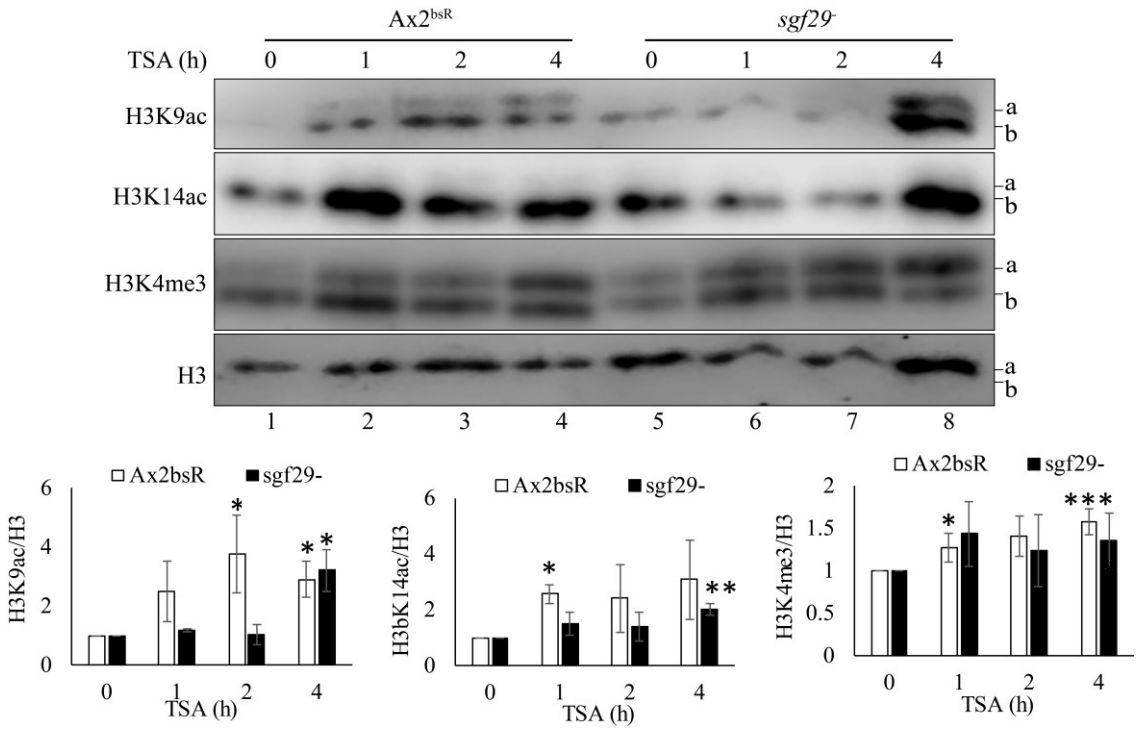

Figure 4.4 *sgf29*⁻ cells failed to accumulate H3K9ac upon TSA treatment during the first two hours.

Histone-enriched acid extracts from TSA (4 μM) treated developing Ax2^{bsR} and *sgf29*⁻ cells were prepared after 0, 1, 2 or 4 hours. Samples were resolved by 18% SDS-PAGE electrophoresis and western blots were performed using anti-H3K9ac, anti-H3bK14ac, anti-H3K4me3 and anti-H3 polyclonal antibodies. The position of histone H3a and H3b are shown on the right of each blot. Western blot results from four biological repeats (two from *sgf29*⁻ clone 1, one each from clone 2 and clone 3) were quantified using Image Studio Lite. Data for each timepoint was normalized to the level of total H3. The starting signal (0h) is denoted as 1. Data is presented as mean ± SD. Statistical significance was obtained using T-Test by comparing samples to 0h timepoint (*, $p < 0.05$; **, $p < 0.01$; ***, $p < 0.001$)).

4.3.5 Loss of dynamic acetylation of H3K4me3 in developing *sgf29*$^{-}$ cells under TSA treatment

Though *sgf29*$^{-}$ cells have defects in accumulating acetylation on histone H3 upon TSA treatment, it is unclear if dynamic acetylation of H3K4 *tri*-methylated histone was particularly affected. To address the question, acid urea gel electrophoresis was used. Under an acidic environment, most proteins become positively charged and this will make them migrate towards the cathode (−). However, any change in net charge on proteins, especially small proteins like histones, markedly changes the speed of migration thus allowing separation of histones with different charges due to PTM states such as phosphorylation or acetylation and results in a "histone ladder" (Cieniewicz et al., 2014). In the case of TSA treatment, the change of net charge is most likely due to accumulation of acetylation which neutralizes the positive charge of lysine residues, thus slowing down histones in acid-urea gel electrophoresis. Therefore, exponential Ax2^{bsR} and *sgf29*$^{-}$ cells were collected and washed twice with KK2 followed by incubation with 4 μM TSA in KK2 for up to 4 hours. Acid extraction was performed after 0, 1, 2 and 4 hours of TSA treatment and the samples were resolved by acid-urea gel. The change in acetylation of bulk histone H3 or K4-trimethylated histone H3 was analyzed by western blot using anti-H3 and anti-H3K4me3 antibodies.

In *Dictyostelium* acid extracts, four bands are apparent in the histone H3 ladder with decreasing net positive charge from band 0 to band 3 (Fig. 4.5A). In parental cells, most histone H3 was found at bands 0-2 with only 12.5% at band 3 prior to TSA treatment. Upon TSA treatment, band 0 and band 3 showed opposite trends. The percentage of band 0 started to decrease while that of band 3 increased and both reached 2-fold change after 4 hours of TSA treatment. A similar pattern of bulk histone H3 was found in *sgf29*$^{-}$ cells (Fig. 4.5A & B).

In the case of H3K4-trimethylated histone H3, in control cells, a more rapid acetylation of the trimethylated histone H3 was apparent as previously reported (Hsu et al., 2012). The percentage of band 0 decreased and that of band 3 increased by TSA treatment, but both reached 2-fold change at 2 hours, confirming that H3K4me3 histones were subjected to preferential acetylation upon TSA treatment (Fig.4.5A, lane 1 – 4). However, this more rapid acetylation was lost in *sgf29*$^{-}$ cells. Though the band 0 of H3K4me3 histones decreased from 20% to 12% after 4 hours of TSA treatment, the percentage of band 3 did not increase significantly (Fig. 4.5A & B). Two independent clones of *sgf29*$^{-}$ cells were used to further confirm the phenotype is due to loss of Sgf29 and the result was the same as found in the first clone (Fig. 4.5C).

The results confirm that rapid acetylation of H3K4me3 is lost in *sgf29*$^{-}$ cells upon TSA treatment. Failure to accumulate acetylation on H3K4me3 histones may explain why total accumulation of H3K9ac was delayed in *sgf29*$^{-}$ cells (Fig. 4.4). However, more direct evidence supporting the hypothesis is needed.

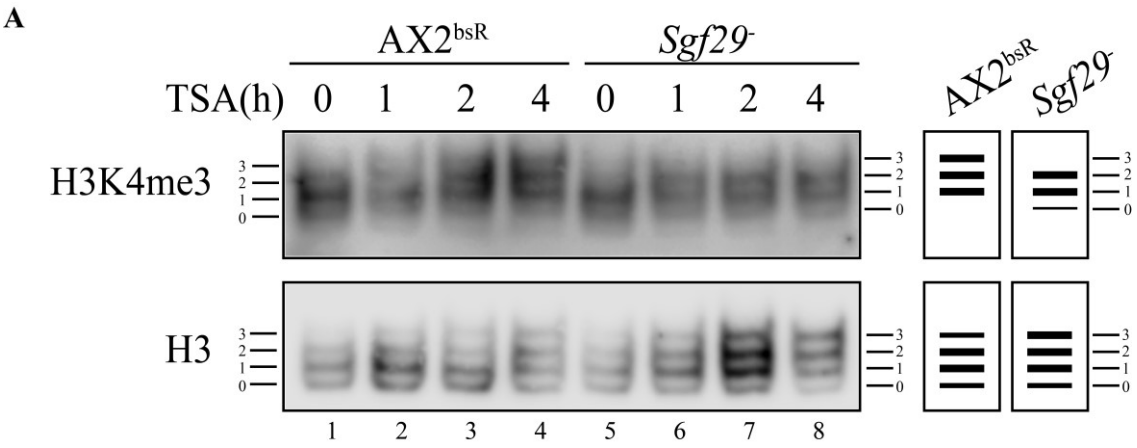

Figure 4.5 *sgf29*$^{-}$ cells lost dynamic acetylation upon TSA treatment
(A.) Histone-enriched acid extracts from TSA (4 μM) treated developing Ax2^{bsR} and *sgf29*$^{-}$ cells were prepared after 0, 1, 2 or 4 hours of TSA treatment. Samples were resolved by 20% acid-urea electrophoresis and western blots were performed using anti-H3K4me3 and anti-H3 polyclonal antibodies. Position of histone H3 with decreasing net positive charge (0 – 3) are shown on both sides of each blot. A schematic illustration of the 4h timepoints are included.

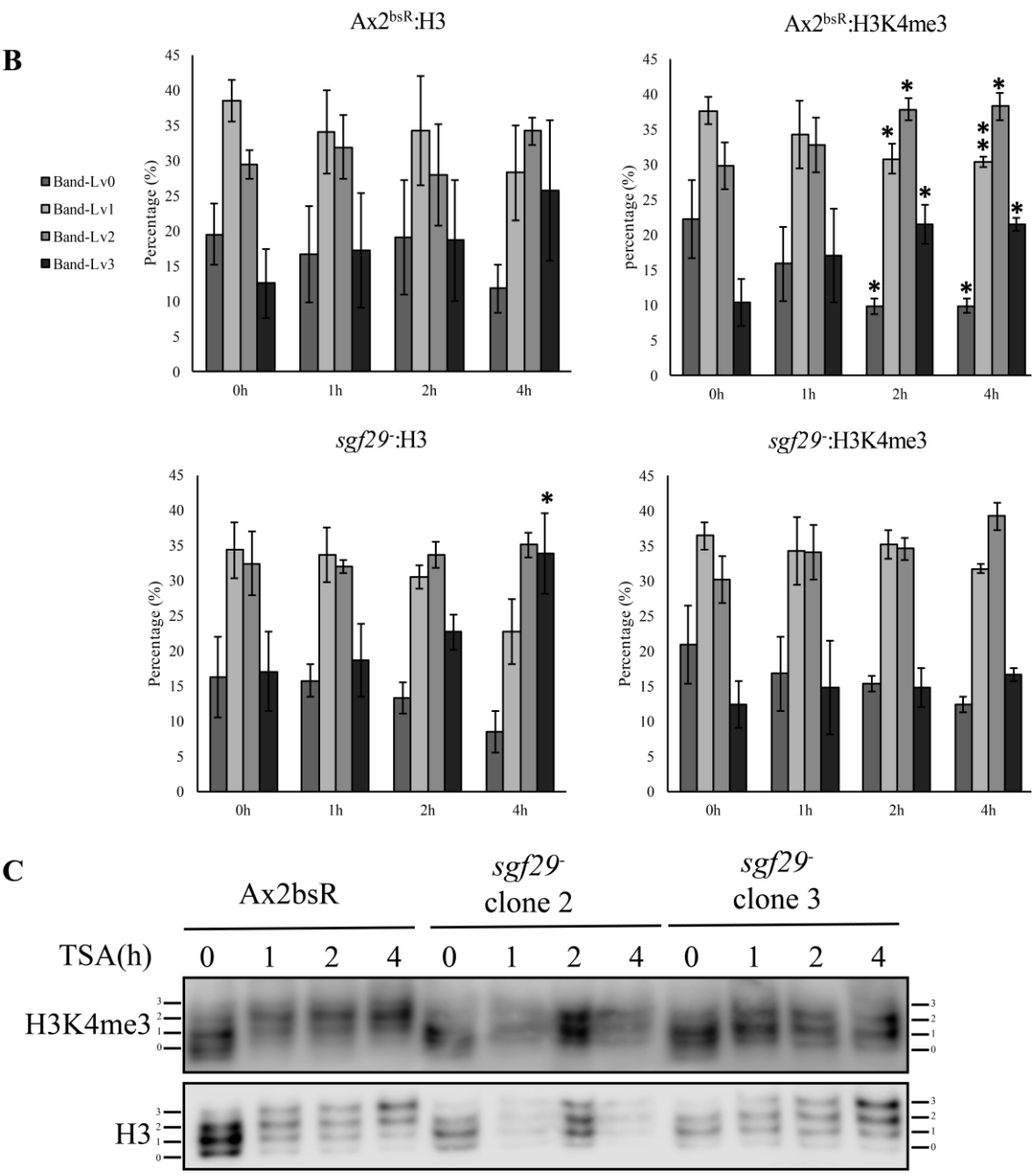

Figure 4.5 continued. *sgf29*⁻ cells lost dynamic acetylation upon TSA treatment **(B.)** Western blot results from three biological repeats were quantified using ImageJ. Percentage of each band in one histone ladder was calculated. Data is presented as mean ± SD. Statistical significance was obtained using T-Test by comparing samples to 0h timepoint (*, $p < 0.05$; **, $p < 0.01$). (**C.**). Experiment as in A. was repeated on two independent *sgf29*⁻ clones.

4.3.6 Sensitivity of development and growth of *sgf29*$^{-}$ cells to TSA treatment

Sgf29^{-} cells exhibited a delay of histone acetylation and loss of dynamic acetylation of H3K4me3 (Fig 4.4 and 4.5). However, how *sgf29*$^{-}$ cells respond to TSA-induced developmental inhibition is still unclear. To address the question, three independent *sgf29*$^{-}$ clones were exposed to DMSO or 1 μM TSA throughout development and images were taken after 24 hours.

The result showed that all three independent *sgf29*$^{-}$ clones were more resistant to 1 μM TSA compared to Ax2^{bsR} cells (Fig. 4.6A). In Ax2^{bsR} cells, development was severely delayed. By 24 hours, cells were still at loose aggregate stage. In contrast, all three independent *sgf29*$^{-}$ clones have fruiting bodies, though some cells were still at slug stage. To understand if *sgf29*$^{-}$ cells are still resistant at higher concentration of TSA, *sgf29*$^{-}$ clone 1 was subjected to development under 0 - 4 μM TSA for 24 hours (Fig. 4.6B). The result showed that even at highest concentration of TSA, *sgf29*$^{-}$ cells were still able to form fruiting bodies. To understand if growth of *sgf29*$^{-}$ cells under TSA treatment is also affected, three clones of *sgf29*$^{-}$ cells were subjected to growth assay in 24-well plates under 4 μM TSA, 20 μM SAHA or 1 mM VPA treatment for 48 hours. The result showed that all three clones are significantly more sensitive to TSA than its parental cells, but not to VPA. However, only clone 2 was more sensitive to SAHA and the overall phenotype

was subtle (Fig. 4.6C).

Disruption of the gene encoding *Dd*Sgf29 not only results in delay of histone acetylation and loss of rapid dynamic acetylation of H3K4me3, but also makes cells resistant to TSA-induced developmental inhibition (Fig. 4.4, 4.5 and 4.6). These results support the hypothesis that *Dd*Sgf29 mediates the cross-talk between H3K4me3 and histone acetylation, and that cross-talk is important for the mode of action of TSA. If the hypothesis is true, then re-introducing wildtype *Dd*Sgf29 back into *sgf29*$^{-}$ cells should re-sensitize the cells to TSA during development.

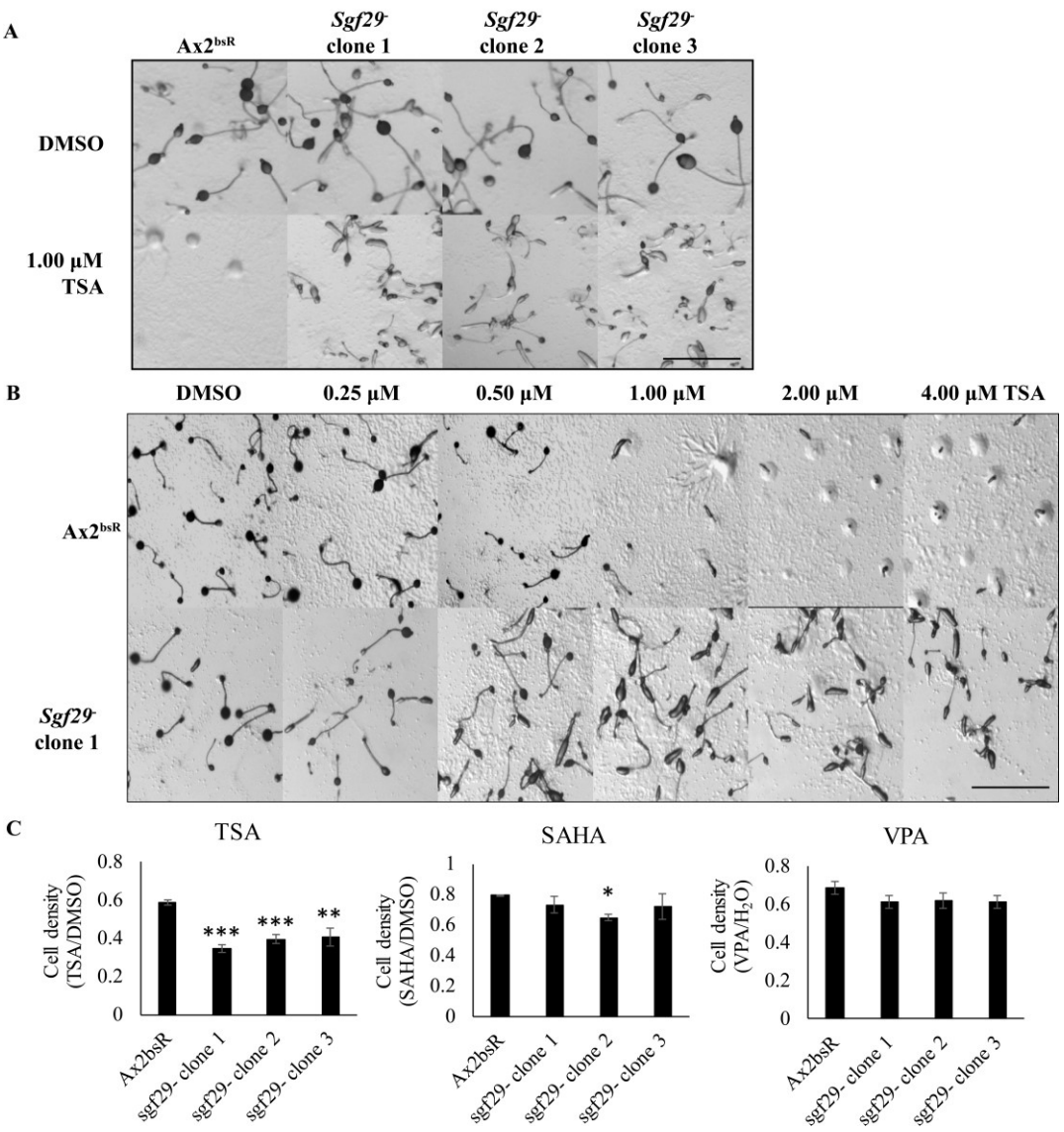

Figure 4.6 *sgf29*$^{-}$ cells are resistant to TSA-induced developmental inhibition

TSA was applied on top of 1.5% agar (w/v) in a 24-well plate and allowed to dry for 2 hours at 22°C. **(A.)** Exponential Ax2^{bsR} and *sgf29*$^{-}$ (clones 1 – 3) cells were collected and washed twice with KK2. Cells were then transferred to agar (2.8×10^6 cells/well) containing 1 µM TSA. **(B.)** Exponential Ax2^{bsR} and *sgf29*$^{-}$ (clone 1) cells were collected and washed twice with KK2. Cells were then transferred to agar (2.8×10^6 cells/well) containing increasing concentration of TSA up to 4 µM. Images were taken after 24 hours of development. Figures are representative of three biological repeats. Scale bar represents 1 mm. **(C.)** Growth assay of *sgf29*$^{-}$ cells in the presence of KDACi. Exponentially growing cells were cultured in HL5 in a 24-well plate (5×10^3 cells/well) with 4 µM TSA, 20 µM SAHA or 1 mM VPA. Relative cell density (inhibitor/vehicle) was calculated after 48 hours of growth and data was shown as mean ± SD from three independent experiments. Statistical significance was assessed using T-Test (*, $p < 0.05$)

4.3.7 Overexpression of wildtype Sgf29 in *sgf29-* cells

To understand if reintroducing Sgf29 into *sgf29-* cells could re-sensitize cells to TSA during development, the coding sequence of wildtype or mutated *sgf29* was cloned into the pDM304 vector (Veltman et al., 2009) using BglII and SpeI sites to allow Sgf29 overexpression driven by the actin 15 promoter. The mutated *sgf29* sequence harbours two site-directed mutations in the Tudor domain as described in Fig. 4.2, which reduce binding to H3K4me3 *in vitro*. To detect the expression of Sgf29, a FLAG tag was introduced at the C-terminus. (Fig. 4.7A).

Empty vector, wildtype or mutated construct were introduced into *sgf29*- cells. Whole cell lysate was prepared from transfected cells and the expression of FLAG-tagged Sgf29 was detected using a specific antibody. Cells transfected with overexpression plasmids express wildtype or mutated *Dd*Sgf29-FLAG with the expected size of 55 kDa while the signal was not detectable in cells transfected with empty plasmid (Fig. 4.7B, upper panel). Transfected cells were subject to a development assay on agar with increasing concentrations of TSA up to 4μM for 24 hours before pictures were taken. Ax2 cells were included in the experiment as a positive control for the effect of TSA.

Development of *sgf29*- cells with empty plasmid were more resistant compared to Ax2

cells, consistent with previous results. However, overexpression of wildtype *Dd*Sgf29 did not re-sensitize cells to TSA but in fact made them more resistant. Even at 4 μM TSA, *sgf29*$^{-}$ cells overexpressing wildtype *Dd*Sgf29 formed healthy fruiting bodies normally. Interestingly, overexpressing mutant *Dd*Sgf29 in *sgf29*$^{-}$ cells did not provide the same resistance and the dose-response to TSA was the same as cells with empty vector (Fig. 4.7B, lower panel). This suggests that a functional Tudor domain is necessary for the enhanced resistance phenotype.

One possible explanation for this surprising result is that when wildtype *Dd*Sgf29 is overexpressed, the amount of *Dd*Sgf29 outweighs the available proteins it forms a complex with, leaving excess monomeric *Dd*Sgf29, which could bind to H3K4me3 and deplete most of the available sites for the functional HAT module, resulting in a dominant negative effect. However, the same effect is not seen when mutant *Dd*Sgf29-FLAG is overexpressed as binding of its Tudor domain to H3K4me3 is disrupted (Fig. 4.2). The above interpretation is illustrated in Fig. 4.8. If this reasoning is really the case, overexpressing *Dd*Sgf29-FLAG in Ax2 cells should result in a similar dominant negative effect. Thus, Ax2 cells were transfected with constructs to drive expression of wildtype or mutant *Dd*Sgf29-FLAG and expression was detected in transfected cells (Fig 4.7C, upper panel). The cells were subjected to a development assay in the presence of TSA

and *sgf29*$^{-}$ cells were included as a control.

Ax2 cells transfected with plasmid to drive overexpression of wildtype *Dd*Sgf29 exhibited marked resistance to TSA, forming fruiting bodies at 4 μM TSA and were more resistant than *sgf29*$^{-}$ cells. However, Ax2 cells containing empty vector or expressing mutated *Dd*Sgf29 were still more sensitive compared to *sgf29*$^{-}$ cells. The result supports the hypothesis that overexpressing the wildtype *Dd*Sgf29 results in a dominant negative effect, which depends on a functional Tudor domain. Thus, to re-sensitize *sgf29*$^{-}$ cells to TSA, a system to introduce a single copy gene using an endogenous promoter to drive expression of *Dd*Sgf29 should be considered.

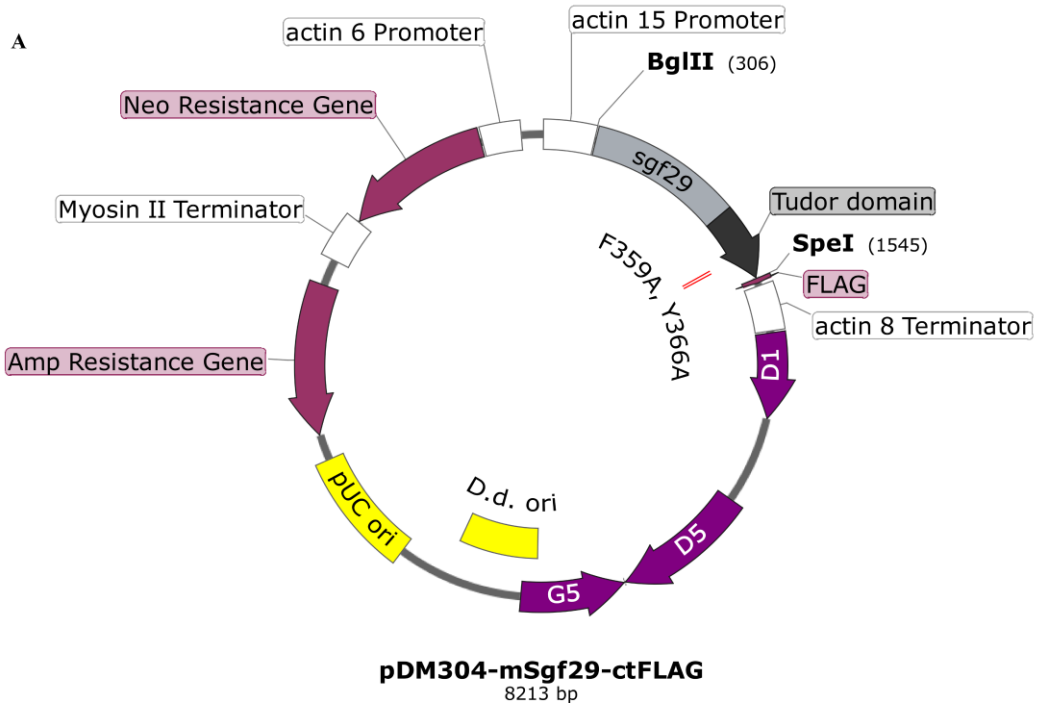

Figure 4.7 Overexpressing wildtype Sgf29-FLAG confers TSA-resistance in *sgf29*⁻ and Ax2 cells during development, dependent on an intact Tudor domain.

(A.) Map of pDM304-mSgf29-ctFLAG. Coding sequence of Sgf29 was cloned into pDM304-ctFLAG vector using BglI and SpeI sites. Both wildtype and mutant Sgf29 were constructed with the later harbouring F359A and Y366A mutations in the Tudor domain as indicated in the map.

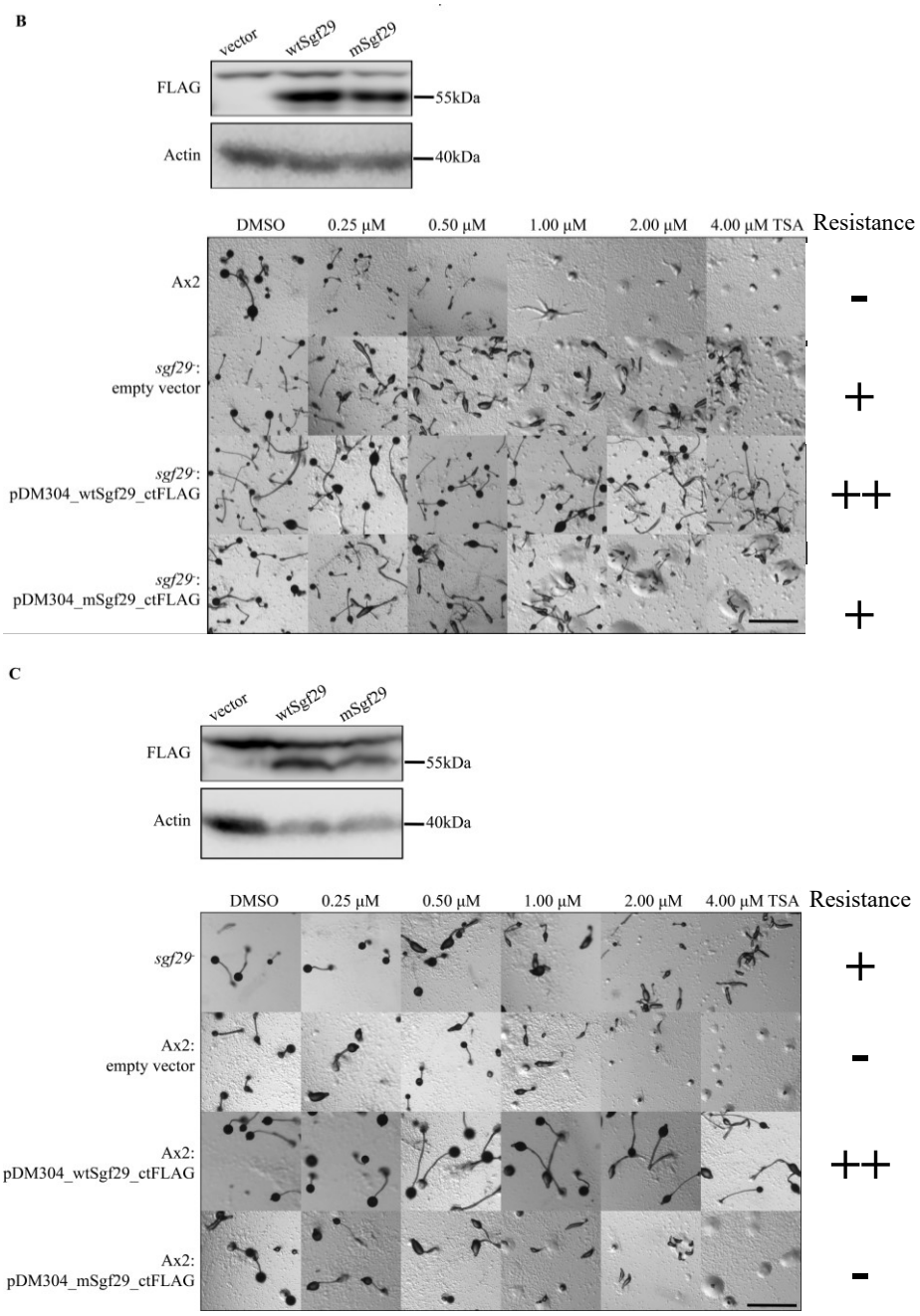

Figure 4.7 continued. Overexpressing wildtype Sgf29-FLAG confers TSA-resistance in *sgf29-* and Ax2 cells during development, dependent on an intact Tudor domain. Development of *sgf29-* **(B)** and Ax2 **(C)** cells overexpressing wildtype or mutant Sgf29-FLAG in the presence of TSA. Expression of wildtype and mutant Sgf29-FLAG were detected in whole cell lysate samples by western blot using an anti-FLAG antibody. Cells developed on agar (2.8×10^6 cells/well) containing increasing concentration of TSA. Images were taken after 24 hours of development. Sensitive (-) and resistant (+/++) phenotypes are indicated at the right-hand side. Figures are representative of three biological repeats. Scale bar represents 1 mm.

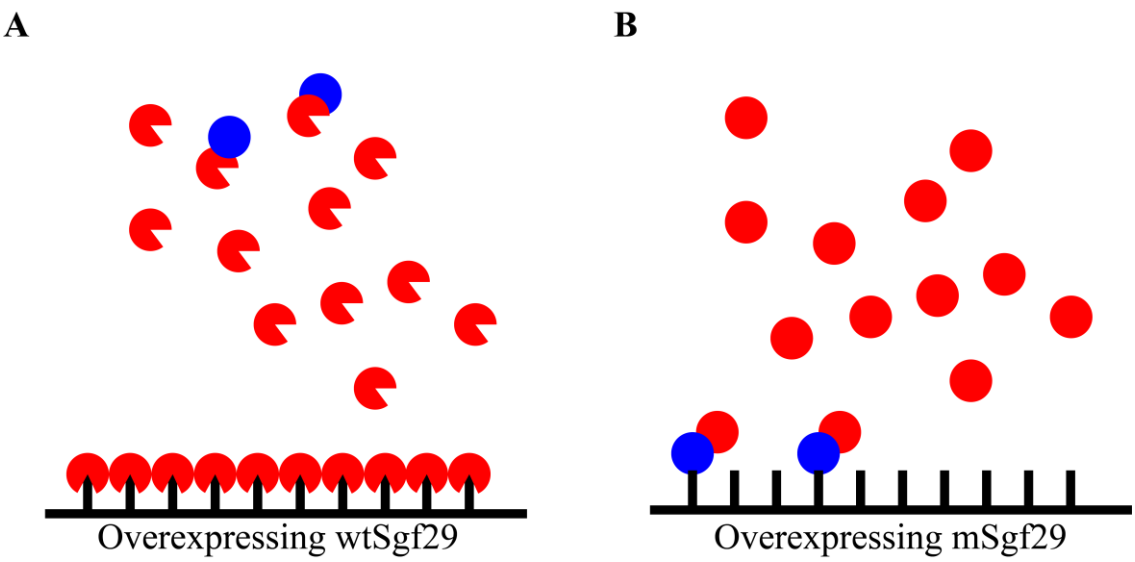

Figure 4.8 Hypothesis explaining the dominant negative effect caused by overexpressing wildtype Sgf29

(A.) When wtSgf29 (open red circle) is overexpressed, it binds to its substrate and depleted the pool, preventing modification of the substrate by its interacting partner (blue circle), thus giving a dominant negative effect. **(B.)** When mSgf29 (red circle) is overexpressed, the mutated Tudor domain is unable to bind to its substrate thus the substrate is open to modification by its interacting partner.

4.4 Discussion

In this chapter I provide further evidence supporting the hypothesis that dynamic acetylation o H3K4me3 is involved in the mode of action of TSA in developmental inhibition by investigating the *in vivo* function of a potential Sgf29 orthologue in *Dictyostelium*.

Summary of results:

- The tandem Tudor domain of the putative *Dd*Sgf29 identified in *Dictyostelium* binds directly and selectively to acid extracts containing H3K4-trimethylated

histones *in vitro*.

- Deletion of *sgf29* results in loss of rapid acetylation of H3K9 and H3bK14 in the first two hours of TSA treatment during development.
- *sgf29* null cells lose dynamic acetylation of H3K4-trimethylated histones upon TSA treatment during development.
- Cell lacking *Dd*Sgf29 are more resistant to TSA-induced developmental inhibition, a phenotype that is found in *set1*$^{-}$, H3aK4A and H3bK4A cells.
- Overexpression of wildtype *Dd*Sgf29-FLAG in parental Ax2 cells confers TSA-resistance during development while overexpressing mutant *Dd*Sgf29-FLAG has no effect.

It has been shown *in vitro* that the tandem Tudor domain of yeast Sgf29 binds preferentially to H3K4me2/3 histone peptides (aa 1-11) (Bian et al., 2011). Similar results were reported using full length human Sgf29 incubated with histone peptides (aa 1 – 17) carrying H3K4me2/3 modification. The results presented here are consistent with the tudor domain binding methylated H3K4 *in vitro* as binding is lost in *set1*$^{-}$ cells which lack all detectable methylation. The interaction between the Tudor domain of *Dictyostelium* Sgf29 was found with acid extracts from H3bK4A but not H3aK4A cells (Fig. 4.2). H3aK4A cells lack all detectable methylation on H3a while *mono* and *di*- but not *tri*-methylation of H3K4 are still detectable on H3b. Methylation of H3b is absent in

H3bK4A cells but all methylation on H3a remains intact (Hsu et al., 2012). This suggest that the Tudor domain of DdSgf29 binds to full length H3 carrying H3K4me3 more strongly than H3K4me2/1.

To further study the function of *Dd*Sgf29 in the context of TSA-induced developmental inhibition, a *sgf29* null strain was created (Fig. 4.3). Sgf29 consists of 411 amino acids, with the tandem Tudor domain at its C-terminus (K297-K411). The disruption strategy was designed to replace nucleotides coding for Q119 to K411 with the bsR cassette. If the insertion does not lead to decay of the mRNA, an extra 5 amino acids may be translated together with the N-terminus of *Dd*Sgf29 (S1-G118) before the translation is terminated by a stop codon introduced by the bsR cassette. The *N*-terminal sequence of Sgf29 does interact with other subunits in HAT module (Nguyen-Huynh et al., 2015). However, deletion of the Tudor domain is sufficient to abolish the recruitment of the HAT module to substrates in other systems (Bian et al., 2011; Ringel and Cieniewicz, 2015). Therefore, the phenotypes discovered in *sgf29*$^{-}$ cells are due to loss of Tudor domain if not a complete loss of Sgf29.

The basal level of H3K9 and K14 acetylation in *sgf29*$^{-}$ cells was similar to control cells (Fig 4.4) which differs from the situation in *S. cerevisiae* where loss of Sgf29 leads to a

reduction in global acetylation levels (Bian et al, 2011) even though its loss does not alter the structural integrity of the SAGA complex (Shukla et al., 2012). However, delay of H3bK9ac and H3bK14ac accumulation on TSA treatment of developing cells was found in *sgf29*$^{-}$ cells, which indicates a general delay of histone H3 acetylation. This agrees with a previous finding that loss of the Tudor domain results in loss of acetylation to H3K4me3 nucleosomes *in vitro* but the reactivity of HAT module remains the same (Ringel and Cieniewicz, 2015). In H3bK4A cells, accumulation of K9ac on H3b upon TSA treatment was lost even after 4 hours of TSA treatment, which suggest methylation of H3K4 is needed for the rapid acetylation induced by TSA (Fig. 3.7). However, *sgf29*$^{-}$ cells only showed a delay in accumulation of H3bK9ac, suggesting the existence of other proteins with similar roles in mediating the cross talk between K4 methylation and acetylation of H3K9 upon TSA treatment. It has been reported that reduced expression of Sgf29 by RNAi leads to a loss of H3K4me3 in human cells (Schram et al., 2013) but that was not the case in this thesis.

Overexpression of *Dd*Sgf29-FLAG in either *sgf29*$^{-}$ or Ax2 cells led to TSA resistance during development, which is a phenotype dependent on a functional tudor domain as overexpressing the mutated protein which does not bind to H3K4me3 *in vitro* had no effect. To detect the expression of *Dd*Sgf29, a FLAG tag was introduced at the C-

terminus (Fig. 4.7A). The crystal structure of Sgf29 alone (Bian et al., 2011), or in complex with Gcn5, Ada2, and Ada3 in the HAT module have been solved (Nguyen-Huynh et al., 2015). The crystal structure shows that the C-terminal tail of Sgf29 is not imbedded inside Sgf29 or interacting with other subunits in the HAT module. Thus, the C-terminus tag of FLAG is expected to have little interference with the function of Sgf29 or the HAT module. These results are consistent with the overexpression of *Dd*Sgf29 acting in a dominant negative way to block recruitment of the HAT activity to the H3K4methylated histone in cells.

Attempts to demonstrate interaction between overexpressed DdSgf29 and epitope tagged and overexpressed Gcn5 in *Dictyostelium* were not successful (data not shown). It has been shown that it is necessary to overexpress all four subunits of the HAT module to stabilize the complex, and demonstrate interaction (Nguyen-Huynh et al., 2015). In future work, if endogenous levels of expressed, tagged *Dd*Sgf29 can be used to rescue the phenotype of *sgf29*$^{-}$ cells, then this should be immunoprecipitated to identify co-precipitating histone acetyltransferase activity and test if this activity is lost in *gcn5Δbromo* cells.

Overall the data in this chapter is consistent with the identified protein (DDB0233189) being the orthologue of Sgf29 and that in *Dictyostelium* early development, an associated HAT complex (most likely containing Gcn5 by analogy with other organisms) is responsible for the majority of dynamic acetylation of H3K4me3 in the presence of TSA and this, in turn, plays a major role in the sensitivity of development to TSA. Either loss or overexpression of Sgf29 in tumour cells would therefore be predicted to lead to resistance to KDACi. It has been reported in rat hepatoma cell lines that Sgf29 was overexpressed as well as the oncogene c-Myc (Kurabe et al., 2007). Deletion of the gene encoding Sgf29 reduced the tumorigenic potential of rat hepatoma K2 cells along with expression from a c-Myc-dependent promoter (reviewed in Kurabe et al., 2015). It will be of interest to investigate whether these cells show altered sensitivity to KDACi.

5. Genome wide screen to identify genes involved in TSA-induced growth inhibition

5.1 Introduction

In chapters 3 and 4, I identified that dynamic acetylation plays a key role in TSA-induced developmental inhibition. However, the mechanisms of growth and developmental inhibition by TSA seem distinct. Cells that are resistant to TSA during development are not resistant during growth and some seem more sensitive. To identify key players involved in TSA-induced growth inhibition in *Dictyostelium*, a genetic screen is the most thorough way. Generating mutants with widespread insertions in the genome by restriction enzyme mediated integration (REMI) is a technique that has been applied in *Dictyostelium* for forward genetics (Adachi et al., 1994; King et al., 2013; Kuspa and Loomis, 1992). However, though generating a large pool of mutants by REMI is relatively easy, the complexity of mutants in each REMI experiment is unknown. There are also difficulties in reusing the pools as the growth reduces the number of clones present and it is inefficient and time consuming to identify individual insertion sites of mutants after a genetic screen (Adachi et al., 1994; Keim et al., 2004).

Recently, a newly-developed technique named REMI-seq, combines REMI and the power of next-generation sequencing to enable generation of a large pool of mutants in

Dictyostelium and parallel phenotyping (Gruenheit et al., 2019). Firstly, thousands of mutants are generated via REMI, which is designed to insert a bsR cassette at DpnII or NlaIII sites in *Dictyostelium* genome. This is predicted to target more than 92% of the genes. The bsR cassettes contains two restriction enzymes, MmeI and I-SceI and a vector tag (Fig. 5.1A). MmeI cuts 18 – 20 bp downstream of the recognition sites in the flanking genomic DNA region while I-SceI cuts inside bsR cassette. Thus, upon digestion with both enzymes, gDNA fragments flanking the insertion sites are released. These fragments can then be ligated to Illumina sequencing adapters thus allowing high-throughput identification of the insertion sites (Fig. 5.2B). Using the technique, the REMI-seq team successfully identified 21,529 independent mutants, collectively named the Genome Wide *Dictyostelium* Insertion (GWDI) bank. These mutants correspond to 12,247 different genomic insertion sites, covering 43% of the predicted genes in the *Dictyostelium* genome (Gruenheit et al., 2019). These strains have been gridded and frozen as single clones and many are stored in the *Dictyostelium* Stock Centre. The individual mutants or pools can be screened. For example, a study using a pool in a traditional screen for resistance has successfully identified mutants resistant to curcumin in *Dictyostelium* (Cocorocchio et al., 2017).

One great advantage of the pool is that it also allows parallel phenotyping of all individual

mutants in the pool. Under external stresses, advantageous mutants are enriched while mutants with disadvantage are depleted over generations. The change in population can be easily detected using the same technique used to identify the insertion sites because the read counts of the next-generation sequencing is proportional to the number of starting DNA fragments. The REMI-seq team has successfully applied this technology to identify mutants with advantage or disadvantage when grown in axenic media or on bacteria (Gruenheit et al., 2019).

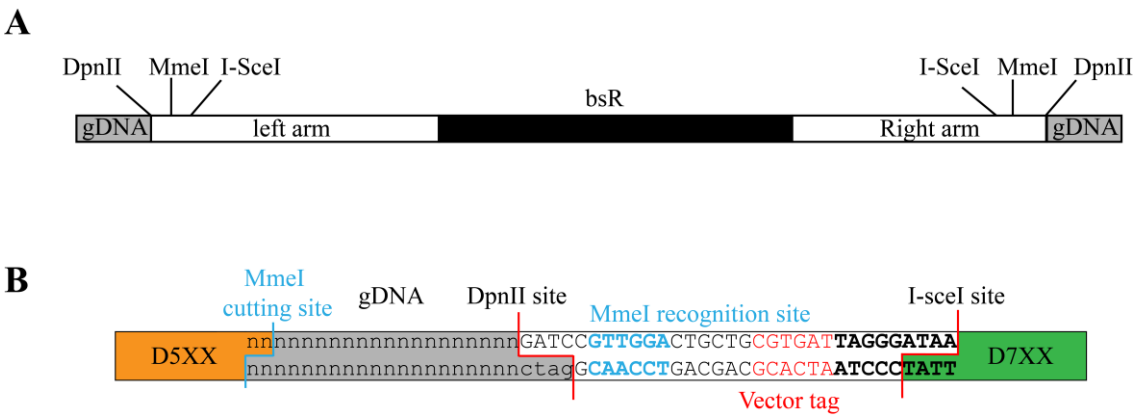

Figure 5.1 Principal of REMI-seq

(A.) Schematic illustration of the bsR cassette used to generate the REMI-seq strains. The bsR cassette is inserted in via restriction-enzyme mediated insertion (REMI) at DpnII or NlaIII sites, though only the DpnII site is shown here. At both 5' and 3' ends of the cassette sit MmeI and I-SceI sites. These restriction enzymes both cut the DNA at a sequence some distance from the recognition site. **(B.)** Digestion with MmeI and I-SceI of genomic DNA from REMI-seq strains releases two fragments flanking the bsR cassette insertion site. The fragments contain 18/20 bp of gDNA upstream of the MmeI recognition site, and a vector tag to facilitate bioinformatic analysis. Adaptors D5 and D7 with different tags can be ligated to digested fragments, which allows parallel sequencing of multiple samples.

5.2 Aims

The first aim of this chapter is to understand if the principal of REMI-seq can be used to identify TSA-resistant mutants during growth. This is done by examining if competition between strains under TSA treatment results in enrichment of advantageous strains. The second aim is to apply REMI-seq using a pool of GWDI mutants and determine if this results in identification of TSA-resistant strains during growth.

5.3 Results

5.3.1 Screen and preparation of library for sequencing

Parallel phenotyping aims to identify genes that when disrupted confer advantage or disadvantage under external stress. Strains with an advantage grow faster than the rest of the population and thus will be enriched over generations under selection pressure. Equally those sensitive to the selective pressure will be under-represented. To utilize the GWDI library to screen for genes involved in TSA-resistance in vegetative cells, it is necessary to determine if the protocol used by its inventors (Gruenheit et al, 2019) also works in my hands.

The concept of parallel phenotyping was verified by utilizing an available strain lacking the genes encoding both H3b and H3c (*H3b/c*$^{-/-}$) variants (Hsu et al., 2012). The resistant phenotype of the strain was discovered in a pilot screen of available strains in lab searching for TSA-resistant cell lines. Using a growth assay in shaking suspension the strain was found to be resistant to growth inhibition in the presence of TSA compared to Ax2 cells (Fig. 5.2A). To understand if competition between advantageous and disadvantageous strains results in a detectable change in doubling time of the population, Ax2 and *H3b/c*$^{-/-}$ cells were subject to TSA treatment independently or in a mixture of both strains (Ax2: *H3b/c*$^{-/-}$ = 9:1). Cells were treated with DMSO or 6 μM TSA at a

starting cell number of 2.3×10^6 cells in Petri dish. The time needed for DMSO-treated cells to reach confluency is defined as one round of treatment within which DMSO and TSA is renewed every 24 hours and the cell density calculated.

After 24 hours of treatment, the doubling time of TSA-treated Ax2 cells increased from 10.6 h to 16.5 h, and by the end of the 1st round, it spiked to 31 h which is markedly slower than DMSO-treated cells (Fig. 5.2B). In the contrast, the doubling time of *H3b/c*$^{-/-}$ cells remained unchanged after 24 hours of TSA treatment then increased from 11 h to 20 h after 48 hours of treatment. The doubling time of the mixed pool firstly increased from 9 h to 14 h after 24 hours of TSA treatment, then further increased to 25.3 h at the end of first round. Both 24 h and 48 h values were lower than the doubling time of Ax2 cells but higher than *H3b/c*$^{-/-}$ cells. Though this pilot experiment was only repeated for twice with large error bars, the results suggest that the existence of an advantageous strain in a pool of disadvantageous cells would reduce the doubling time of the whole population in the presence of TSA. It also indicates that strains with advantage should become dominant in the population over multiple generations. Thus, the same experiment set up could be applied to a pool of GWDI mutants.

A pool of GWDI strains that contains approximately 10,000 different mutants was kindly provided by Prof. Chris Thompson. The pool was subjected to the same conditions as

above and the screen was carried out for eight rounds in three replicates. The doubling time of the DMSO-treated pool was ~15 hours for the first six rounds and increased to ~17 hours at round 8 (Figure 5.2C). Conversely, the doubling time of TSA-treated pool was ~19 hours at first round, increased to ~22 hours during the second round and peaked at ~24 hours at the fourth round. However, from the fifth to seventh rounds the doubling time of TSA-treated pool decreased to ~19 hours and was further reduced to 16 hours by the final round (Fig. 5.2C). The decrease of doubling time at the fifth and eighth rounds indicates enrichment of TSA-resistant strains in the population at early and late stages of selection respectively. To ensure a full coverage of early- and late-enriched strains, cells from both the fifth and eighth rounds were subjected to gDNA preparation (Fig. 5.2D). However, it should be noted that some late-enriched strains may be missed due to the increased doubling time of the DMSO-treated pool at the eighth round.

Two replicates from each round (replicate 1 and 2 for fifth round; replicate 2 and 3 for eighth round) were subjected to downstream library construction. More detail of the library construction is included in Materials and Methods. Briefly, gDNA was digested with MmeI and I-SceI. These fragments from different strains in the pool contain 18/20 bp of gDNA flanking the bsR cassette insertion sites together with a vector tag (Fig. 5.1B). These fragments were then ligated to D5 at one end and different D7 adaptors at the other

end containing unique sequence tags to allow parallel sequencing of multiple samples in one run. The ligated products were then amplified by PCR, generating a 183 bp fragment (Fig. 5.2E). The amplified products were purified twice and pooled for Illumina sequencing.

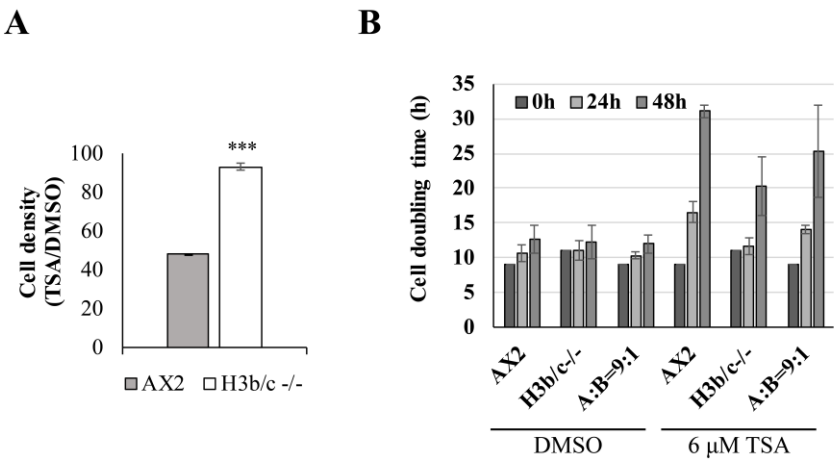

Figure 5.2 Growth of a pool of REMI-seq strains in the presence of TSA followed by construction of library for sequencing

(A.) Growth of Ax2 and *H3b/c*$^{-/-}$ cells under TSA treatment. Cells were inoculated into 25 ml of HL5 at a beginning cell density of 1×10^5 cells/ml in shaking suspension in the presence of DMSO or 4 μM TSA for 24 hours before cell density was recorded. The density in the presence of TSA is plotted as a percentage of that in the presence of DMSO **(B.)** Competition between Ax2 and *H3b/c*$^{-/-}$ cells in the presence of TSA. Exponentially growing cells were subjected to DMSO or 6 μM TSA at a starting cell number of 2×10^6 cells in a Petri dish. Media was changed every 24 hours with fresh DMSO or TSA and cell density was recorded until cells were confluent, which accounts for one round of treatment. From starting cell density to confluency takes about 48 hours for DMSO-treated cells. In the mixed pool (A:B = 9 : 1), Ax2 and *H3b/c*$^{-/-}$ cells were mixed in 9 : 1 ratio. Data is presented as mean ± SD (n = 2).

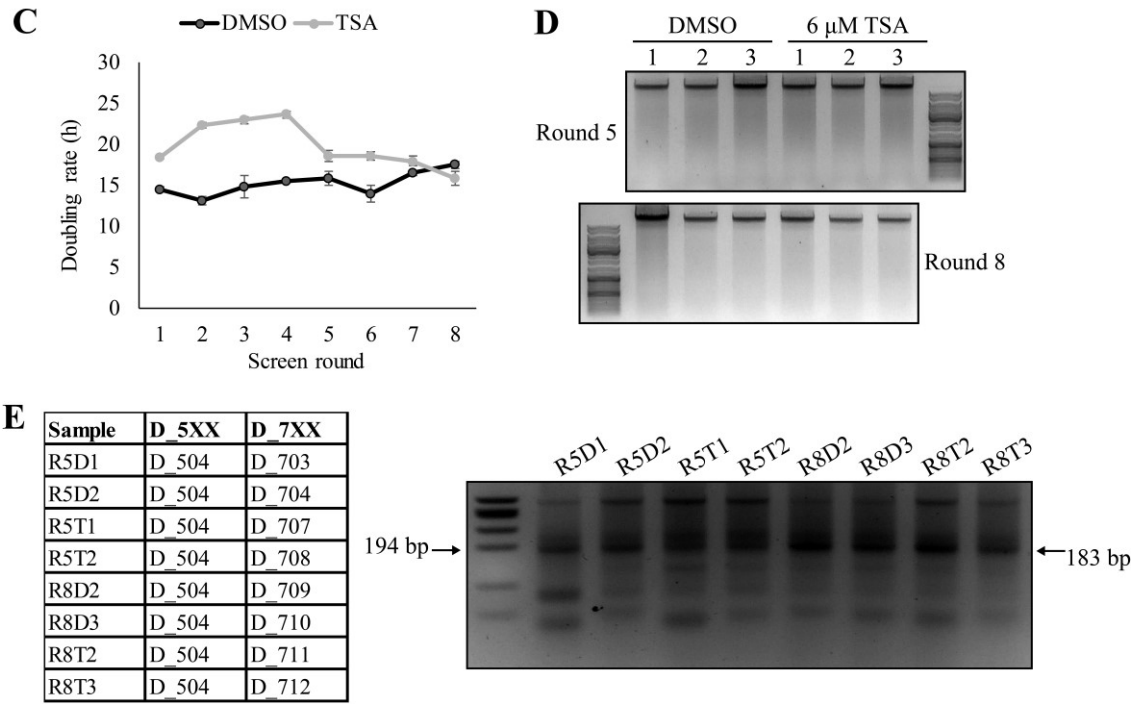

Sample	D_5XX	D_7XX
R5D1	D_504	D_703
R5D2	D_504	D_704
R5T1	D_504	D_707
R5T2	D_504	D_708
R8D2	D_504	D_709
R8D3	D_504	D_710
R8T2	D_504	D_711
R8T3	D_504	D_712

Figure 5.2 continued. Growth of a pool of REMI-seq strains in the presence of TSA followed by construction of library for sequencing

(**C.**) Doubling times of the REMI-seq pool treated with 6 μM TSA. A pool of ~10000 REMI-seq strains were subjected to DMSO or TSA under the same conditions described in figure B. The screen was carried out for eight rounds and the doubling time of each round was recorded. Data is presented as mean ± SD from three biological replicates. **(D.)** gDNA was extracted from the screened pools after five and eight rounds of treatment , run on an 0.8% agarose gel and visualized by ethidium bromide staining. **(E.)** Construction of library for Illumina sequencing. Two out of three extracted gDNA samples of each treatment in fifth and eighth round were digested with MmeI and I-SceI. Different combinations of D5 and D7 adaptors were ligated to digested gDNA. R5D1 indicates the sample is from DMSO-treated replicate 1 of fifth round. The ligated product was amplified using a specific primer P5 and sample-specific D7 primers. The reactions were resolved on an 3.5% agarose gel and visualized by staining with Midori green (NIPPON). The size of the correctly amplified fragment is 183 bp. Amplicons of eight samples were mixed in the same molar ratio and the mixed pool was subjected to Illumina sequencing. Sequences of all adaptors and primers are listed in Appendix 1.

5.3.2 Bioinformatic pipeline

The total number of reads generated by the NextSeq platform was 400 million of which 240 and 160 million reads were generated from round 5 and round 8 samples respectively. In fifth round samples, both replicates of DMSO- and TSA-treated samples generated ~60 million reads each. In eighth round samples, both DMSO-treated replicates generated ~45 million reads, while TSA-treated samples gave 45 and 25 million reads (Fig. 5.3A). Reads without vector tag or found at more than one site in the *Dictyostelium* genome were filtered. After filtering, the number of reads of DMSO- and TSA-treated samples from the fifth round were 10 and 7 million respectively. From the eighth round the number of reads of DMSO-treated samples reduced to 7-8 million while TSA-treated samples were 6.5 and 3 million (Fig. 5.3B).

The number of reads from the same insertion site was calculated and normalized to the total number of reads in each sample to determine its fraction of the whole population. To understand the reproducibility of the REMI-seq screen, normalized read counts of the two replicates were plotted against each other (Fig 5.3C). For strains with normalized read counts below 1000, the value varies markedly between two replicates. But for those higher than 1000, the value correlates well between two replicates.

The number of normalized read counts of the two DMSO replicates were averaged in both rounds, and strains were classified into three bins based on the read counts. Bin 100, 1000 and 10000 were created for strains with less than 100, between 100 to 1000 and more than 1000 normalized read counts respectively. The fold change (TSA/DMSO) of each strain at the fifth and eighth rounds were then calculated, and the numbers of enriched and depleted strains were listed (Table 5.1). The results of the two replicates in both rounds were plotted against each other for each of the three bins (Fig 5.3D). In general, there were more depleted strains than enriched ones in both rounds, confirming TSA selection. However, a different behavior of the overall population was observed in three bins. For bin 10000, more strains were depleted than enriched in both the fifth and eighth rounds, whereas strains in bin 100 had more enriched than depleted in the fifth round but not in the eighth round, possibly due to the increased doubling time of DMSO-treated sample.

To ensure enriched and depleted strains deviated from the overall behavior of the population in each of the three bins, the average fold change (FC) and standard deviation (S) in each bin were calculated. The cutoff for enriched strains was set at "$\log_{10}FC > M + 1.5S$" while for depleted strains the cutoff was "$\log_{10}FC < M - 1S$" (Fig. 5.3E). After applying the cutoff, there were 114 enriched and 13 depleted strains in the fifth round

and 110 and 34 in the eighth round respectively (Table 5.1).

Table 5.1 Number of strains in the three bins before and after applying cut off

Round 5					Round 8				
Average $log_{10}FC$	Bin			total	Average $log_{10}FC$	Bin			total
	100	1000	10000			100	1000	10000	
> 0	839	25	89	953	> 0	238	24	39	301
< 0	253	391	1068	1712	< 0	297	988	920	2205
Number of strains passed cutoff in both repeats									
> 0	17	20	77	114	> 0	47	24	39	110
< 0	N/A	0	13	13	< 0	N/A	2	32	34

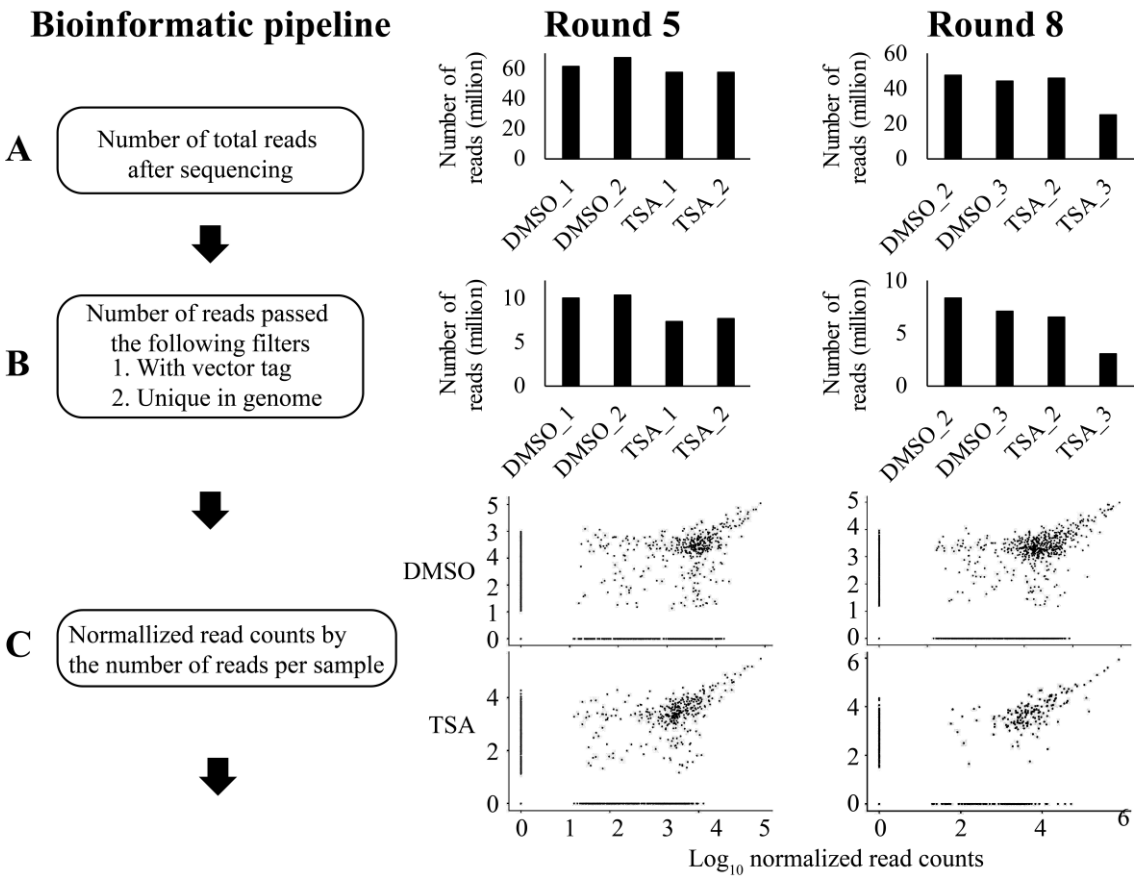

Figure 5.3 Bioinformatic pipeline for processing sequencing data

This figure is divided into three columns. The left column describes the steps carried out to generate figures for fifth round (middle column) and eighth round (right column). **(A.)** The total number of read counts of DMSO- and TSA-treated samples in fifth and eighth round was extracted from raw sequencing data. **(B.)** Reads with vector tag and found to be unique in the *Dictyostelium* genome were subjected to downstream analysis. **(C.)** Read counts were normalized to the total number of reads in each sample and data of two replicates plotted against each other.

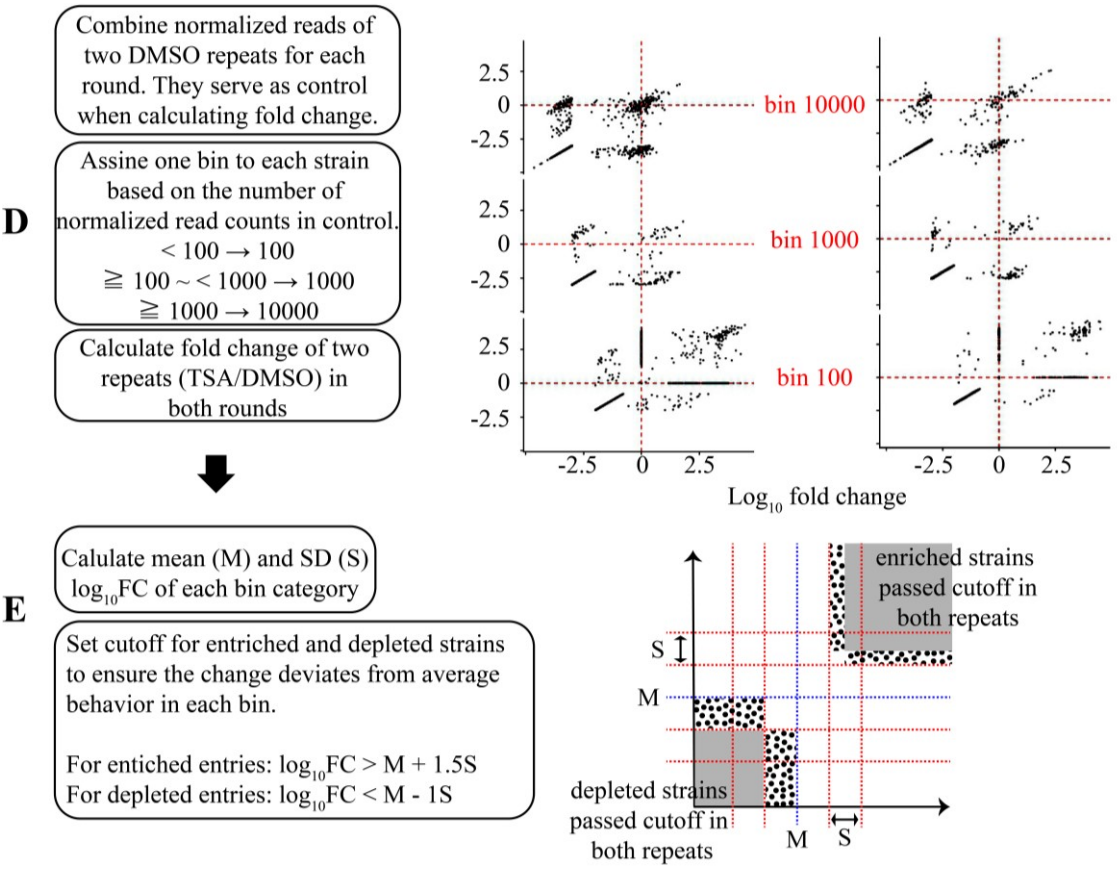

Figure 5.3 continued. Bioinformatic pipeline for processing sequencing data

(D.) Normalized read counts of two DMSO replicates in each round were averaged. This number serves as a reference to calculate fold of enrichment and is used to assign reads to three different bins. The log10 value of enrichment of two TSA-replicates were plotted against each other. **(E.)** Schematic illustration of the cut off set for enriched and depleted strains. The mean (M) and standard deviation (S) in each bin were calculated. Only changes deviating from the average behavior of the population in each bin was considered enriched or depleted. The cut off for enriched and depleted strains are "$\log_{10}FC > M + 1.5S$" and "$\log_{10}FC < M - 1S$" respectively. Blue-dotted line indicates the average fold of enrichment, while the space between the two lines indicates the standard deviation. The grey area represents strains that pass the cut off in both replicates while the black dotted area represents strains that only pass the cut off in one replicate.

The complete list of the strains and their corresponding genes are included in Appendix 3. The strains demonstrated dynamic changes of the population under TSA treatment when looking at both rounds. Fifty five strains were found enriched only in round 5 while 63 were found only in round 8. A total number of 47 strains were enriched in the fifth round and were also present in the eighth round samples. The depleted strains in the fifth round were absent in eighth round or remained depleted. No strains switched from depleted in fifth round to enriched in eighth round but 12 strains switched from enriched to depleted (Fig. 5.4A). The fold change of these filtered strains showed a similar pattern in both replicates of the fifth or eighth round (Fig. 5.4B).

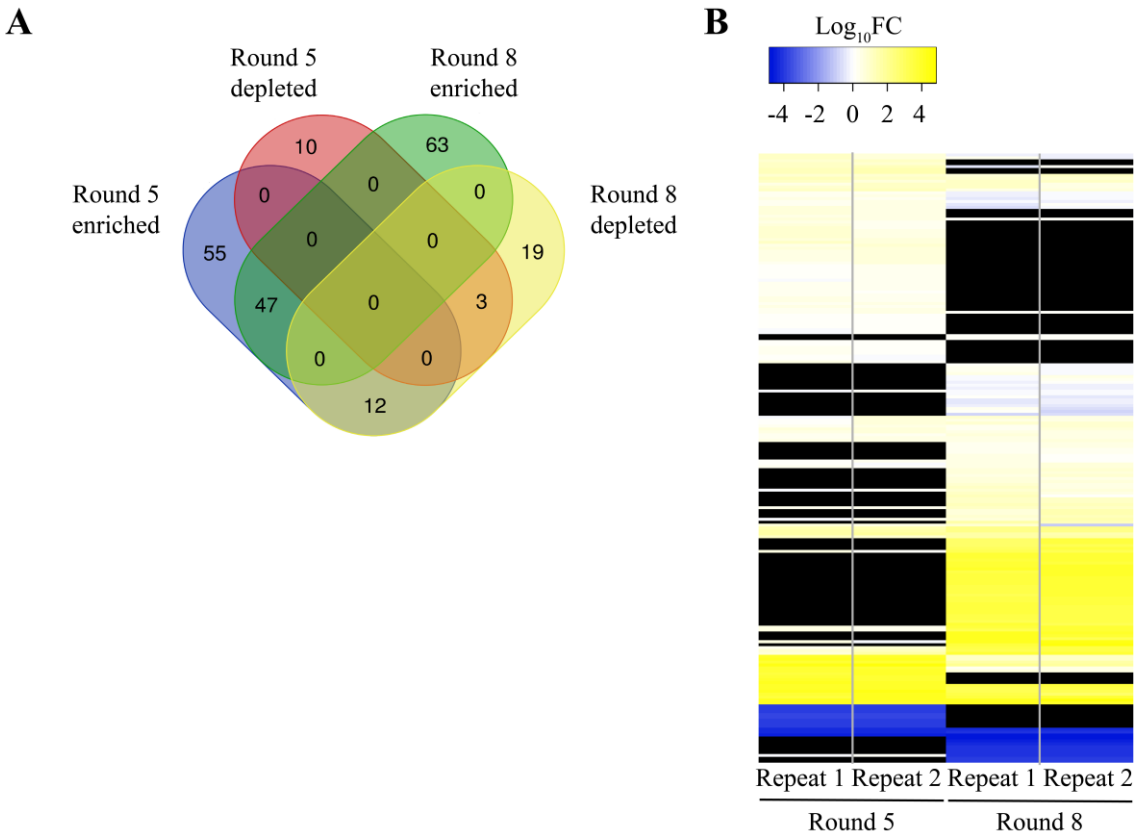

Figure 5.4 Venn diagram and heat map of enriched and depleted strains in fifth and eight rounds

(A.) Venn diagram showing the overlap between strains passing the cut off in the fifth and eighth rounds. The diagram is generated using a webtool (http://bioinformatics.psb.ugent.be/webtools/Venn/). **(B)**. Heat map of enriched and depleted strains in fifth or eighth rounds. Log10 fold change values of enriched and depleted strains from both replicates in each round were subjected to heat map analysis (http://www.heatmapper.ca/expression/). Enriched and depleted strain are represented by yellow and blue blocks respectively. Black blocks are strains with a missing value in one of the rounds.

5.3.3 Validation of enriched strains from screen

Many of the individual GWDI strains are available from the *Dictyostelium* Stock Centre, which is a resource that can be used to verify the results of the screen. Therefore, seven genes were selected based on the extent of enrichment (FC > 4 in either round and passed

the set cutoff) along with their availability in the Stock Centre. For each gene, the strain carrying the insertion site identified in screen (site 1), as well as a second strain with a different insertion site at the same gene (site 2) were included in the subsequent analysis (Fig. 5.5A). Among the seven genes selected, two have insertion sites in the promoter region while the others are in gene body. These genes are numbered from 1 to 7 according to the bin category and number of gene ID. Of note, gene Nos. 4 and 7 show rapid growth in HL5 and so will have a selective advantage (Gruenheit et al., 2019). Both strains of selected genes were subjected to a growth assay on plastic in HL5 under DMSO or 4 μM TSA treatment for 48 hours with a starting cell number of $5 \times 10^{3.}$ cells in 24-well plates.

Among the 7 genes tested, 4, 5 and 6 showed significant TSA resistance in the strains identified by screen (site 1). The growth inhibition by TSA in these strains ranged from 33 to 39% while in Ax4bsR cells it was 51% ($p < 0.05$). Though growth inhibition of site 1 strains of gene 3 (40%) and 7 (27%) was also lower than control cells, the large error bar made the result insignificant. Thus, except for gene 1 and 2, among 7 genes tested, 5 of the site 1 strains have shown resistance to TSA to different extent (Fig. 5.5B). The site 2 strains of gene 3 ,6 and 7 were also more resistant to TSA (inhibited by 18 to 43%, $p < 0.05$). This suggests that the resistant phenotype observed in site 1 strains of gene 3, 6 and 7 are likely due to mutation of the corresponding genes, not a consequence of a

second unknown insertion. However, the result of gene 2 is intriguing. Though its site 1 strain is not resistant to TSA, the site 2 strain is significantly more resistant (26%, $p < 0.05$). The result confirms that the majority of enriched strains discovered by REMI-seq screen are indeed resistant to TSA to various extent, at least for those with a minimum FC > 4 in either round. Interestingly, insertions into gene No.7 have been reported to cause fast-growth in HL5, but this strain also showed TSA-resistance in growth.

Strains with disruption of H3K4 trimethylation such as *set1*$^{-}$ and H3K4A cells showed resistance to TSA during development but not during growth, where they were in fact more sensitive than parental cells, suggesting that resistance during growth and development are mechanistically distinct (See chapter 3). To understand if these strains selected for resistance during growth are also resistant to TSA during development, the 14 strains were subjected to development in the presence of 2 μM TSA on agar and pictures were taken after 24 hours of development.

The development assay showed that none of the tested strains is more resistant to TSA-induced developmental inhibition compared to Ax4^{bsR} cells (Fig. 5.5C). Instead, some strains that were resistant in growth under TSA treatment were more sensitive during development. For example, development of site 1 strains of gene 3 to 5, and site 2 strains

of gene 2, 3 and 6, were at tight aggregate stage while that of Ax4^{bsR} cells were at slug stage.

A

No.	Gene ID	Site 1*	Site 2	Bin	Adv	$Log_{10}FC$ R5	$Log_{10}FC$ R8	Description
1	DDB_G0267844	712	132	100	No	4.00	3.25	similar to plant expansins
2	DDB_G0270586	672	1430	100	No	N/A	3.67	putative transporter
3	DDB_G0270934	1154	182	100	No	N/A	3.67	Putative triacylglycerol lipase-like protein
4	*DDB_G0270964	-318	439	100	Yes	N/A	3.31	putative pseudogene
5	DDB_G0270452	1836	1274	1000	No	0.59	N/A	cyclin-like F-box containing protein
6	*DDB_G0269028	-281	-136	1000	No	1.16	0.90	hypothetical protein
7	DDB_G0270640	461	2963	10000	Yes	0.84	1.13	putative spindle pole body-interacting protein

*Site 1 is the bsR insrtion site carried by strains identified by screen, while site 2 is in an independent strain with a different insertion at the same gene. The position of the insertion site is indicated by relative distance to the first nucleotide of the indicated genes.

B

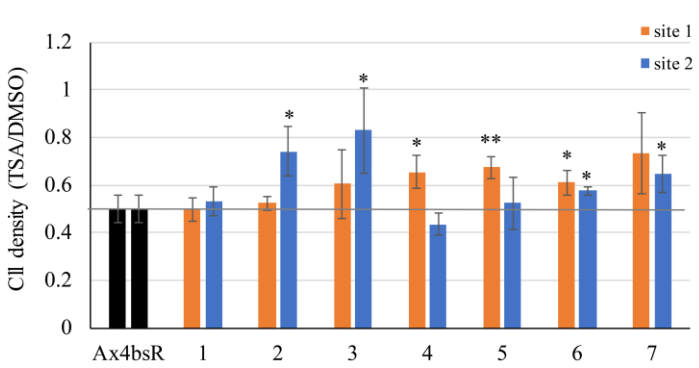

Figure 5.5 Validation of REMI-seq results using available individual GWDI strains **(A.)** List of genes covered by strains purchased from *Dictyostelium* Stock Centre. A total of 14 strains covering two insertion sites of 7 genes were selected. More detail of the 14 strains are listed in Appendix 4. **(B.)** Cells were cultured in HL5 in 24-well plates (5×10^3 cells/well starting density) under DMSO or 4 μM TSA treatment. Relative cell density (TSA/DMSO) was calculated after 48 hours of growth, data shown as mean ± SD from three independent experiments. The statistical significance was calculated using T-Test relative to Ax4^{bsR} cells (*, $p < 0.05$; **, $p < 0.01$).

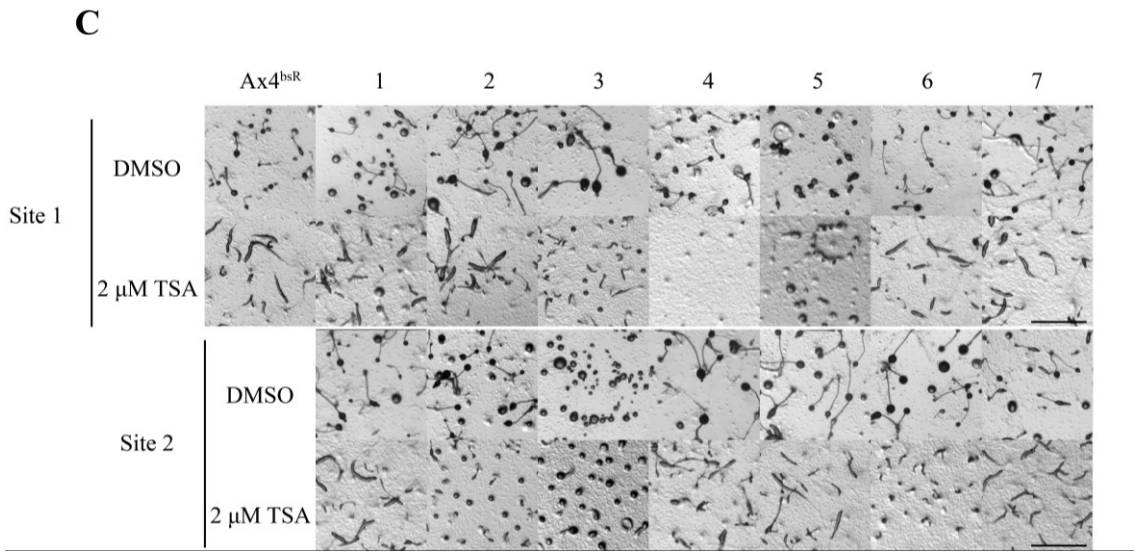

Figure 5.5 continued. Validation of REMI-seq results using available individual GWDI strains

(C.) TSA was applied on top of 1.5% agar (w/v) in a 24-well plate and allowed to dry for 2 hours at 22°C. Exponential $Ax4^{bsR}$ and insertional mutant cells were collected and washed twice with KK2. Cells were then transferred to agar (2.8×10^6 cells/well) containing 2 µM TSA. Images were taken after 24 hours of development. Figures are representative of two biological repeats. Scale bar represents 1 mm.

5.3.4 Candidate genes and pathways involved in TSA-induced growth inhibition

To understand which functional category and pathways are over-represented in the enriched genes, annotated genes with minimum FC > 4 in either round (44 in total) were subjected to STRING analysis (https://string-db.org/).

The analysis revealed that genes involved in signal transduction and response to external stress are overrepresented (Fig. 5.6A). These include genes encoding for protein kinases and genes involved in Ras signaling pathway (Appendix 5). STRING analysis also

showed that genes in the pathway "polo-like kinase mediated events" were strongly enriched with false discovery rate less than 0.0043. The term is associated with regulation of G2/M transition, which involves WEE kinase that inhibits the entry of mitosis (Kellogg, 2003). In *Dictyostelium* three potential WEE kinases have been reported (Goldberg et al., 2006). Surprisingly, strains with mutation in two out of the three genes encoding WEE kinases were found enriched after the TSA screen (Fig. 5.6B). Interestingly, *ku70* and *fhkD*, a protein similar to the mammalian cell cycle checkpoint kinase *chk2*, were also found in the list and these two proteins have been reported to be co-expressed in other species (Fig. 5.6B). The results suggest that genes involved in DNA repair and the resulting G2/M cell cycle check point may play an important role in the mode of action of TSA-induced growth inhibition. To understand if mutation of *ku70* results in TSA resistance during growth, a *ku70*$^-$ strain which is available in our lab (Couto et al., 2011) was subjected to 4 μM TSA treatment for 24 and 48 hours with a starting cell number of 5×10^3 cells/ml in 24-well plates. The result confirms that in the absence of ku70, cells are more resistant to TSA-induced growth inhibition. The cell density of TSA-treated Ax2 cells was 69% and 58% relative to DMSO-treated cells after 24 and 48 hours respectively (Fig. 5.6C). However, TSA-treated *ku70*$^-$ cells were at 88% ($p < 0.01$) and 73% ($p < 0.05$) after 24 and 48 hours respectively.

A

Biological Process (GO)				
#term ID	**term description**	**count**	**background**	**FDR**
GO:0006468	protein phosphorylation	5	282	0.043
GO:0033554	cellular response to stress	5	296	0.043
GO:0035556	intracellular signal transduction	5	267	0.043
GO:0060255	regulation of macromolecule metabolic process	6	435	0.043
GO:0006468	protein phosphorylation	5	282	0.043
Molecular Function (GO)				
#term ID	**term description**	**count**	**background**	**FDR**
GO:0000166	nucleotide binding	9	888	0.028
GO:0004674	protein serine/threonine kinase activity	4	240	0.0286
GO:0004386	helicase activity	2	45	0.0395
GO:0005085	guanyl-nucleotide exchange factor activity	2	45	0.0395
Reactome Pathways				
#term ID	**term description**	**count**	**background**	**FDR**
DDI-156711	Polo-like kinase mediated events	2	4	0.0043

Figure 5.6 GO term, pathway and co-expression analysis of genes mutated in enriched strains

Annotated genes mutated in strains with FC > 4 in either round were subjected to STRING analysis (https://string-db.org/). **(A.)** List of enriched GO terms and pathways in the genes analyzed.

B

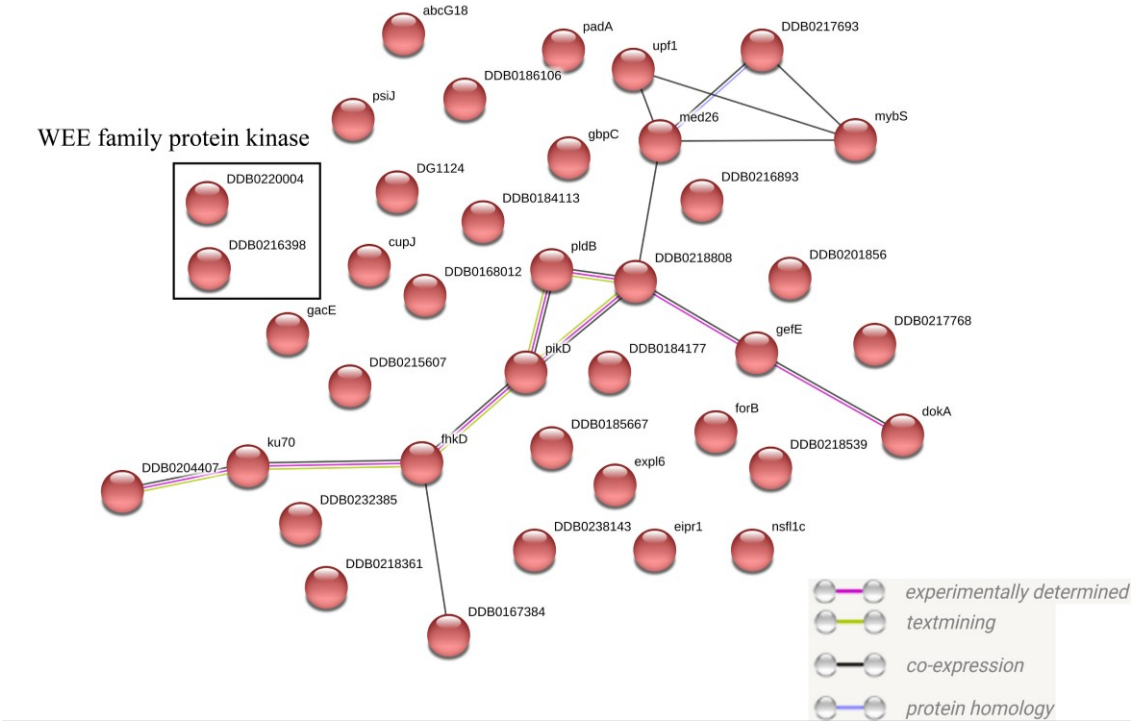

C

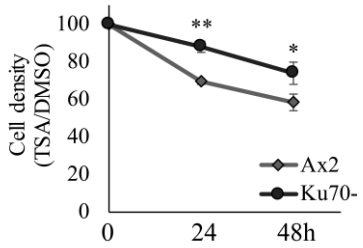

Figure 5.6 continued. GO term, pathway and co-expression analysis of genes mutated in enriched strains

(B.) Network of analyzed genes showing potential co-expression (black lines), putative interaction determined by experiment (purple lines). Genes that are often mentioned together are linked by yellow lines. Blue lines indicate that the protein sequence of the two genes have some sequence similarity. **(C.)** Cells were cultured in HL5 in 24-well plates (5×10^3 cells/well starting density) under DMSO or 4 µM TSA treatment. Relative cell density (TSA/DMSO) was calculated after 24 and 48 hours of growth. Data shown as mean ± SD from three independent experiments. The statistical significance was calculated using T-Test relative to $Ax4^{bsR}$ cells (*, $p < 0.05$; **, $p < 0.01$).

5.4 Discussion

In this chapter I successfully applied REMI-seq technology to identify mutants resistant to TSA during growth. However, we are the first lab except for the REMI-seq team to report use of this technology so there are several things worth discussing.

This technology worked very well in our hands. The screen is a population-based experiment that allows parallel phenotyping and we successfully identified potential genes that when mutated confer an advantage or disadvantage under TSA-treatment. Second, the available individual GWDI strains enable a quick verification of the screen using identified clones and/or clones with a second insertion site in the same gene. Growth of a single clone in the presence of drug is a very different assay to the population-based assay used for identification, but initial analysis suggests that the majority of mutants identified by REMI-seq are resistant to TSA under more standard growth conditions and validates this as a screening approach. I did not have an opportunity to test the sensitivity of depleted strains in the presence of TSA but this needs to be carried out to verify this technology to identify sensitive mutants.

However, there are also some disadvantages of the technology. One technical issue is that when digesting gDNA with I-SceI, the enzyme also cuts *rnlA* (IG7) in mitochondrial

DNA due to star activity. The consequence of the undesired digestion is contamination of the library with *rnlA* fragments of a similar size. Although the issue is dealt with by digesting the DNA sample with pshAI, which is enriched in mitochondrial DNA, the proportion of mitochondrial reads was still high in our hands. Prior to sending the library for Illumina sequencing, the library was quality-checked by cloning into pJET1.2 vectors followed by Sanger sequencing. Among 23 sequenced clones, 26% of them belong to mitochondrial DNA while 18% of them could not be mapped onto the genome of *Dictyostelium*. These contribute to the reads filtered out in the first step of analysis (Fig. 5.3A).

Another issue is the low confidence of strains in bin 100. Most of the enriched strains were found in bin 100 before applying the cutoff. However, the variation between the two replicates in bin 100 is large (Fig. 5.3A). Though most of the strains in bin 100 were filtered after applying the cutoff, validation of the selected 4 site 1 strains in bin 100 only confirmed one significantly resistant and one potentially resistant strain (Fig. 5.5B). Of note, the log10 fold enrichment of gene 1 is high, with a value of 4 and 3.25 in round 5 and 8 respectively. However, the validation failed to support these numbers.

The final issue is that not all strains identified by screen are available in the GWDI bank

deposited in the *Dictyostelium* Stock Centre. This markedly reduced the choices I had when deciding which strains should be verified experimentally. In addition, a second insertion site or a random mutation besides the identified site is possible so even if the strain is resistant, this might not be due to loss of the identified gene. This issue can be partially resolved by verifying two individual clones that have the same insertion site or another insertion to disrupt the same gene, reducing the chance that a second unknown insertion or random mutation is the cause of identified phenotype. However, it is always essential to remake mutants for important targets to verify the resistance phenotype. It should also be pointed out that all the strains screened are insertion mutants, predicted to lead to loss of expression or expression of truncated proteins. Therefore, gain-of -function phenotypes due to overexpression or point mutations may not be detected by REMI-seq.

Of the strains identified, at least three are resistant during growth, and if both insertion sites are considered, 6 out of 7 show resistance in at least one strain. However, none of the strains showed resistance during development, further reinforcing the suggestion that different mechanisms underlie TSA inhibition of these two processes. In gene 3, insertion near the 5' end of the gene led to a developmental phenotype not apparent in the original insertion, confirming that the phenotypes of the strains with insertions in the same gene are not always equivalent. This could be due to a mutation elsewhere in the genome in

one of the strains, or could reflect the expression of a residual truncated protein for an insertion near the 3’ end of the gene.

6: General discussion

In this thesis I examined how loss of dynamic acetylation (i.e. rapid acetylation of H3K4me3 in the presence of TSA) affects the inhibitory effects of TSA on cellular growth and development of *Dictyostelium*. This was achieved by utilizing cells lacking H3K4me3 due to loss of the gene encoding a methyltransferase (Set1) or carrying a point mutation on K4 on H3a or H3b. In addition, a gene encoding for a potential *Dictyostelium* orthologue of Sgf29 was identified and its role in dynamic acetylation was revealed.

All three KDACis (TSA, SAHA, and VPA) tested in this thesis inhibit the development of *Dictyostelium*. However, cells lacking H3K4me3 exhibited resistance to hydroxamates-induced developmental inhibition (Fig. 3.3). This was further investigated in detail with a focus on TSA. Loss of *Set1* or mutation of H3K4 on H3a/b confers resistance to the developmental inhibition by TSA, suggesting that methylation of H3K4 plays a key role (Fig. 3.4 and 3.5). The phenotype was then connected to loss of dynamic acetylation supported by the similar resistance phenotype of *sgf29*$^{-}$ cells. Loss of *sgf29* not only confers developmental resistance to TSA but directly impacted on dynamic acetylation (Fig. 4.5 and 4.6). These results strongly suggest that, the development barrier set by TSA can be overcome by impaired dynamic acetylation due to loss of H3K4me3

(*set1*-, H3aK4A and H3bK4A cells) or *sgf29*. But how could impairing dynamic acetylation lead to the escape of developing *Dictyostelium* cells from TSA-induced development inhibition?

During the development of *Dictyostelium*, expression of genes related to vegetative growth are repressed while genes related to development are activated, and the proportion of down-regulated genes (65% to 83%) is larger than up-regulated ones (Driessche et al., 2002; Iranfar et al., 2003). The regulation is time sensitive with the expression of a small portion of vegetative and development genes being inhibited and activated respectively in the first 4 hours of development. The up- and down- regulation of the majority of these genes happens after 6 hours of development (Katoh et al., 2007). Interestingly, the global change of the levels of the active transcription mark H3K4me3 during *Dictyostelium* development coincides with the major trend of gene down-regulation. Between 4 to 8 hours after the onset of development, the level of bulk H3K4me3 starts to decrease and stabilizes after 20 hours of development (Chubb et al. 2006). It has been shown that during development of *Dictyostelium*, loss of H3K4me3 at the 5'end of a gene locus correlates to decrease of gene expression as in the case of *rasG5* (Chubb et al. 2006). However, while the bulk of the H3K4me3 decreases, some genes gain H3K4me3 and their expression increases as in the case of *acaA* (Chubb et al. 2006). Thus, one can

hypothesize that changes in H3K4me3 levels at particular locations may be critical for correct gene regulation during development of *Dictyostelium*. However, in the absence of H3K4me3 there may be a compensation mechanism to ensure proper development as evidenced by the normal development of *set1* null cells.

Upon TSA treatment, developing *Dictyostelium* cells accumulate H3K9 acetylation rapidly within 4 hours (Fig. 3.7). Moreover, H3K4me3 histones are subjected to rapid accumulation of acetylation upon TSA treatment and this process is mediated by Sgf29 (Fig. 4.5). This could result in genes associated with the H3K4me3 mark being kept in the active state while its down-regulation marks developmental progress, thus impacting the entry into certain development stages. However, TSA-induced development inhibition is only observed if cells are exposed to TSA during the first 4 hours of development (Fig. 3.6). This indicates either 1) the developmental regulation of genes subject to TSA influence is complete after the first 4 hours or 2) the development program has passed a critical checkpoint such that the TSA-induced change becomes a minor factor. Of course, both speculations could be true at the same time. Interestingly, it has been shown that *Dictyostelium* cells are committed to development after the first 4 hours of development and after that timepoint the developmental process is irreversible even in the presence of food source (Katoh et al., 2007). When bacteria or a mixture of amino

acids is provided to developing cells within the first 4 hours, development is terminated, suggesting that metabolic regulation of amino acids is involved in the commitment (Katoh et al., 2007). In agreement with this discovery, down regulation of genes in ribosomal biogenesis has been reported during *Dictyostelium* development (Driessche et al., 2002; Iranfar et al., 2003; Rosengarten et al., 2015). It will be interesting to examine if the expression pattern of genes involved in ribosomal biogenesis is changed by TSA during development. Nevertheless, the running hypothesis is that change in H3K4me3 is critical for correct up- and down-regulation of genes during *Dictyostelium* development, and upon TSA treatment the dynamic acetylation interferes with the process by bringing in more acetylation to H3K4me3 marked chromatin. The consequence of this interference in the case of *Dictyostelium* is inhibition of development. However, the scenario may be cell-type specific and even dependent on the developmental stage in human cells. It is known that in human the pattern of the H3K4me3 mark across the genome is cell type-specific (Koch et al., 2007), and is dynamically changed during development (Shulha et al., 2013). Thus, targeting both KDACs and key components mediating dynamic acetylation may induce undiscovered synergetic effect(s) that are worth investigating in disease models.

Though loss of Set1 confers resistance to hydroxamates (TSA and SAHA) during

development, it also sensitizes cells to these compounds during growth, and similar results were observed in H3aK4a and H3bK4a cells (Fig. 3.2). In addition, *sgf29*$^{-}$ cells also showed the same phenotype in response to TSA, suggesting the increased sensitivity is due to loss of dynamic acetylation (Fig. 4.6). However, the mechanism underlying the phenotype is unclear. To this point, mutations have been identified that make cells resistant to TSA either during growth or during development but not both, although the screens are not saturating and such mutations may exist. This separation of function however, does raise an interesting question as to sensitivity of tumour cells to KDACi inhibition and acquired resistance during treatment. Depending on the mechanism of action of the KDACi, for example inducing differentiation or apoptosis of the tumour cells, different mutations may lead to resistance. It will be of interest to determine the consequences of introducing the mutations identified in this work into a range of human tumour cells to assess the KDACi resistance.

Potential genes involved in TSA-induced growth inhibition were revealed in this study by the REMI-seq screen (Appendix 3). Strains carrying plasmid insertions into these genes were enriched in the population under TSA treatment, indicating resistance to TSA. A small number of these were verified as TSA-resistant when grown as single clones, rather than in a mixed population (Fig. 5.5) validating this approach. This growth of a

population of cells can be argued to better mimic the situation in which a whole tumour is being subjected to drug during treatment regimes. Examples of these genes include ABC transporters, protein kinases, transcription factors and genes involved in DNA repair and cell cycle check points (Fig. 5.6). It has been reported that increased efflux of a KDACi Romidepsin due to the increased expression of ABCC, an ABC transporter, contributes to cellular resistance to KDACi Romidepsin in human cancer cells (Xiao et al., 2005). One of the ABC transporter genes identified as enriched in the presence of TSA by the REMI-seq screen in this study is *abcG18*, which has been shown to be involved in endocytosis in *Dictyostelium* (Brazill et al., 2001). Thus, resistance to TSA could also arise from mutation of influx transporters. In human cells only a very small number of other mutations leading to resistance mechanisms to KDACi have been reported and are all due to increased expression of genes encoding for thioredoxin, anti-apoptotic proteins or KDACs (reviewed in Robey et al., 2011). It is not surprising that these genes were not identified in this study as REMI-seq will favour identification of loss of function leading to resistance, not overexpression. It is possible that plasmid insertion in a negative regulatory element, for example in a promoter, will lead to increased expression, or that it could lead to expression of a truncated, activated protein but this is less likely than the insertion leading to loss of function. It is also possible that deletion of negative regulator(s) of the above genes could lead to their subsequent

activation.

In summary, the major finding of this thesis is the identification of dynamic acetylation as a key mechanism in the mode of action of KDACis, especially hydroxamates, in development in *Dictyostelium*. This provides a future research direction in mammalian systems to determine the consequence of simultaneously targeting KDAC and components in dynamic acetylation in different disease models. In addition, the newly established technique REMI-seq has been utilized in this thesis and proven successful in identifying mutations leading to resistance to TSA during growth, providing a useful reference for future users of the technique. The result of the screen also provides a list of candidate genes whose mutation are likely to result in TSA resistance.

7. References

Adachi, H., Hasebe, T., Yoshinaga, K., Ohta, T., Sutoh, K. (1994). **Isolation of Dictyostelium discoideum Cytokinesis Mutants by Restriction Enzyme-Mediated Integration of the Blasticidin S Resistance Marker** Biochemical and Biophysical Research Communications 205(3), 1808-1814. https://dx.doi.org/10.1006/bbrc.1994.2880

Archer, S., Meng, S., Shei, A., Hodin, R. (1998). **p21WAF1 is required for butyrate-mediated growth inhibition of human colon cancer cells** Proceedings of the National Academy of Sciences 95(12), 6791-6796. https://dx.doi.org/10.1073/pnas.95.12.6791

Ashkenazi, A. (2002). **Targeting death and decoy receptors of the tumour-necrosis factor superfamily** Nature Reviews Cancer 2(6), nrc821. https://dx.doi.org/10.1038/nrc821

Avvakumov, N., Côté, J. (2007). **The MYST family of histone acetyltransferases and their intimate links to cancer** Oncogene 26(37), 1210608. https://dx.doi.org/10.1038/sj.onc.1210608

Baptista, T., Grünberg, S., Minoungou, N., Koster, M., Timmers, H., Hahn, S., Devys, D., Tora, L. (2017). **SAGA Is a General Cofactor for RNA Polymerase II Transcription** Molecular Cell 68(1), 130-143.e5. https://dx.doi.org/10.1016/j.molcel.2017.08.016

Barbaric, S., Reinke, H., Hörz, W. (2003). **Multiple Mechanistically Distinct Functions of SAGA at the PHO5 Promoter** Molecular and Cellular Biology 23(10), 3468-3476. https://dx.doi.org/10.1128/mcb.23.10.3468-3476.2003

Batova, A., Shao, L., Diccianni, M., Yu, A., Tanaka, T., Rephaeli, A., Nudelman, A., Yu, J. (2002). **The histone deacetylase inhibitor AN-9 has selective toxicity to acute leukemia and drug-resistant primary leukemia and cancer cell lines** Blood 100(9), 3319-3324. https://dx.doi.org/10.1182/blood-2002-02-0567

Berger, S., Piña, B., Silverman, N., Marcus, G., Agapite, J., Regier, J., Triezenberg, S., Guarente, L. (1992). **Genetic isolation of ADA2: A potential transcriptional adaptor required for function of certain acidic activation domains** Cell 70(2), 251-265. https://dx.doi.org/10.1016/0092-8674(92)90100-q

Bian, C., Xu, C., Ruan, J., Lee, K., Burke, T., Tempel, W., Barsyte, D., Li, J., Wu, M., Zhou, B. (2011). **Sgf29 binds histone H3K4me2/3 and is required for SAGA complex recruitment and histone H3 acetylation** The EMBO journal 30(14), 2829-2842. https://dx.doi.org/10.1038/emboj.2011.193

Bolden, J., Peart, M., Johnstone, R. (2006). **Anticancer activities of histone deacetylase inhibitors** Nature Reviews Drug Discovery 5(9), nrd2133. https://dx.doi.org/10.1038/nrd2133

Bonnet, J., Wang, C., Baptista, T., Vincent, S., Hsiao, W., Stierle, M., Kao, C., Tora, L., Devys, D. (2014). **The SAGA coactivator complex acts on the whole transcribed genome and is required for RNA polymerase II transcription** Genes & Development 28(18), 1999-2012. https://dx.doi.org/10.1101/gad.250225.114

Bowers, E., Yan, G., Mukherjee, C., Orry, A., Wang, L., Holbert, M., Crump, N., Hazzalin, C., Liszczak, G., Yuan, H., Larocca, C., Saldanha, S., Abagyan, R., Sun, Y., Meyers, D., Marmorstein, R., Mahadevan, L., Alani, R., Cole, P. (2010). **Virtual Ligand Screening of the p300/CBP Histone Acetyltransferase: Identification of a Selective Small Molecule Inhibitor** Chemistry & Biology 17(5), 471-482. https://dx.doi.org/10.1016/j.chembiol.2010.03.006

Bracker, T., Sommer, A., Fichtner, I., Faus, H., Haendler, B., Hess-Stumpp, H. (2009). **Efficacy of MS-275, a selective inhibitor of class I histone deacetylases, in human colon cancer models** International Journal of Oncology 35(4), 909-20. https://dx.doi.org/10.3892/ijo_00000406

Brazill, D., Meyer, L., Hatton, R., Brock, D., Gomer, R. (2001). **ABC transporters required for endocytosis and endosomal pH regulation in Dictyostelium.** Journal of cell science 114(Pt 21), 3923-32. https://www.ncbi.nlm.nih.gov/pubmed/11719559

Briggs, S., Bryk, M., Strahl, B., Cheung, W., Davie, J., Dent, S., Winston, F., Allis, C. (2001). **Histone H3 lysine 4 methylation is mediated by Set1 and required for cell**

growth and rDNA silencing in Saccharomyces cerevisiae Genes & Development 15(24), 3286-3295. https://dx.doi.org/10.1101/gad.940201

Bu, P., Evrard, Y., Lozano, G., Dent, S. (2007). **Loss of Gcn5 Acetyltransferase Activity Leads to Neural Tube Closure Defects and Exencephaly in Mouse Embryos** Molecular and Cellular Biology 27(9), 3405-3416. https://dx.doi.org/10.1128/mcb.00066-07

Burgess, A., Ruefli, A., Beamish, H., Warrener, R., Saunders, N., Johnstone, R., Gabrielli, B. (2004). **Histone deacetylase inhibitors specifically kill nonproliferating tumour cells** Oncogene 23(40), 1207893. https://dx.doi.org/10.1038/sj.onc.1207893

Butler, L., Agus, D., Scher, H., Higgins, B., Rose, A., Cordon-Cardo, C., Thaler, H., Rifkind, R., Marks, P., Richon, V. (2000). **Suberoylanilide hydroxamic acid, an inhibitor of histone deacetylase, suppresses the growth of prostate cancer cells in vitro and in vivo.** Cancer research 60(18), 5165-70. https://www.ncbi.nlm.nih.gov/pubmed/11016644

Butler, J., Dent, S. (2013). **The role of chromatin modifiers in normal and malignant hematopoiesis** Blood 121(16), 3076-3084. https://dx.doi.org/10.1182/blood-2012-10-451237

Candau, R., Zhou, J., Allis, C., Berger, S. (1997). **Histone acetyltransferase activity and interaction with ADA2 are critical for GCN5 function in vivo** The EMBO Journal 16(3), 555-565. https://dx.doi.org/10.1093/emboj/16.3.555

Carrozza, M., Utley, R., Workman, J., Côté, J. (2003). **The diverse functions of histone acetyltransferase complexes** Trends in Genetics 19(6), 321-329. https://dx.doi.org/10.1016/s0168-9525(03)00115-x

Cerbo, V., Schneider, R. (2013). **Cancers with wrong HATs: the impact of acetylation** Briefings in Functional Genomics 12(3), 231-243. https://dx.doi.org/10.1093/bfgp/els065

Chen, L., Wei, T., Si, X., Wang, Q., Li, Y., Leng, Y., Deng, A., Chen, J., Wang, G., Zhu, S., Kang, J. (2013). **Lysine Acetyltransferase GCN5 Potentiates the Growth of Non-small Cell Lung Cancer via Promotion of E2F1, Cyclin D1, and Cyclin E1**

Expression Journal of Biological Chemistry 288(20), 14510-14521. https://dx.doi.org/10.1074/jbc.m113.458737

Cheng, G., Liu, F., Asai, T., Lai, F., Man, N., Xu, H., Chen, S., Greenblatt, S., Hamard, P., Ando, K., Chen, X., Wang, L., Martinez, C., Tadi, M., Wang, L., Xu, M., Yang, F., Shiekhattar, R., Nimer, S. (2017). **Loss of p300 accelerates MDS-associated leukemogenesis** Leukemia 31(6), 1382. https://dx.doi.org/10.1038/leu.2016.347

Chubb, J., Bloomfield, G., Xu, Q., Kaller, M., Ivens, A., Skelton, J., Turner, B., Nellen, W., Shaulsky, G., Kay, R., Bickmore, W., Singer, R. (2006). **Developmental timing in Dictyostelium is regulated by the Set1 histone methyltransferase** Developmental Biology 292(2), 519-532. https://dx.doi.org/10.1016/j.ydbio.2005.12.054

Cieniewicz, A., Moreland, L., Ringel, A., Mackintosh, S., Raman, A., Gilbert, T., Wolberger, C., Tackett, A., Taverna, S. (2014). **The Bromodomain of Gcn5 Regulates Site Specificity of Lysine Acetylation on Histone H3** Molecular & Cellular Proteomics 13(11), 2896-2910. https://dx.doi.org/10.1074/mcp.m114.038174

Ciurciu, A., Komonyi, O., Pankotai, T., Boros, I. (2006). **The Drosophila Histone Acetyltransferase Gcn5 and Transcriptional Adaptor Ada2a Are Involved in Nucleosomal Histone H4 Acetylation** ▾ Molecular and Cellular Biology 26(24), 9413-9423. https://dx.doi.org/10.1128/mcb.01401-06

Cocorocchio, M., Baldwin, A., Stewart, B., Kim, L., Harwood, A., Thompson, C., Andrews, P., Williams, R. (2017). **Curcumin and derivatives function through protein phosphatase 2A and presenilin orthologues in Dictyostelium discoideum** Disease Models & Mechanisms 11(1), dmm.032375. https://dx.doi.org/10.1242/dmm.032375

Cohen, L., Amin, S., Marks, P., Rifkind, R., Desai, D., Richon, V. (1999). **Chemoprevention of carcinogen-induced mammary tumorigenesis by the hybrid polar cytodifferentiation agent, suberanilohydroxamic acid (SAHA).** Anticancer research 19(6B), 4999-5005. https://www.ncbi.nlm.nih.gov/pubmed/10697502

Consortium, T. (2012). **Large-Scale Screening for Targeted Knockouts in the Caenorhabditis elegans Genome** G3: Genes|Genomes|Genetics 2(11), 1415-1425. https://dx.doi.org/10.1534/g3.112.003830

Couto, A., Wang, H., Green, J., Kiely, R., Siddaway, R., Borer, C., Pears, C., Lakin, N. (2011). **PARP regulates nonhomologous end joining through retention of Ku at double-strand breaks** The Journal of Cell Biology 194(3), 367-375. https://dx.doi.org/10.1083/jcb.201012132

Crump, N., Hazzalin, C., Bowers, E., Alani, R., Cole, P., Mahadevan, L. (2011). **Dynamic acetylation of all lysine-4 trimethylated histone H3 is evolutionarily conserved and mediated by p300/CBP** Proceedings of the National Academy of Sciences 108(), 7814-7819. https://dx.doi.org/10.1073/pnas.1100099108

Daly, K., Shirazi-Beechey, S. (2006). **Microarray Analysis of Butyrate Regulated Genes in Colonic Epithelial Cells** DNA and Cell Biology 25(1), 49-62. https://dx.doi.org/10.1089/dna.2006.25.49

Driessche, N., Shaw, C., Katoh, M., Morio, T., Sucgang, R., Ibarra, M., Kuwayama, H., Saito, T., Urushihara, H., Maeda, M., Takeuchi, I., Ochiai, H., Eaton, W., Tollett, J., Halter, J., Kuspa, A., Tanaka, Y., Shaulsky, G. (2002). **A transcriptional profile of multicellular development in Dictyostelium discoideum.** Development (Cambridge, England) 129(7), 1543-52. https://www.ncbi.nlm.nih.gov/pubmed/11923193

Drogaris, P., Villeneuve, V., Pomiès, C., Lee, E., Bourdeau, V., Bonneil, É., Ferbeyre, G., Verreault, A., Thibault, P. (2012). **Histone Deacetylase Inhibitors Globally Enhance H3/H4 Tail Acetylation Without Affecting H3 Lysine 56 Acetylation** Scientific Reports 2(1), 220. https://dx.doi.org/10.1038/srep00220

Eickholt, B., Towers, G., Ryves, W., Eikel, D., Adley, K., Ylinen, L., Chadborn, N., Harwood, A., Nau, H., Williams, R. (2005). **Effects of Valproic Acid Derivatives on Inositol Trisphosphate Depletion, Teratogenicity, Glycogen Synthase Kinase-3β Inhibition, and Viral Replication: A Screening Approach for New Bipolar Disorder Drugs Derived from the Valproic Acid Core Structure** Molecular Pharmacology 67(5), 1426-1433. https://dx.doi.org/10.1124/mol.104.009308

.

El-Habr, E.A.; Dubois, L.G.; Burel-Vandenbos, F.; Bogeas, A.; Lipecka, J.; Turchi, L.; Lejeune, F.-X.; Coehlo, P.; Yamaki, T.; Wittmann, B.M. (2016). **A driver role for GABA metabolism in controlling stem and proliferative cell state through GHB production in glioma** Acta Neuropathol 133, 645–660. https://doi.org/10.1007/s00401-

016-1659-5

Escriva, H., Bertrand, S., Laudet, V. (2004). **The evolution of the nuclear receptor superfamily** Essays In Biochemistry 40(), 11-26. https://dx.doi.org/10.1042/bse0400011

Finnin, M., Donigian, J., Cohen, A., Richon, V., Rifkind, R., Marks, P., Breslow, R., Pavletich, N. (1999). **Structures of a histone deacetylase homologue bound to the TSA and SAHA inhibitors** Nature 401(6749), 43710. https://dx.doi.org/10.1038/43710

Gao, B., Kong, Q., Zhang, Y., Yun, C., Dent, S., Song, J., Zhang, D., Wang, Y., Li, X., Fang, D. (2017). **The Histone Acetyltransferase Gcn5 Positively Regulates T Cell Activation.** Journal of immunology (Baltimore, Md. : 1950) 198(10), 3927-3938. https://dx.doi.org/10.4049/jimmunol.1600312

Gayther, S., Batley, S., Linger, L., Bannister, A., Thorpe, K., Chin, S., Daigo, Y., Russell, P., Wilson, A., Sowter, H., Delhanty, J., Ponder, B., Kouzarides, T., Caldas, C. (2000). **Mutations truncating the EP300 acetylase in human cancers** Nature Genetics 24(3), 300-303. https://dx.doi.org/10.1038/73536

Glick, R., Swendeman, S., Coffey, D., Rifkind, R., Marks, P., Richon, V., Quaglia, M. (1999). **Hybrid polar histone deacetylase inhibitor induces apoptosis and CD95/CD95 ligand expression in human neuroblastoma.** Cancer research 59(17), 4392-9. https://www.ncbi.nlm.nih.gov/pubmed/10485488

Goldberg, J., Manning, G., Liu, A., Fey, P., Pilcher, K., Xu, Y., Smith, J. (2006). **The Dictyostelium Kinome—Analysis of the Protein Kinases from a Simple Model Organism** PLoS Genetics 2(3), e38. https://dx.doi.org/10.1371/journal.pgen.0020038

Göttlicher, M., Minucci, S., Zhu, P., Krämer, O., Schimpf, A., Giavara, S., Sleeman, J., Coco, F., Nervi, C., Pelicci, P., Heinzel, T. (2001). **Valproic acid defines a novel class of HDAC inhibitors inducing differentiation of transformed cells** The EMBO Journal 20(24), 6969-6978. https://dx.doi.org/10.1093/emboj/20.24.6969

Green, M., Sambrook, J. (2012). **Molecular Cloning: A LABORATORY MANUAL** Cold Spring Harbor, N.Y.: Cold Spring Harbor Laboratory Press

Gruenheit, N., Baldwin, A., Stewart, B., Jaques, S., Keller, T., Parkinson, K., Chisholm,

R., Harwood, A., Thompson, C. (2019). **REMI-seq: Development of methods and resources for functional genomics in Dictyostelium** bioRxiv https://dx.doi.org/10.1101/582072

Hallson, G., Hollebakken, R., Li, T., Syrzycka, M., Kim, I., Cotsworth, S., Fitzpatrick, K., Sinclair, D., Honda, B. (2012). **dSet1 Is the Main H3K4 Di- and Tri-Methyltransferase Throughout Drosophila Development** Genetics 190(1), 91-100. https://dx.doi.org/10.1534/genetics.111.135863

Halsall, J., Gupta, V., O'Neill, L., Turner, B., Nightingale, K. (2012). **Genes Are Often Sheltered from the Global Histone Hyperacetylation Induced by HDAC Inhibitors** PLoS ONE 7(3), e33453. https://dx.doi.org/10.1371/journal.pone.0033453

Hassan, A., Prochasson, P., Neely, K., Galasinski, S., Chandy, M., Carrozza, M., Workman, J. (2002). **Function and Selectivity of Bromodomains in Anchoring Chromatin-Modifying Complexes to Promoter Nucleosomes** Cell 111(3), 369-379. https://dx.doi.org/10.1016/s0092-8674(02)01005-x

Hayashi, A., Horiuchi, A., Kikuchi, N., Hayashi, T., Fuseya, C., Suzuki, A., Konishi, I., Shiozawa, T. (2010). **Type-specific roles of histone deacetylase (HDAC) overexpression in ovarian carcinoma: HDAC1 enhances cell proliferation and HDAC3 stimulates cell migration with downregulation of E-cadherin** International Journal of Cancer 127(6), 1332-1346. https://dx.doi.org/10.1002/ijc.25151

Hazzalin, C., Mahadevan, L. (2005). **Dynamic Acetylation of All Lysine 4–Methylated Histone H3 in the Mouse Nucleus: Analysis at c-fos and c-jun** PLoS Biol 3(), e393. https://dx.doi.org/10.1371/journal.pbio.0030393

Heintzman, N., Stuart, R., Hon, G., Fu, Y., Ching, C., Hawkins, R., Barrera, L., Calcar, S., Qu, C., Ching, K., Wang, W., Weng, Z., Green, R., Crawford, G., Ren, B. (2007). **Distinct and predictive chromatin signatures of transcriptional promoters and enhancers in the human genome** Nature Genetics 39(3), 311-318. https://dx.doi.org/10.1038/ng1966

Hemshekhar, M., Santhosh, M., Kemparaju, K., Girish, K. (2012). **Emerging Roles of Anacardic Acid and Its Derivatives: A Pharmacological Overview** Basic & Clinical

Pharmacology & Toxicology 110(2), 122-132. https://dx.doi.org/10.1111/j.1742-7843.2011.00833.x

Henry, R., Kuo, Y., Andrews, A. (2013). **Differences in Specificity and Selectivity Between CBP and p300 Acetylation of Histone H3 and H3/H4** Biochemistry 52(34), 5746-59. https://dx.doi.org/10.1021/bi400684q

Hoshikawa, Y., Kwon, H., Yoshida, M., Horinouchi, S., Beppu, T. (1994). **Trichostatin A Induces Morphological Changes and Gelsolin Expression by Inhibiting Histone Deacetylase in Human Carcinoma Cell Lines** Experimental Cell Research 214(1), 189-197. https://dx.doi.org/10.1006/excr.1994.1248

Hsu, D., Chubb, J., Muramoto, T., Pears, C., Mahadevan, L. (2012). **Dynamic acetylation of lysine-4-trimethylated histone H3 and H3 variant biology in a simple multicellular eukaryote** Nucleic Acids Research 40(15), 7247-7256. https://dx.doi.org/10.1093/nar/gks367

Huang, J., Ling, K. (2017). **EZH2 and histone deacetylase inhibitors induce apoptosis in triple negative breast cancer cells by differentially increasing H3 Lys27 acetylation in the BIM gene promoter and enhancers** Oncology Letters 14(5), 5735-5742. https://dx.doi.org/10.3892/ol.2017.6912

Huang, M., Zhang, J., Yan, C., Li, X., Zhang, J., Ling, R. (2019). **Small molecule HDAC inhibitors: promising agents for breast cancer treatment** Bioorganic Chemistry 91(), 103184. https://dx.doi.org/10.1016/j.bioorg.2019.103184

Hung, T., Binda, O., Champagne, K., Kuo, A., cell, J. (2009). **ING4 mediates crosstalk between histone H3 K4 trimethylation and H3 acetylation to attenuate cellular transformation** Molecular Cell 33(), 248-256.

Hyun, K., Jeon, J., Park, K., Kim, J. (2017). **Writing, erasing and reading histone lysine methylations** Experimental & Molecular Medicine 49(4), e324. https://dx.doi.org/10.1038/emm.2017.11

Insinga, A., Monestiroli, S., Ronzoni, S., Gelmetti, V., Marchesi, F., Viale, A., Altucci, L., Nervi, C., Minucci, S., Pelicci, P. (2004). **Inhibitors of histone deacetylases induce tumor-selective apoptosis through activation of the death receptor pathway** Nature

Medicine 11(1), nm1160. https://dx.doi.org/10.1038/nm1160

Iranfar, N., Fuller, D., Loomis, W. (2003). **Genome-Wide Expression Analyses of Gene Regulation during Early Development of Dictyostelium discoideum** Eukaryotic Cell 2(4), 664-670. https://dx.doi.org/10.1128/ec.2.4.664-670.2003

Ito, A., Kawaguchi, Y., Lai, C., Kovacs, J., Higashimoto, Y., Appella, E., Yao, T. (2002). **MDM2–HDAC1-mediated deacetylation of p53 is required for its degradation** The EMBO Journal 21(22), 6236-6245. https://dx.doi.org/10.1093/emboj/cdf616

Jamaladdin, S., Kelly, R., O'Regan, L., Dovey, O., Hodson, G., Millard, C., Portolano, N., Fry, A., Schwabe, J., Cowley, S. (2014). **Histone deacetylase (HDAC) 1 and 2 are essential for accurate cell division and the pluripotency of embryonic stem cells** Proceedings of the National Academy of Sciences 111(27), 9840-9845. https://dx.doi.org/10.1073/pnas.1321330111

Jiang, Z., Li, W., Hu, X., Zhang, Q., Sun, T., Cui, S., Wang, S., Ouyang, Q., Yin, Y., Geng, C., Tong, Z., Cheng, Y., Pan, Y., Sun, Y., Wang, H., Ouyang, T., Gu, K., Feng, J., Wang, X., Wang, S., Liu, T., Gao, J., Cristofanilli, M., Ning, Z., Lu, X. (2019). **Tucidinostat plus exemestane for postmenopausal patients with advanced, hormone receptor-positive breast cancer (ACE): a randomised, double-blind, placebo-controlled, phase 3 trial** The Lancet Oncology 20(6), 806-815. https://dx.doi.org/10.1016/s1470-2045(19)30164-0

Jin, Q., Yu, L., Wang, L., Zhang, Z., Kasper, L., Lee, J., Wang, C., Brindle, P., Dent, S., Ge, K. (2011). **Distinct roles of GCN5/PCAF-mediated H3K9ac and CBP/p300-mediated H3K18/27ac in nuclear receptor transactivation** The EMBO Journal 30(2), 249-262. https://dx.doi.org/10.1038/emboj.2010.318

Kang-Decker, N., Tong, C., Boussouar, F., Baker, D., Xu, W., Leontovich, A., Taylor, W., Brindle, P., Deursen, J. (2004). **Loss of CBP causes T cell lymphomagenesis in synergy with p27Kip1 insufficiency** Cancer Cell 5(2), 177-189. https://dx.doi.org/10.1016/s1535-6108(04)00022-4

Karmodiya, K., Krebs, A., Oulad-Abdelghani, M., Kimura, H., Tora, L. (2012). **H3K9 and H3K14 acetylation co-occur at many gene regulatory elements, while H3K14ac marks a subset of inactive inducible promoters in mouse embryonic stem cells** BMC Genomics 13(1), 424. https://dx.doi.org/10.1186/1471-2164-13-424

Katoh, M., Chen, G., Roberge, E., Shaulsky, G., Kuspa, A. (2007). **Developmental Commitment in Dictyostelium discoideum** ▾ † Eukaryotic Cell 6(11), 2038-2045. https://dx.doi.org/10.1128/ec.00223-07

Keim, M., Williams, R., Harwood, A. (2004). **An inverse PCR technique to rapidly isolate the flanking DNA of Dictyostelium insertion mutants** Molecular Biotechnology 26(3), 221-224. https://dx.doi.org/10.1385/mb:26:3:221

Kellogg, D. (2003). **Wee1-dependent mechanisms required for coordination of cell growth and cell division** Journal of Cell Science 116(24), 4883-4890. https://dx.doi.org/10.1242/jcs.00908

Kijima, M., Yoshida, M., Sugita, K., Horinouchi, S., Beppu, T. (1993). **Trapoxin, an antitumor cyclic tetrapeptide, is an irreversible inhibitor of mammalian histone deacetylase.** The Journal of biological chemistry 268(30), 22429-35. https://www.ncbi.nlm.nih.gov/pubmed/8226751

King, J., Gueho, A., Hagedorn, M., Gopaldass, N., Leuba, F., Soldati, T., Insall, R. (2013). **WASH is required for lysosomal recycling and efficient autophagic and phagocytic digestion** Molecular Biology of the Cell 24(17), 2714-2726. https://dx.doi.org/10.1091/mbc.e13-02-0092

Klose, R., Gardner, K., Liang, G., Erdjument-Bromage, H., Tempst, P., Zhang, Y. (2007). **Demethylation of Histone H3K36 and H3K9 by Rph1: a Vestige of an H3K9 Methylation System in Saccharomyces cerevisiae?** ▾ Molecular and Cellular Biology 27(11), 3951-3961. https://dx.doi.org/10.1128/mcb.02180-06

Knipstein, J., Gore, L. (2011). **Entinostat for treatment of solid tumors and hematologic malignancies** Expert Opinion on Investigational Drugs 20(10), 1455-1467. https://dx.doi.org/10.1517/13543784.2011.613822

Kuo, Y., Andrews, A. (2013). **Quantitating the Specificity and Selectivity of Gcn5-Mediated Acetylation of Histone H3** PLoS ONE 8(2), e54896. https://dx.doi.org/10.1371/journal.pone.0054896

Kurabe, N., Katagiri, K., Komiya, Y., Ito, R., Sugiyama, A., Kawasaki, Y., Tashiro, F.

(2007). **Deregulated expression of a novel component of TFTC/STAGA histone acetyltransferase complexes, rat SGF29, in hepatocellular carcinoma: possible implication for the oncogenic potential of c-Myc** Oncogene 26(38), 1210349. https://dx.doi.org/10.1038/sj.onc.1210349

Kurabe, N., Murakami, S., Tashiro, F. (2015). **SGF29 and Sry pathway in hepatocarcinogenesis** World Journal of Biological Chemistry 6(3), 139-147. https://dx.doi.org/10.4331/wjbc.v6.i3.139

Kuspa, A., Loomis, W. (1992). **Tagging developmental genes in Dictyostelium by restriction enzyme-mediated integration of plasmid DNA.** Proceedings of the National Academy of Sciences 89(18), 8803-8807. https://dx.doi.org/10.1073/pnas.89.18.8803

Kwon, H., Kim, M., Kim, M., Nakajima, H., Kim, K. (2002). **Histone deacetylase inhibitor FK228 inhibits tumor angiogenesis** International Journal of Cancer 97(3), 290-296. https://dx.doi.org/10.1002/ijc.1602

Kwon, S., Zhang, Y., Matthias, P. (2007). **The deacetylase HDAC6 is a novel critical component of stress granules involved in the stress response** Genes & Development 21(24), 3381-3394. https://dx.doi.org/10.1101/gad.461107

Lau, O., Kundu, T., Soccio, R., Ait-Si-Ali, S., Khalil, E., Vassilev, A., Wolffe, A., Nakatani, Y., Roeder, R., Cole, P. (2000). **HATs off Selective Synthetic Inhibitors of the Histone Acetyltransferases p300 and PCAF** Molecular Cell 5(3), 589-595. https://dx.doi.org/10.1016/s1097-2765(00)80452-9

Lee, K., Sardiu, M., Swanson, S., Gilmore, J., Torok, M., Grant, P., Florens, L., Workman, J., Washburn, M. (2011). **Combinatorial depletion analysis to assemble the network architecture of the SAGA and ADA chromatin remodeling complexes** Molecular Systems Biology 7(1), 503. https://dx.doi.org/10.1038/msb.2011.40

Lee, K., Workman, J. (2007). **Histone acetyltransferase complexes: one size doesn't fit all** Nature Reviews Molecular Cell Biology 8(4), 284-295. https://dx.doi.org/10.1038/nrm2145

Li, J., Xue, X., Ruan, J., Wu, M., Zhu, Z., Zang, J. (2010). **Cloning, purification,**

crystallization and preliminary crystallographic analysis of the tandem tudor domain of Sgf29 from Saccharomyces cerevisiae Acta Crystallographica Section F: Structural Biology and Crystallization Communications 66(8), 902-4. https://dx.doi.org/10.1107/s1744309110016726

Li, Y., Seto, E. (2016). **HDACs and HDAC Inhibitors in Cancer Development and Therapy** Cold Spring Harbor Perspectives in Medicine 6(10), a026831. https://dx.doi.org/10.1101/cshperspect.a026831

Li, Y., Shin, D., Kwon, S. (2013). **Histone deacetylase 6 plays a role as a distinct regulator of diverse cellular processes** FEBS Journal 280(3), 775-793. https://dx.doi.org/10.1111/febs.12079

Li, H., Wu, X. (2004). **Histone deacetylase inhibitor, Trichostatin A, activates p21WAF1/CIP1 expression through downregulation of c-myc and release of the repression of c-myc from the promoter in human cervical cancer cells** Biochemical and Biophysical Research Communications 324(2), 860-867. https://dx.doi.org/10.1016/j.bbrc.2004.09.130

Li, S., Shogren-Knaak, M. (2009). **The Gcn5 Bromodomain of the SAGA Complex Facilitates Cooperative and Cross-tail Acetylation of Nucleosomes** Journal of Biological Chemistry 284(14), 9411-9417. https://dx.doi.org/10.1074/jbc.m809617200

Li, Q., Wang, D., Ju, L., Yao, J., Gao, C., Lei, P., Li, L., Zhao, X., Wu, M. (2019). **The hyper-activation of transcriptional enhancers in breast cancer** Clinical Epigenetics 11(1), 48. https://dx.doi.org/10.1186/s13148-019-0645-x

Lohia, R., Jain, P., Jain, M., Mishra, H., Burma, P., Shrivastava, A., Saran, S. (2018). **Deletion of Dictyostelium discoideum Sir2A impairs cell proliferation and inhibits autophagy.** Journal of biosciences 43(2), 351-364. https://www.ncbi.nlm.nih.gov/pubmed/29872023

Loomis, W. (2015). **Genetic control of morphogenesis in Dictyostelium** Developmental Biology 402(2), 146-161. https://dx.doi.org/10.1016/j.ydbio.2015.03.016

Ludwig, E., Francisco, R., Francisco, R., Kaller, M., Nellen, W., Chubb, J. (2006).

Dictyostelium discoideum Protocols Methods Mol. Biol 346(), 491-505. https://dx.doi.org/10.1385/1-59745-144-4:491

Mann, B., Johnson, J., Cohen, M., Justice, R., Pazdur, R. (2007). **FDA approval summary: vorinostat for treatment of advanced primary cutaneous T-cell lymphoma** The oncologist 12(10)https://www.ncbi.nlm.nih.gov/pubmed/17962618

Mariño-Ramírez, L., Levine, K., Morales, M., Zhang, S., Moreland, R., Baxevanis, A., Landsman, D. (2011). **The Histone Database: an integrated resource for histones and histone fold-containing proteins** Database 2011(0), bar048. https://dx.doi.org/10.1093/database/bar048

Marks, P., Breslow, R. (2007). **Dimethyl sulfoxide to vorinostat: development of this histone deacetylase inhibitor as an anticancer drug** Nature Biotechnology 25(1), 84-90. https://dx.doi.org/10.1038/nbt1272

Marks, P., Richon, V., Rifkind, R. (2000). **Histone Deacetylase Inhibitors: Inducers of Differentiation or Apoptosis of Transformed Cells** JNCI: Journal of the National Cancer Institute 92(15), 1210-1216. https://dx.doi.org/10.1093/jnci/92.15.1210

Muñoz-Braceras, S., Mesquita, A., Escalante, R. (2013). **Dictyostelium discoideum as a model in biomedical research. In: Romeralo M, Baldauf S, Escalante R, eds. Dictyostelids Evolution, Genomics and Cell Biology.** Berlin: Springer, 2013:1-34. https://dx.doi.org/10.1007/978-3-642-38487-5_1

Muraoka, M., Konishi, M., Kikuchi-Yanoshita, R., Tanaka, K., Shitara, N., Chong, J., Iwama, T., Miyaki, M. (1996). **p300 gene alterations in colorectal and gastric carcinomas.** Oncogene 12(7), 1565-9. https://www.ncbi.nlm.nih.gov/pubmed/8622873

Müller-Taubenberger, Bönisch, Hake, B. (2011). **The histone methyltransferase Dot1 is required for DNA damage repair and proper development in Dictyostelium** Biochemical and Biophysical Research Communications 404(), 1016-1022. https://dx.doi.org/10.1016/j.bbrc.2010.12.101

Nakata, S., Yoshida, T., Horinaka, M., Shiraishi, T., Wakada, M., Sakai, T. (2004). **Histone deacetylase inhibitors upregulate death receptor 5/TRAIL-R2 and sensitize apoptosis induced by TRAIL/APO2-L in human malignant tumor cells**

Oncogene 23(37), 1207830. https://dx.doi.org/10.1038/sj.onc.1207830

Nebbioso, A., Clarke, N., Voltz, E., Germain, E., Ambrosino, C., Bontempo, P., Alvarez, R., Schiavone, E., Ferrara, F., Bresciani, F., Weisz, A., Lera, A., Gronemeyer, H., Altucci, L. (2004). **Tumor-selective action of HDAC inhibitors involves TRAIL induction in acute myeloid leukemia cells** Nature Medicine 11(1), nm1161. https://dx.doi.org/10.1038/nm1161

Neuwald, A., Landsman, D. (1997). **GCN5-related histone N-acetyltransferases belong to a diverse superfamily that includes the yeast SPT10 protein** Trends in Biochemical Sciences 22(5), 154-155. https://dx.doi.org/10.1016/s0968-0004(97)01034-7

Nguyen-Huynh, N., Sharov, G., Potel, C., Fichter, P., Trowitzsch, S., Berger, I., Lamour, V., Schultz, P., Potier, N., Leize-Wagner, E. (2015). **Chemical cross-linking and mass spectrometry to determine the subunit interaction network in a recombinant human SAGA HAT subcomplex.** Protein science : a publication of the Protein Society 24(8), 1232-46. https://dx.doi.org/10.1002/pro.2676

Ogryzko, V., Schiltz, R., Russanova, V., Howard, B., Nakatani, Y. (1996). **The Transcriptional Coactivators p300 and CBP Are Histone Acetyltransferases** Cell 87(5), 953-959. https://dx.doi.org/10.1016/s0092-8674(00)82001-2

Piekarz, R., Frye, R., Turner, M., Wright, J., Allen, S., Kirschbaum, M., Zain, J., Prince, H., Leonard, J., Geskin, L., Reeder, C., Joske, D., Figg, W., Gardner, E., Steinberg, S., Jaffe, E., Stetler-Stevenson, M., Lade, S., Fojo, A., Bates, S. (2009). **Phase II Multi-Institutional Trial of the Histone Deacetylase Inhibitor Romidepsin As Monotherapy for Patients With Cutaneous T-Cell Lymphoma** Journal of Clinical Oncology 27(32), 5410-5417. https://dx.doi.org/10.1200/jco.2008.21.6150

Plumb, J., Finn, P., Williams, R., Bandara, M., Romero, M., Watkins, C., Thangue, N., Brown, R. (2003). **Pharmacodynamic response and inhibition of growth of human tumor xenografts by the novel histone deacetylase inhibitor PXD101.** Molecular cancer therapeutics 2(8), 721-8. https://www.ncbi.nlm.nih.gov/pubmed/12939461

Ponte, E., Bracco, E., Faix, J., Bozzaro, S. (1998). **Detection of subtle phenotypes: The case of the cell adhesion molecule csA in Dictyostelium** Proceedings of the

National Academy of Sciences 95(16), 9360-9365. https://dx.doi.org/10.1073/pnas.95.16.9360

R, E. (1996). **p300 and CBP as transcriptional regulators and targets of oncogenic events** Biol Chem 377(), 685 - 688.

Rack, J., Lutter, T., Bjerga, G., Guder, C., Ehrhardt, C., Värv, S., Ziegler, M., Aasland, R. (2014). **The PHD finger of p300 Influences Its Ability to Acetylate Histone and Non-Histone Targets** Journal of Molecular Biology 426(24), 3960-3972. https://dx.doi.org/10.1016/j.jmb.2014.08.011

Rada-Iglesias, A., Enroth, S., Ameur, A., Koch, C., Clelland, G., Respuela-Alonso, P., Wilcox, S., Dovey, O., Ellis, P., Langford, C., Dunham, I., Komorowski, J., Wadelius, C. (2007). **Butyrate mediates decrease of histone acetylation centered on transcription start sites and down-regulation of associated genes** Genome Research 17(6), 708-719. https://dx.doi.org/10.1101/gr.5540007

Rafehi, H., Balcerczyk, A., Lunke, S., Kaspi, A., Ziemann, M., KN, H., Okabe, J., Khurana, I., Ooi, J., Khan, A., Du, X., Chang, L., Haviv, I., Keating, S., Karagiannis, T., El-Osta, A. (2014). **Vascular histone deacetylation by pharmacological HDAC inhibition** Genome Research 24(8), 1271-1284. https://dx.doi.org/10.1101/gr.168781.113

Richon, V., Emiliani, S., Verdin, E., Webb, Y., Breslow, R., Rifkind, R., Marks, P. (1998). **A class of hybrid polar inducers of transformed cell differentiation inhibits histone deacetylases** Proceedings of the National Academy of Sciences 95(6), 3003-3007. https://dx.doi.org/10.1073/pnas.95.6.3003

Richon, V., Sandhoff, T., Rifkind, R., Marks, P. (2000). **Histone deacetylase inhibitor selectively induces p21WAF1 expression and gene-associated histone acetylation** Proceedings of the National Academy of Sciences 97(18), 10014-10019. https://dx.doi.org/10.1073/pnas.180316197

Richon, V., Webb, Y., Merger, R., Sheppard, T., Jursic, B., Ngo, L., Civoli, F., Breslow, R., Rifkind, R., Marks, P. (1996). **Second generation hybrid polar compounds are potent inducers of transformed cell differentiation** Proceedings of the National Academy of Sciences 93(12), 5705-5708. https://dx.doi.org/10.1073/pnas.93.12.5705

Ringel, A., Cieniewicz, A. (2015). **Nucleosome competition reveals processive acetylation by the SAGA HAT module** Proceedings of the National Academy of Sciences 112(), E5461-70.

Riss, A., Scheer, E., Joint, M., Trowitzsch, S., Berger, I., Tora, L. (2015). **Subunits of ADA-two-A-containing (ATAC) or Spt-Ada-Gcn5-acetyltrasferase (SAGA) Coactivator Complexes Enhance the Acetyltransferase Activity of GCN5** Journal of Biological Chemistry 290(48), 28997-29009. https://dx.doi.org/10.1074/jbc.m115.668533

Robey, R., Chakraborty, A., Basseville, A., Luchenko, V., Bahr, J., Zhan, Z., Bates, S. (2011). **Histone deacetylase inhibitors: emerging mechanisms of resistance.** Molecular pharmaceutics 8(6), 2021-31. https://dx.doi.org/10.1021/mp200329f

Rosato, R., Almenara, J., Grant, S. (2003). **The histone deacetylase inhibitor MS-275 promotes differentiation or apoptosis in human leukemia cells through a process regulated by generation of reactive oxygen species and induction of p21CIP1/WAF1 1.** Cancer research 63(13), 3637-45. https://www.ncbi.nlm.nih.gov/pubmed/12839953

Rosengarten, R., Santhanam, B., Fuller, D., Katoh-Kurasawa, M., Loomis, W., Zupan, B., Shaulsky, G. (2015). **Leaps and lulls in the developmental transcriptome of Dictyostelium discoideum** BMC Genomics 16(1), 294. https://dx.doi.org/10.1186/s12864-015-1491-7

Roth, S., Denu, J., Allis, C. (2001). **HISTONE ACETYLTRANSFERASES** Annual Review of Biochemistry 70(1), 81-120. https://dx.doi.org/10.1146/annurev.biochem.70.1.81

Sakimura, R., Tanaka, K., Yamamoto, S., Matsunobu, T., Li, X., Hanada, M., Okada, T., Nakamura, T., Li, Y., Iwamoto, Y. (2007). **The Effects of Histone Deacetylase Inhibitors on the Induction of Differentiation in Chondrosarcoma Cells** Clinical Cancer Research 13(1), 275-282. https://dx.doi.org/10.1158/1078-0432.ccr-06-1696

Saksouk, N., Avvakumov, N., Champagne, K., Hung, T., Doyon, Y., Cayrou, C., Paquet, E., Ullah, M., Landry, A., Côté, V., Yang, X., Gozani, O., Kutateladze, T., Côté, J.

(2009). **HBO1 HAT Complexes Target Chromatin throughout Gene Coding Regions via Multiple PHD Finger Interactions with Histone H3 Tail** Molecular Cell 33(2), 257-265. https://dx.doi.org/10.1016/j.molcel.2009.01.007

Sandor, V., Senderowicz, A., Mertins, S., Sackett, D., Sausville, E., Blagosklonny, M., Bates, S. (2000). **P21-dependent G 1 arrest with downregulation of cyclin D1 and upregulation of cyclin E by the histone deacetylase inhibitor FR901228** British Journal of Cancer 83(6), 817-825. https://dx.doi.org/10.1054/bjoc.2000.1327

Sapountzi, V., Côté, J. (2011). **MYST-family histone acetyltransferases: beyond chromatin** Cellular and Molecular Life Sciences 68(7), 1147-1156. https://dx.doi.org/10.1007/s00018-010-0599-9

Sasakawa, Y., Naoe, Y., Inoue, T., Sasakawa, T., Matsuo, M., Manda, T., Mutoh, S. (2002). **Effects of FK228, a novel histone deacetylase inhibitor, on human lymphoma U-937 cells in vitro and in vivo** Biochemical Pharmacology 64(7), 1079-1090. https://dx.doi.org/10.1016/s0006-2952(02)01261-3

Sawarkar, R., Visweswariah, S., Nellen, W., Nanjundiah, V. (2009). **Histone Deacetylases Regulate Multicellular Development in the Social Amoeba Dictyostelium discoideum** Journal of Molecular Biology 391(5), 833-848. https://dx.doi.org/10.1016/j.jmb.2009.06.067

Schneider, J., Wood, A., Lee, J., Schuster, R., Dueker, J., Maguire, C., Swanson, S., Florens, L., Washburn, M., Shilatifard, A. (2005). **Molecular Regulation of Histone H3 Trimethylation by COMPASS and the Regulation of Gene Expression** Molecular Cell 19(6), 849-856. https://dx.doi.org/10.1016/j.molcel.2005.07.024

Schram, A., Baas, R., Jansen, P., Riss, A., Tora, L., Vermeulen, M., Timmers, T. (2013). **A Dual Role for SAGA-Associated Factor 29 (SGF29) in ER Stress Survival by Coordination of Both Histone H3 Acetylation and Histone H3 Lysine-4 Trimethylation** PLoS ONE 8(7), e70035. https://dx.doi.org/10.1371/journal.pone.0070035

Schübeler, D., MacAlpine, D., Scalzo, D., Wirbelauer, C., Kooperberg, C., Leeuwen, F., Gottschling, D., O'Neill, L., Turner, B., Delrow, J., Bell, S., Groudine, M. (2004). **The histone modification pattern of active genes revealed through genome-wide**

chromatin analysis of a higher eukaryote Genes & Development 18(11), 1263-1271. https://dx.doi.org/10.1101/gad.1198204

Seto, E., Yoshida, M. (2014). **Erasers of Histone Acetylation: The Histone Deacetylase Enzymes** Cold Spring Harbor Perspectives in Biology 6(4), a018713. https://dx.doi.org/10.1101/cshperspect.a018713

Shamas-Din, A., Kale, J., Leber, B., Andrews, D. (2013). **Mechanisms of Action of Bcl-2 Family Proteins** Cold Spring Harbor Perspectives in Biology 5(4), a008714. https://dx.doi.org/10.1101/cshperspect.a008714

Shrivastava, A., Burma, P., Jain, M., Jain, P., Lohia, R., Saran, S. (2016). **Dictyostelium discoideum Sir2D modulates cell-type specific gene expression and is involved in autophagy** International Journal of Developmental Biology 61(1-2), 95-104. https://dx.doi.org/10.1387/ijdb.160038ss

Shukla, A., Lahudkar, S., Durairaj, G., Bhaumik, S. (2012). **Sgf29p Facilitates the Recruitment of TATA Box Binding Protein but Does Not Alter SAGA's Global Structural Integrity in Vivo** Biochemistry 51(2), 706-714. https://dx.doi.org/10.1021/bi201708z

Shulha, H., Cheung, I., Guo, Y., Akbarian, S., Weng, Z. (2013). **Coordinated Cell Type–Specific Epigenetic Remodeling in Prefrontal Cortex Begins before Birth and Continues into Early Adulthood** PLoS Genetics 9(4), e1003433. https://dx.doi.org/10.1371/journal.pgen.1003433

Smith, E., Belote, J., Schiltz, R., Yang, X., Moore, P., Berger, S., Nakatani, Y., Allis, C. (1998). **Cloning of Drosophila GCN5: Conserved features among metazoan GCN5 family members** Nucleic Acids Research 26(12), 2948-2954. https://dx.doi.org/10.1093/nar/26.12.2948

Sterner, D., Berger, S. (2000). **Acetylation of histones and transcription-related factors** Microbiology and Molecular Biology Reviews 64(), 435-59. https://dx.doi.org/10.1128/MMBR.64.2.435-459.2000

Stevense, M., Chubb, J., Muramoto, T. (2011). **Nuclear organization and transcriptional dynamics in Dictyostelium** Develop. Growth Differ. 53(4), 576-586.

https://dx.doi.org/10.1111/j.1440-169X.2011.01271.x

Strmecki, L., Greene, D., Pears, C. (2005). **Developmental decisions in Dictyostelium discoideum** Developmental Biology 284(1)https://dx.doi.org/10.1016/j.ydbio.2005.05.011

Sugita, K., Koizumi, K., Yoshida, H. (1992). **Morphological reversion of sis-transformed NIH3T3 cells by trichostatin A.** Cancer research 52(1), 168-72. https://www.ncbi.nlm.nih.gov/pubmed/1727377

Syntichaki, P., Topalidou, I., Thireos, G. (2000). **The Gcn5 bromodomain co-ordinates nucleosome remodelling** Nature 404(6776), 414. https://dx.doi.org/10.1038/35006136

Tanaka, M., Levy, J., Terada, M., Breslow, R., Rifkind, R., Marks, P. (1975). **Induction of erythroid differentiation in murine virus infected eythroleukemia cells by highly polar compounds** Proceedings of the National Academy of Sciences 72(3), 1003-1006. https://dx.doi.org/10.1073/pnas.72.3.1003

Tang, Z., Chen, W., Shimada, M., Nguyen, U., Kim, J., Sun, X., Sengoku, T., McGinty, R., Fernandez, J., Muir, T., Roeder, R. (2013). **SET1 and p300 Act Synergistically, through Coupled Histone Modifications, in Transcriptional Activation by p53** Cell 154(2), 297-310. https://dx.doi.org/10.1016/j.cell.2013.06.027

Taverna, S., Ilin, S., Rogers, R., Tanny, J., Lavender, H., Li, H., Baker, L., Boyle, J., Blair, L., Chait, B., Patel, D., Aitchison, J., Tackett, A., Allis, C. (2006). **Yng1 PHD Finger Binding to H3 Trimethylated at K4 Promotes NuA3 HAT Activity at K14 of H3 and Transcription at a Subset of Targeted ORFs** Molecular Cell 24(5), 785-796. https://dx.doi.org/10.1016/j.molcel.2006.10.026

Tillner, J., Winckler, T., Dingermann, T. (1996). **Developmentally regulated promoters from Dictyostelium discoideum as molecular markers for testing potential teratogens.** Die Pharmazie 51(11), 902-6. https://www.ncbi.nlm.nih.gov/pubmed/8985980

TSUJI, N., KOBAYASHI, M., NAGASHIMA, K., WAKISAKA, Y., KOIZUMI, K. (1976). **A NEW ANTIFUNGAL ANTIBIOTIC, TRICHOSTATIN** The Journal of Antibiotics 29(1), 1-6. https://dx.doi.org/10.7164/antibiotics.29.1

VanderMolen, K., McCulloch, W., Pearce, C. (2011). **Romidepsin (Istodax, NSC 630176, FR901228, FK228, depsipeptide): a natural product recently approved for cutaneous T-cell lymphoma** The Journal of Antibiotic 64(), 525-531. https://dx.doi.org/10.1038/ja.2011.35

Veltman, D., Akar, G., Bosgraaf, L., Haastert, P. (2009). **A new set of small, extrachromosomal expression vectors for Dictyostelium discoideum** Plasmid 61(2), 110-118. https://dx.doi.org/10.1016/j.plasmid.2008.11.003

Vidal, A., Koff, A. (2000). **Cell-cycle inhibitors: three families united by a common cause** Gene 247(1-2), 1-15. https://dx.doi.org/10.1016/s0378-1119(00)00092-5

Voss, A., Thomas, T. (2018). **Histone Lysine and Genomic Targets of Histone Acetyltransferases in Mammals** BioEssays 40(10), e1800078. https://dx.doi.org/10.1002/bies.201800078

Wang, Z., Zang, C., Rosenfeld, J., Schones, D., Barski, A., Cuddapah, S., Cui, K., Roh, T., Peng, W., Zhang, M., Zhao, K. (2008). **Combinatorial patterns of histone acetylations and methylations in the human genome** Nature Genetics 40(7), 897-903. https://dx.doi.org/10.1038/ng.154

Wang, Y., Zhang, R., Wu, D., Lu, Z., Sun, W., Cai, Y., Wang, C., Jin, J. (2013). **Epigenetic change in kidney tumor: downregulation of histone acetyltransferase MYST1 in human renal cell carcinoma** Journal of Experimental & Clinical Cancer Research 32(1), 8. https://dx.doi.org/10.1186/1756-9966-32-8

Wang, L., Koutelou, E., Hirsch, C., McCarthy, R., Schibler, A., Lin, K., Lu, Y., Jeter, C., Shen, J., Barton, M., Dent, S. (2018). **GCN5 Regulates FGF Signaling and Activates Selective MYC Target Genes during Early Embryoid Body Differentiation** Stem Cell Reports 10(1), 287-299. https://dx.doi.org/10.1016/j.stemcr.2017.11.009

Wang, L., Mizzen, C., Ying, C., Candau, R., Barlev, N., Brownell, J., Allis, C., Berger, S. (1997). **Histone acetyltransferase activity is conserved between yeast and human GCN5 and is required for complementation of growth and transcriptional activation.** Molecular and Cellular Biology 17(1), 519-527. https://dx.doi.org/10.1128/mcb.17.1.519

Wang, X., Wei, X., Pang, Q., Yi, F. (2012). **Histone deacetylases and their inhibitors: molecular mechanisms and therapeutic implications in diabetes mellitus** Acta Pharmaceutica Sinica B 2(4), 387-395. https://dx.doi.org/10.1016/j.apsb.2012.06.005

West, A., Johnstone, R. (2014). **New and emerging HDAC inhibitors for cancer treatment** The Journal of Clinical Investigation 124(1)https://dx.doi.org/10.1172/JCI69738

Williams, R., Cheng, L., Mudge, A., Harwood, A. (2002). **A common mechanism of action for three mood-stabilizing drugs** Nature 417(6886), 292. https://dx.doi.org/10.1038/417292a

Xiao, J., Foraker, A., Swaan, P., Liu, S., Huang, Y., Dai, Z., Chen, J., Sadée, W., Byrd, J., Marcucci, G., Chan, K. (2005). **Efflux of Depsipeptide FK228 (FR901228, NSC-630176) Is Mediated by P-Glycoprotein and Multidrug Resistance-Associated Protein 1** Journal of Pharmacology and Experimental Therapeutics 313(1), 268-276. https://dx.doi.org/10.1124/jpet.104.072033

Xu, X., Müller-Taubenberger, A., Adley, K., Pawolleck, N., Lee, V., Wiedemann, C., Sihra, T., Maniak, M., Jin, T., Williams, R. (2007). **Attenuation of Phospholipid Signaling Provides a Novel Mechanism for the Action of Valproic Acid ▾ †** Eukaryotic Cell 6(6), 899-906. https://dx.doi.org/10.1128/ec.00104-06

Xu, W., Edmondson, D., Evrard, Y., Wakamiya, M., Behringer, R., Roth, S. (2000). **Loss of Gcn5l2 leads to increased apoptosis and mesodermal defects during mouse development** Nature Genetics 26(2), ng1000_229. https://dx.doi.org/10.1038/79973

Xue, Y., Wen, H., Shi, X. (2018). **CBP/p300: intramolecular and intermolecular regulations** Frontiers in Biology 13(3), 168-179. https://dx.doi.org/10.1007/s11515-018-1502-6

Yamauchi, T., Yamauchi, J., Kuwata, T., Tamura, T., Yamashita, T., Bae, N., Westphal, H., Ozato, K., Nakatani, Y. (2000). **Distinct but overlapping roles of histone acetylase PCAF and of the closely related PCAF-B/GCN5 in mouse embryogenesis** Proceedings of the National Academy of Sciences 97(21), 11303-11306. https://dx.doi.org/10.1073/pnas.97.21.11303

Yan, G., Eller, M., Elm, C., Larocca, C., Ryu, B., Panova, I., Dancy, B., Bowers, E., Meyers, D., Lareau, L., Cole, P., Taverna, S., Alani, R. (2013). **Selective Inhibition of p300 HAT Blocks Cell Cycle Progression, Induces Cellular Senescence, and Inhibits the DNA Damage Response in Melanoma Cells** Journal of Investigative Dermatology 133(10), 2444-2452. https://dx.doi.org/10.1038/jid.2013.187

Yoshida, H., Sugita, K. (1992). **A Novel Tetracyclic Peptide, Trapoxin, Induces Phenotypic Change from Transformed to Normal in sis-Oncogene-transformed NIH3T3 Cells** Japanese Journal of Cancer Research 83(4), 324-328. https://dx.doi.org/10.1111/j.1349-7006.1992.tb00109.x

Yoshida, M., Nomura, S., Beppu, T. (1987). **Effects of trichostatins on differentiation of murine erythroleukemia cells.** Cancer research 47(14), 3688-91. https://www.ncbi.nlm.nih.gov/pubmed/2439196

Yuan, H., Marmorstein, R. (2013). **Histone acetyltransferases: Rising ancient counterparts to protein kinases** Biopolymers 99(2), 98-111. https://dx.doi.org/10.1002/bip.22128

Zeng, F., Peng, S., Li, L., Mu, L., Zhang, Z., Zhang, Z., Huang, N. (2013). **Structure-based identification of drug-like inhibitors of p300 histone acetyltransferase.** Yao xue xue bao = Acta pharmaceutica Sinica 48(5), 700-8. https://www.ncbi.nlm.nih.gov/pubmed/23888693

Zhang, Q., Wang, T., Geng, C., Zhang, Y., Zhang, J., Ning, Z., Jiang, Z., China, D., China, D., China, T., China, S. (2018). **Exploratory clinical study of chidamide, an oral subtype-selective histone deacetylase inhibitor, in combination with exemestane in hormone receptor-positive advanced breast cancer** Chinese Journal of Cancer Research 30(6), 605-612. https://dx.doi.org/10.21147/j.issn.1000-9604.2018.06.05

Zhao, Y., Garcia, B. (2015). **Comprehensive Catalog of Currently Documented Histone Modifications.** Cold Spring Harbor perspectives in biology 7(9), a025064. https://dx.doi.org/10.1101/cshperspect.a025064

Zhou, K., Gaullier, G., Luger, K. (2019). **Nucleosome structure and dynamics are**

coming of age Nature Structural & Molecular Biology 26(1), 3-13. https://dx.doi.org/10.1038/s41594-018-0166-x

8. Appendixes

Appendix 1

Primer name	sequence (5' → 3')	restriction enzyme sites	mutation
Cloning primers			
Tudor-F	GCGAATTCAGTAGTGGAAATGGATTCCATGG	EcoRI, NcoI	N/A
Tudor-R	CTCGAGACTAGTCTTATTTAAGGCCAC	XhoI, SpeI	N/A
Tudor-N-R	AAAGGCGGTGGTATCGGGAGCCAT	N/A	AA to GC
Tudor-C-F	CCCGATACCACCGCCTTTGCTCC	N/A	TA to GC
DdSgf29_1-854_F	GGATCCAGATCTATGTCCGATGCTC	BamHI, BglII	N/A
DdSgf29_1-854_R	GTTGCATACCATGGAATCCA	NcoI	N/A
Gcn5KO_LR_F	GTTCAAATTTCTCTCTATCTGCTG	N/A	N/A
Gcn5KO_LR_R	TACCCACATTATCACATTATTTAATTTATTATC	N/A	N/A
Gcn5KO_RR_F	GAAAATTCACCTTATTATGATAACGCAG	N/A	N/A
Gcn5KO_LR_R	GAATTTTGACAAATTTCATAATCTTTTAACCAAG	N/A	N/A
Sgf29KO_LR_R	GACCAACCTGATCACTCTTTTCTTCATC	N/A	N/A
Sgf29KO_RR_F	CATGTTGTGGCCTTAAATAAGTAGTTG	N/A	N/A
Sgf29KO_RR_R	CAATTGTTTGTTTTGAAAATTCACCACCAC	N/A	N/A
P1	CTAAAATGTAGGTAGGTGACCAAATC	N/A	N/A
P2	GAAGTTATCATATGCCGCATGG	N/A	N/A

P3	ATGCTATACGAAGTTATCCGTGG	N/A	N/A
P4	ATGCTATACGAAGTTATCCGTGG	N/A	N/A
P5	CTCACATTCCACCATATACAC	N/A	N/A
P6	CATTTCCATATTTATTTGTTGAGTCCC	N/A	N/A
***Gcn5Δbromo* genotyping primers**			
bromo_F	CAACAATTGGCAGTTGTATTACAAAG	N/A	N/A
bromo_R	CTGCGTTATCATAATAAGGTG	N/A	N/A
Gcn5_F	CATGGTCAAAGACGCATACCC	N/A	N/A
Gcn5_R	The same as bromo_R	N/A	N/A
acetyl_F	CACCATCATACTCTTGGATGAAAC	N/A	N/A
acetyl_R	GGACCAGAAGATGGTTTACAAATTG	N/A	N/A
5'bsr_F	The same as Gcn5_F	N/A	N/A
5'bsr_R	GTTGAGAAATGTTAAATTGATCC	N/A	N/A
3'bsr_F	ATAGAAATGAATGGCAAGTTAG	N/A	N/A
3'bsr_R	The same as bromo_R	N/A	N/A
ig7_F	TCCAAGAGGAAGAGGAGAACTGC	N/A	N/A
ig7_R	TGGGGAGGTCGTTACACCATTC	N/A	N/A
gpda_F	GGTTGTCCCAATTGGTATTAATGG	N/A	N/A
gpda_R	CCGTGGGTTGAATCATATTTGAAC	N/A	N/A
gDNA_F	GTAGGTGATTTTCGAGCAC	N/A	N/A
gDNA_R	GAATTTGTAAACCATCTTCTGGTCC	N/A	N/A
REMI-seq primers			

D_504_a	AATGATACGGCGACCACCGAGATCTACACGGCTCTGAACACTCTTTCCCTACACGACGCTCTTCCGATCTNN
D_504_b	AGATCGGAAGAGCGTCGTGTAGGGAAAGAGTGTTCAGAGCCGTGTAGATCTCGGTGGTCGCCGTATCATT
D_703_a	CAAGCAGAAGACGGCATACGAGATAATGAGCGGTGACTGGAGTTCAGACGTGTGCTCTTCCGATCTTTAT
D_703_b	AGATCGGAAGAGCACACGTCTGAACTCCAGTCACCGCTCATTATCTCGTATGCCGTCTTCTGCTTG
D_704_a	CAAGCAGAAGACGGCATACGAGATGGAATCTCGTGACTGGAGTTCAGACGTGTGCTCTTCCGATCTTTAT
D_704_b	AGATCGGAAGAGCACACGTCTGAACTCCAGTCACGAGATTCCATCTCGTATGCCGTCTTCTGCTTG
D_707_a	CAAGCAGAAGACGGCATACGAGATAGCTTCAGGTGACTGGAGTTCAGACGTGTGCTCTTCCGATCTTTAT
D_707_b	AGATCGGAAGAGCACACGTCTGAACTCCAGTCACCTGAAGCTATCTCGTATGCCGTCTTCTGCTTG
D_708_a	CAAGCAGAAGACGGCATACGAGATGCGCATTAGTGACTGGAGTTCAGACGTGTGCTCTTCCGATCTTTAT
D_708_b	AGATCGGAAGAGCACACGTCTGAACTCCAGTCACTAATGCGCATCTCGTATGCCGTCTTCTGCTTG
D_709_a	CAAGCAGAAGACGGCATACGAGATCATAGCCGGTGACTGGAGTTCAGACGTGTGCTCTTCCGATCTTTAT
D_709_b	AGATCGGAAGAGCACACGTCTGAACTCCAGTCACCGGCTATGATCTCGTATGCCGTCTTCTGCTTG
D_710_a	CAAGCAGAAGACGGCATACGAGATTTCGCGGAGTGACTGGAGTTCAGACGTGTGCTCTTCCGATCTTTAT
D_710_b	AGATCGGAAGAGCACACGTCTGAACTCCAGTCACTCCGCGAAATCTCGTATGCCGTCTTCTGCTTG
D_711_a	CAAGCAGAAGACGGCATACGAGATGCGCGAGAGTGACTGGAGTTCAGACGTGTGCTCTTCCGATCTTTAT
D_711_b	AGATCGGAAGAGCACACGTCTGAACTCCAGTCACTCTCGCGCATCTCGTATGCCGTCTTCTGCTTG
D_712_a	CAAGCAGAAGACGGCATACGAGATCTATCGCTGTGACTGGAGTTCAGACGTGTGCTCTTCCGATCTTTAT
D_712_b	AGATCGGAAGAGCACACGTCTGAACTCCAGTCACAGCGATAGATCTCGTATGCCGTCTTCTGCTTG
P5	AATGATACGGCGACCACCGA

Appendix 2

1st Antibody	Supplier	Cat. Number	Poly/mono	Host	Dilution		
					whole cell lysate	Acid extract	corresponding 2nd antibody
H3K9ac	homemade	N/A	p	Rabbit	N/A	1:4000	Swine anti-rabbit (DAKO), 1:3000
H3K14ac	homemade	N/A	p	Rabbit	N/A	1:13000	Swine anti-rabbit (DAKO), 1:3000
H3K4me3	homemade	N/A	p	Rabbit	N/A	1:26000 (SDS-PAGE) 1:10000 (AU gel)	Swine anti-rabbit (DAKO), 1:3000
H3	Abcam	ab12079	p	Goat	N/A	1:4000	SDS-PAGE: IRDye 680RD Donkey anti-goat (LICOR), 1:15000 AU gel: Rabbit anti-goat (DAKO), 1:3000
FLAG	Sigma	F1804	m	mouse	1:1000	N/A	Rabbit anti-mouse (DAKO), 1:10000
Actin	Santa Cruz	sc-1615	p	Goat	1:1000	N/A	Goat anti-rabbit (DAKO), 1:10000

Appendix 3

gene	chr	pos	bin	fast-growing?	R5_TSA_1 (log10FC)	R5_TSA_2 (log10FC)	R5 average	R8_TSA_2 (log10FC)	R8_TSA_3 (log10FC)	R8 average	short	desc
DDB_G0286385	DDB0232431	4393579	100	NA	NA	NA	NA	3.67	4.50	4.09	padA	involved in development and cell differentiation;B modulates the expression of extracellular cAMP relay genes during aggregation
DDB_G0287169	DDB0232431	5428716	100	NA	NA	NA	NA	3.83	4.03	3.93	DDB_G0287169	NA
DDB_G0274577	DDB0232429	3894327	100	Yes	NA	NA	NA	3.57	4.01	3.79	DG1124	calcium-binding EF-hand domain-containing protein. shares a short region of similarity with H. sapiens DBC protein (deleted in breast cancer)
DDB_G0282297	DDB0232430	5645037	100	NA	NA	NA	NA	3.98	4.01	3.99	forB	actin binding protein, formin homology domain-containing protein
NA	DDB0232428	1508797	100	NA	NA	NA	NA	3.41	4.00	3.70	NA	NA
DDB_G0275861	DDB0232429	5746977	100	NA	NA	NA	NA	4.25	3.92	4.08	DDB_G0275861	conserved eukaryotic protein
NA	DDB0232430	3499103	100		NA	NA	NA	3.16	3.86	3.51	NA	NA
DDB_G0270934	DDB0232428	3487098	100	NA	NA	NA	NA	3.49	3.84	3.67	DDB_G0270934	Putative triacylglycerol lipase-like protein
DDB_G0275687	DDB0232429	5759285	100	NA	NA	NA	NA	3.35	3.83	3.59	abcG18	full transporter consisting of two ABC domains and two transmembrane domains
DDB_G0282535	DDB0232430	5895115	100	NA	NA	NA	NA	4.16	3.83	3.99	DDB_G0282535	NA

DDB_G0277095	DDB0232429	7497501	100	NA	NA	NA	NA	3.65	3.83	3.74	DDB_G0277095	NA
DDB_G0276713	DDB0232429	7116001	100	NA	NA	NA	NA	3.79	3.80	3.79	DDB_G0276713	NA
NA	DDB0232431	122208	100	NA	NA	NA	NA	3.76	3.80	3.78	NA	NA
DDB_G0287099	DDB0232431	5340555	100	NA	NA	NA	NA	3.57	3.77	3.67	DDB_G0287099	NA
NA	DDB0232430	3669755	100		NA	NA	NA	3.40	3.76	3.58	NA	NA
NA	DDB0232430	1355759	100		NA	NA	NA	3.36	3.75	3.55	NA	NA
NA	DDB0232429	8290991	100		NA	NA	NA	3.51	3.74	3.62	NA	NA
DDB_G0278171	DDB0232430	395199	100	NA	NA	NA	NA	2.82	3.59	3.20	DDB_G0278171	NA
DDB_G0291842	DDB0232433	823045	100	Yes	NA	NA	NA	3.44	3.58	3.51	DDB_G0291842	putative protein tyrosine kinase; similar to S. pombe WEE1, inhibitor of mitosis through phosphorylation of cdc2
DDB_G0280157	DDB0232430	3031416	100	NA	NA	NA	NA	3.58	3.57	3.58	DDB_G0280157	NA
DDB_G0270586	DDB0232428	3182265	100	NA	NA	NA	NA	3.78	3.56	3.67	DDB_G0270586	putative transporter
NA	DDB0232428	3615829	100	Yes	NA	NA	NA	3.08	3.55	3.31	NA	NA
DDB_G0274101	DDB0232429	4566767	100	Yes	NA	NA	NA	3.40	3.53	3.47	dokA	histidine kinase DokA
NA	DDB0232429	3596962	100		NA	NA	NA	2.81	3.50	3.15	NA	NA
DDB_G0274577	DDB0232429	3895130	100	Yes	NA	NA	NA	3.54	3.39	3.46	DG1124	calcium-binding EF-hand domain-containing protein. shares a short region of similarity with H. sapiens DBC protein (deleted in breast cancer)
NA	DDB0232429	3442402	100		NA	NA	NA	3.53	3.38	3.46	NA	NA

DDB_G0286459	DDB0232431	4378499	100	NA	NA	NA	NA	3.42	3.33	3.38	DDB_G0286459	contains one C1 domain (protein kinase C conserved region 1) which is involved in phorbol ester diacylglycerol binding;B contains one coiled-coil domain
NA	DDB0232432	86236	100		NA	NA	NA	3.51	3.33	3.42	NA	NA
DDB_G0268914	DDB0232428	2374716	100	NA	NA	NA	NA	3.30	3.31	3.31	DDB_G0268914	NA
DDB_G0270640	DDB0232428	3582734	100	Yes	NA	NA	NA	3.20	3.30	3.25	DDB_G0270640	putative spindle pole body-interacting protein
NA	DDB0232432	4534015	100		NA	NA	NA	2.83	3.28	3.06	NA	NA
DDB_G0275733	DDB0232429	5917196	100	Yes	NA	NA	NA	3.72	3.26	3.49	med26	putative ortholog of the poorly conserved mediator of RNA polymerase II transcription subunit 26;B the mediator complex functions as a bridge to convey information from gene-specific regulatory proteins to the basal RNA polymerase II transcription machinery
NA	DDB0232431	477641	100	NA	NA	NA	NA	4.10	3.26	3.68	NA	NA
DDB_G0290317	DDB0232432	3948807	100	NA	4.32	4.47	4.39	1.98	1.86	1.92	psiJ	contains a PA14 (anthrax protection antigen) domain and 6 Dictyostelium (CTDC) repeats
DDB_G0274981	DDB0232429	4761262	100	NA	4.10	4.31	4.20	3.25	3.18	3.22	DDB_G0274981	NA
DDB_G0293468	DDB0232433	2925216	100	NA	4.12	4.20	4.16	4.19	4.48	4.34	mybS	contains one Myb DNA-binding domain
DDB_G0274825	DDB0232429	4035058	100	NA	4.12	4.15	4.14	1.05	1.15	1.10	DDB_G0274825	similar to Dictystelium cell surface glycoproteins gp130, and GP138A, B, C, and D
DDB_G0274279	DDB0232429	4038443	100	NA	4.22	4.03	4.12	4.11	4.02	4.06	tssc1	similar to Tumor Suppressing Subtransferable Candidate 1

DDB_G0269252	DDB0232428	4047430	100	Yes	4.23	3.90	4.06	NA	NA	NA	gefE	putative Ras guanine nucleotide exchange factor;B promotes the exchange of GDP for GTP on Ras small GTPases thus converting them into the active form
DDB_G0267844	DDB0232428	961864	100	NA	4.02	3.99	4.00	3.19	3.31	3.25	expl6	similar to plant expansins, which modify the cell wall to allow expansion during cell growth;B contains a predicted signal peptide
DDB_G0276251	DDB0232429	6503513	100	NA	3.97	4.03	4.00	3.40	3.57	3.48	DDB_G0276251	similar to H. sapiens GP17, involved in modification of glycosylphosphatidylinositol; contains 16 transmembrane domains
DDB_G0269486	DDB0232428	2861962	100	Yes	3.76	4.16	3.96	3.30	2.89	3.10	DDB_G0269486	NA
DDB_G0277961	DDB0232430	67393	100	NA	4.00	3.90	3.95	1.01	1.04	1.03	DDB_G0277961	NA
NA	DDB0232429	6804362	100		4.04	3.81	3.93	NA	NA	NA	NA	NA
DDB_G0294002	DDB0232433	3602047	100	NA	3.66	4.11	3.89	3.62	3.72	3.67	DDB_G0294002_RTE	ORF1 protein of tRNA-specific non-long terminal repeat retrotransposon TRE5-B;B refer to GenBank GenBank AF298209 for consensus full-length element
DDB_G0280869	DDB0232430	3815678	100	Yes	3.84	3.88	3.86	0.77	0.48	0.63	DDB_G0280869	NA
DDB_G0284625	DDB0232431	2257802	100	Yes	3.63	3.98	3.81	NA	NA	NA	DDB_G0284625	onserved hypothetical Dictyostelium protein, contains one EGF-like, type 3 domain
DDB_G0271660	DDB0232429	686804	100	NA	3.81	3.79	3.80	0.33	0.42	0.38	fmoB	belongs to the fmo family;B similar to flavin-containing monooxygenases from a variety of eukaryotes;B involved in the metabolism of xenobiotic compounds

NA	DDB0232432	2589633	100	Yes	3.76	3.78	3.77	1.55	1.71	1.63	NA	NA
DDB_G0292036	DDB0232433	1060701	100	NA	3.78	3.75	3.76	NA	NA	NA	ric8	similar to human RIC8A (synembryn-A); non-receptor guanine nucleotide exchange factor for Gα protein; important for chemotaxis and development
NA	DDB0232431	3747153	1000		NA	NA	NA	0.75	1.39	1.07	NA	NA
DDB_G0288923	DDB0232432	2134091	1000	NA	NA	NA	NA	1.32	1.34	1.33	upf1	ortholog of yeast NAM7 and the mammalian UPF1 (up-frameshift suppressor 1) or RENT1 protein%2C part of a post-splicing multiprotein complex and involved in nonsense-mediated decay (NMD) of mRNAs containing premature stop codons
DDB_G0285963	DDB0232431	3876747	1000	NA	NA	NA	NA	0.94	1.32	1.13	fhkD	CAMK group RAD53 family protein kinase;B similar to mammalian cell cycle checkpoint kinases chk2;B contains a forkhead-associated (FHA) domain, a phosphopeptide recognition domain found in many regulatory proteins
DDB_G0274577	DDB0232429	3896724	1000	Yes	NA	NA	NA	1.70	1.32	1.51	DG1124	calcium-binding EF-hand domain-containing protein. shares a short region of similarity with H. sapiens DBC protein (deleted in breast cancer)
NA	DDB0232433	770652	1000		NA	NA	NA	1.15	1.07	1.11	NA	NA
DDB_G0291884	DDB0232433	881141	1000	NA	NA	NA	NA	0.70	0.80	0.75	DDB_G0291884_RTE	ORF2 protein encoding endonuclease and reverse transcriptase of tRNA-specific non-long terminal repeat

												retrotransposon TRE3-A;B refer to GenBank AF134169 for full-length consensus element
NA	DDB0232432	1592045	1000		NA	NA	NA	0.69	0.72	0.70	NA	NA
DDB_G0282137	DDB0232430	5423611	1000	NA	NA	NA	NA	0.98	0.58	0.78	DDB_G0282137	related to sterol desaturase
NA	DDB0237465	71230	1000		NA	NA	NA	0.88	0.57	0.73	NA	NA
DDB_G0275213	DDB0232429	5011028	1000	NA	NA	NA	NA	0.72	0.51	0.61	DDB_G0275213	NA
DDB_G0288269	DDB0232432	1291047	1000	NA	NA	NA	NA	0.39	0.50	0.44	fslE	similar to G-protein-coupled receptors;B weak frizzled cystein-rich domain;B predicted to have 7 transmembrane domains and a putative signal peptide
DDB_G0288725	DDB0232432	1881450	1000	NA	NA	NA	NA	1.15	0.48	0.81	DDB_G0288725	NA
DDB_G0288833	DDB0232432	2045949	1000	NA	NA	NA	NA	-0.02	0.33	0.15	derl1	component of endoplasmic reticulum-associated degradation (ERAD) for misfolded lumenal proteins;B contains 5 putative transmembrane domains
DDB_G0283725	DDB0232431	1036269	1000	NA	NA	NA	NA	1.31	0.19	0.75	DDB_G0283725_ps	putative pseudogene, very similar to pyridoxal phosphate-dependent decarboxylase family genes
DDB_G0276911	DDB0232429	7252351	1000	NA	NA	NA	NA	0.50	-0.15	0.18	DDB_G0276911	NA
NA	DDB0232428	2675112	1000		NA	NA	NA	0.28	-0.63	-0.17	NA	NA
NA	DDB0232429	3504006	1000		1.68	1.79	1.74	1.63	1.50	1.57	NA	NA
DDB_G0291079	DDB0232432	4967317	1000	Yes	1.23	1.54	1.38	NA	NA	NA	gbpC	member of the TKL (tyrosine kinase-like) group and ROCO family of protein kinases; belongs to the LRRK family of protein kinases; contains LRR, Roc, COR,

												RasGEF, protein kinase, DEP, cyclic nucleotide-binding, and GRAM domains; involved in cGMP-mediated chemotaxis; catalyzes GDP to GTP exchange on its own Roc domain; translocates from cytoplasm to cell cortex after cAMP stimulation; GRAM domain binds directly to plasma membrane
DDB_G0272532	DDB0232429	1829135	1000	NA	1.21	1.48	1.35	NA	NA	NA	DDB_G0272532	NA
NA	DDB0232428	2368271	1000		1.23	1.09	1.16	0.92	0.87	0.90	NA	NA
DDB_G0279503	DDB0232430	2171451	1000	NA	1.04	1.25	1.15	0.41	0.66	0.54	DDB_G0279503	NA
DDB_G0275035	DDB0232429	5295040	1000	NA	1.12	1.17	1.15	-0.49	0.13	-0.18	zizA	zizimin- related DOCK family protein. DOCK family protein putative. guanine nucleotide exchange factor (GEF)
NA	DDB0232428	3136237	1000	Yes	0.63	1.64	1.14	3.73	3.77	3.75	NA	NA
DDB_G0279483	DDB0232430	2124128	1000	NA	1.12	0.93	1.03	NA	NA	NA	pldB	phospholipase D1 catalyzes the reaction a phosphatidylcholine + H2O <=> choline + a phosphatidate; plays a role in quorum sensing during aggrega
DDB_G0293654	DDB0232433	3218614	1000	NA	0.89	0.99	0.94	NA	NA	NA	gacE	GTPase Activating factor for raC
DDB_G0282471	DDB0232430	5812827	1000	NA	1.01	0.70	0.85	NA	NA	NA	DDB_G0282471	NA
DDB_G0288485	DDB0232432	1619822	1000	NA	1.09	0.59	0.84	-0.34	-0.32	-0.33	pikD	subunit of PI4K, responsible for the phosphorylation of phosphatidylinositol (PI) to PI4P (ATP + 1-

												phosphatidyl-1D-myo-inositol = ADP + 1-phosphatidyl-1D-myo-inositol 4-phosphate), the first committed step in the generation of phosphatidylinositol 4,5-bisphosphate (PIP2), a precursor of the second messenger inositol 1,4,5-trisphosphate (InsP3)
DDB_G0273949	DDB0232429	3587618	1000	NA	0.57	1.02	0.80	1.00	0.56	0.78	DDB_G0273949	Putative glycerophosphodiester phosphodiesterase 5 (Automated). there is a second copy of this gene.
NA	DDB0232431	968553	1000		0.86	0.55	0.71	NA	NA	NA	NA	NA
DDB_G0269870	DDB0232428	3768940	1000	NA	0.54	0.87	0.70	NA	NA	NA	DDB_G0269870	NA
DDB_G0286069	DDB0232431	4024280	1000	NA	0.83	0.56	0.70	NA	NA	NA	ku70	part of the heterodimer ku70 and ku80 complex, which binds to DNA double-strand break ends;B involved in double-strand break repair via nonhomologous end joining (NHEJ)
DDB_G0290923	DDB0232432	4760046	1000	NA	0.76	0.59	0.67	NA	NA	NA	DDB_G0290923	NA
DDB_G0270452	DDB0232428	4908049	1000	NA	0.48	0.70	0.59	NA	NA	NA	DDB_G0270452	cyclin-like F-box containing protein
NA	DDB0232433	3137296	1000		0.62	0.48	0.55	NA	NA	NA	NA	NA
DDB_G0269770	DDB0232428	3524802	1000	NA	0.43	0.65	0.54	NA	NA	NA	fam63A	DUF544 family protein
NA	DDB0232429	5850919	1000		0.58	0.42	0.50	NA	NA	NA	NA	NA
NA	DDB0232430	3708125	10000		NA	NA	NA	0.71	1.44	1.08	NA	NA

DDB_G0283885	DDB0232431	1166561	10000	NA	NA	NA	NA	1.09	1.15	1.12	DDB_G0283885	member of a gene family comprising DDB_G0283887, DDB_G0283885, DDB_G0275891_ps, and DDB_G0275279, similar to hypothetical protein MT3488 from Mycobacterium tuberculosis
NA	DDB0232429	4917169	10000		NA	NA	NA	0.57	0.78	0.67	NA	NA
DDB_G0277539	DDB0232429	8011924	10000	Yes	NA	NA	NA	0.67	0.62	0.64	DDB_G0277539	putative protein tyrosine kinase; similar to human wee1, inhibitor of mitosis through phosphorylation of cdc2
DDB_G0290915	DDB0232432	4743245	10000	Yes	NA	NA	NA	0.27	0.42	0.35	DDB_G0290915	NA
DDB_G0283595	DDB0232431	806963	10000	Yes	NA	NA	NA	-0.04	0.42	0.19	DDB_G0283595	member of the patatin family of glycoproteins, which are storage proteins but also possess lipase activity
DDB_G0285763	DDB0232431	3440030	10000	NA	NA	NA	NA	0.31	0.28	0.29	DDB_G0285763	NA
NA	DDB0232433	1675139	10000		NA	NA	NA	0.22	0.27	0.25	NA	NA
DDB_G0279637	DDB0232430	2347441	10000	Yes	NA	NA	NA	0.50	0.16	0.33	DDB_G0279637	NA
DDB_G0287593	DDB0232432	526711	10000	NA	NA	NA	NA	0.58	0.15	0.36	abcC6	full transporter, consisting of two ABC domains and two transmembrane domains

DDB_G0295421	DDB0232433	2598542	10000	NA	NA	NA	NA	-0.34	0.10	-0.12	tRNA-Thr-AGU-18	transfers a threonine residue to a growing polypeptide chain during protein synthesis
DDB_G0274483	DDB0232429	4423715	10000	NA	NA	NA	NA	0.12	0.10	0.11	DDB_G0274483	NA
NA	DDB0232430	6008658	10000		NA	NA	NA	0.08	0.01	0.05	NA	NA
DDB_G0277789	DDB0232429	8384851	10000	NA	NA	NA	NA	0.25	-0.07	0.09	DDB_G0277789	similar to a conserved eukaryotic protein: contains two transmembrane domains
DDB_G0291257	DDB0232433	14649	10000	NA	NA	NA	NA	-0.17	-0.16	-0.16	DDB_G0291257_TE	ORF1 encoding a protein of unknown function of the putative DNA transposon DDT-A;B refer to AF298201 for full-length consensus element
NA	DDB0232432	3761819	10000		NA	NA	NA	0.19	-0.16	0.01	NA	NA
DDB_G0282897	DDB0232430	6256880	10000	Yes	NA	NA	NA	0.25	-0.19	0.03	tom7	homologous to mitochondrial import protein 7 kDa subunit; associates with TOM40 in yeast
DDB_G0277497	DDB0232429	8020742	10000	NA	NA	NA	NA	-0.26	-0.22	-0.24	aco	oxidoreductase
NA	DDB0232430	491081	10000		NA	NA	NA	-0.15	-0.28	-0.21	NA	NA

DDB_G0267524	DDB0232428	271521	10000	Yes	NA	NA	NA	-0.52	-0.31	-0.41	ssr3	subunit of the TRAP complex aids in the translocation of nascent polypeptides into the lumen of the endoplasmic reticulum
DDB_G0292714	DDB0232433	1783808	10000	NA	NA	NA	NA	-0.41	-0.36	-0.39	DDB_G0292714	NA
DDB_G0291079	DDB0232432	4964845	10000	Yes	NA	NA	NA	0.01	-0.44	-0.22	gbpC	member of the TKL (tyrosine kinase-like) group and ROCO family of protein kinases; belongs to the LRRK family of protein kinases; contains LRR, Roc, COR, RasGEF, protein kinase, DEP, cyclic nucleotide-binding, and GRAM domains; involved in cGMP-mediated chemotaxis; catalyzes GDP to GTP exchange on its own Roc domain; translocates from cytoplasm to cell cortex after cAMP stimulation; GRAM domain binds directly to plasma membrane
NA	DDB0232428	272275	10000		NA	NA	NA	-0.34	-0.54	-0.44	NA	NA
DDB_G0272554	DDB0232429	1838299	10000	NA	NA	NA	NA	-0.83	-0.62	-0.73	DDB_G0272554_RTE	ORF2 protein fragment of DIRS1 retrotransposon;B refer to Genbank M11339 for full-length element
DDB_G0285033	DDB0232431	2840259	10000	NA	NA	NA	NA	0.05	-0.79	-0.37	DDB_G0285033	belongs to the short-chain dehydrogenase/reductase family

DDB_G0285329	DDB0232431	3094501	10000	NA	NA	NA	NA	-4.01	-4.01	-4.01	DDB_G0285329	C-terminal half very similar to nucleotide binding protein 1;B belongs to the highly conserved ATP-binding protein family
NA	DDB0232431	60172	10000		NA	NA	NA	-4.02	-4.02	-4.02	NA	NA
NA	DDB0232428	4877292	10000		NA	NA	NA	-4.07	-4.07	-4.07	NA	NA
DDB_G0278945	DDB0232430	1252700	10000	NA	NA	NA	NA	-4.12	-4.12	-4.12	DDB_G0278945	NA
DDB_G0293630	DDB0232433	3177480	10000	NA	NA	NA	NA	-4.12	-4.12	-4.12	DDB_G0293630_RTE	ORF2 protein encoding endonuclease and reverse transcriptase of tRNA-specific non-long terminal repeat retrotransposon TRE5-B;B refer to GenBank AF298209 for consensus full-length element
DDB_G0290961	DDB0232432	4811344	10000	NA	NA	NA	NA	-4.38	-4.38	-4.38	zfaA	putative pseudogene; similar to a family of D. discoideum zinc finger containing genes, including zfaA and DDB_G0290965
NA	DDB0232430	6242829	10000		NA	NA	NA	-4.59	-4.59	-4.59	NA	NA
DDB_G0272861	DDB0232429	2071738	10000	NA	NA	NA	NA	-4.66	-4.66	-4.66	cosA	belongs to the costars family;B similar to the C terminal region of mammalian striated muscle activator of Rho signaling

DDB_G0273949	DDB0232429	3587042	10000	NA	1.55	1.64	1.60	2.24	2.30	2.27	DDB_G0273949	Putative glycerophosphodiester phosphodiesterase 5 (Automated). there is a second copy of this gene.
DDB_G0278657	DDB0232430	682095	10000	NA	1.47	1.53	1.50	2.20	2.22	2.21	DDB_G0278657_ps	putative pseudogene, similar to DDB_G0293286 and DDB_G0293288
DDB_G0272218	DDB0232429	1691598	10000	NA	0.93	1.16	1.05	1.00	0.57	0.79	DDB_G0272218	NA
DDB_G0281291	DDB0232430	4361428	10000	NA	0.85	1.19	1.02	3.25	3.46	3.35	DDB_G0281291	putative ortholog of the transcription cofactor 30 kDa HIV-1 Tat interactive protein 2 (HTATIP2)
DDB_G0282059	DDB0232430	5354850	10000	NA	0.98	0.95	0.96	1.69	1.64	1.66	DDB_G0282059	NA
DDB_G0283773	DDB0232431	1083032	10000	Yes	0.92	0.87	0.89	0.65	1.06	0.85	DDB_G0283773	putative GTPase, very conserved in protozoa and fungi
DDB_G0293980	DDB0232433	3518992	10000	NA	1.12	0.61	0.87	0.28	-0.37	-0.04	DDB_G0293980	NA
DDB_G0270640	DDB0232428	3582360	10000	Yes	1.00	0.68	0.84	1.14	1.13	1.13	DDB_G0270640	matches PFAM HMM for SPB_interacting (spindle pole body) protein;B similar to D.purpureum protein
DDB_G0272470	DDB0232429	1735865	10000	NA	0.68	0.75	0.71	NA	NA	NA	DDB_G0272470	NA
DDB_G0278303	DDB0232430	653440	10000	NA	0.62	0.74	0.68	0.26	0.71	0.49	DDB_G0278303_ps	putative pseudogene;B beta-ketoacyl synthase family protein

DDB_G0278079	DDB0232430	244929	10000	NA	0.86	0.49	0.67	NA	NA	NA	exdl2A	very similar to mammalian exonuclease 3'-5' domain-like-containing protein 2 (EXDL2); the upstream Dictyostelium gene is very similar
DDB_G0270774	DDB0232428	4624308	10000	Yes	0.51	0.76	0.63	NA	NA	NA	DDB_G0270774	NA
DDB_G0271016	DDB0232428	4112783	10000	Yes	0.28	0.87	0.57	3.31	3.38	3.35	DDB_G0271016	NA
DDB_G0275155	DDB0232429	5261813	10000	NA	0.49	0.62	0.55	NA	NA	NA	DDB_G0275155	NA
NA	DDB0232428	85261	10000		0.59	0.51	0.55	-0.75	-0.04	-0.40	NA	NA
DDB_G0277581	DDB0232429	8273990	10000	NA	0.41	0.68	0.54	0.43	0.45	0.44	DDB_G0277581	NA
DDB_G0289051	DDB0232432	2276567	10000	NA	0.64	0.40	0.52	0.89	-1.06	-0.09	DDB_G0289051	NA
NA	DDB0232432	3938176	10000		0.81	0.23	0.52	NA	NA	NA	NA	NA
DDB_G0275181	DDB0232429	5328159	10000	Yes	0.60	0.44	0.52	0.18	0.01	0.09	mcee	catalyzes the reaction L-methylmalonyl-CoA <=> D-methylmalonyl-CoA
DDB_G0275157	DDB0232429	5217861	10000	NA	0.48	0.53	0.51	NA	NA	NA	limF	LIM-type zinc finger-containing protein. contains three LIM domain repeats

DDB_G0291964	DDB0232433	896066	10000	NA	0.34	0.64	0.49	NA	NA	NA	DDB_G0291964_RTE	partial ORF1 and ORF2 of tRNA-specific non-long terminal repeat retrotransposon TRE3-B;B refer to GenBank AF134170 for full-length consensus element
DDB_G0295361	DDB0232433	3132394	10000	NA	0.51	0.44	0.47	0.56	0.66	0.61	tRNA-Ala-AGC-11	transfers an alanine residue to a growing polypeptide chain during protein synthesis%0A
DDB_G0295371	DDB0232433	3235091	10000	NA	0.36	0.52	0.44	-0.04	-0.30	-0.17	tRNA-Asn-GUU-18	transfers an asparagine residue to a growing polypeptide chain during protein synthesis%0A
DDB_G0295757	DDB0232428	2506297	10000	NA	0.57	0.31	0.44	NA	NA	NA	DDB_G0295757	NA
DDB_G0276713	DDB0232429	7115818	10000	NA	0.34	0.52	0.43	0.32	0.82	0.57	DDB_G0276713	NA
DDB_G0283289	DDB0232431	466384	10000	NA	0.39	0.47	0.43	NA	NA	NA	DDB_G0283289	NA
NA	DDB0232429	3276085	10000		0.61	0.23	0.42	NA	NA	NA	NA	NA
DDB_G0295649	DDB0237465	71778	10000	NA	0.33	0.46	0.40	-0.58	0.10	-0.24	17S_rRNA-2	component of the ribosomal small (40S) subunit
DDB_G0288919	DDB0232432	2121297	10000	NA	0.40	0.37	0.39	NA	NA	NA	psiI	contains a signal peptide, a PA14 (anthrax protection antigen) domain, 6 Dictyostelium (CTDC) repeats and a C-terminal transmembrane domain

DDB_G0291964	DDB0232433	894117	10000	NA	0.01	0.74	0.38	0.53	0.55	0.54	DDB_G0291964_RTE	partial ORF1 and ORF2 of tRNA-specific non-long terminal repeat retrotransposon TRE3-B;B refer to GenBank AF134170 for full-length consensus element
DDB_G0291079	DDB0232432	4962097	10000	Yes	0.34	0.41	0.38	0.09	0.08	0.09	gbpC	member of the TKL (tyrosine kinase-like) group and ROCO family of protein kinases; belongs to the LRRK family of protein kinases; contains LRR, Roc, COR, RasGEF, protein kinase, DEP, cyclic nucleotide-binding, and GRAM domains; involved in cGMP-mediated chemotaxis; catalyzes GDP to GTP exchange on its own Roc domain; translocates from cytoplasm to cell cortex after cAMP stimulation; GRAM domain binds directly to plasma membrane
NA	DDB0232431	4131502	10000		0.34	0.40	0.37	-0.29	-0.09	-0.19	NA	NA
NA	DDB0232429	8474792	10000		0.00	0.73	0.36	0.79	0.95	0.87	NA	NA
DDB_G0270520	DDB0232428	2767188	10000	NA	0.45	0.27	0.36	-0.52	-0.15	-0.33	DDB_G0270520	NA
NA	DDB0232429	8173828	10000		0.31	0.39	0.35	0.56	0.51	0.53	NA	NA

DDB_G0282371	DDB0232430	6081570	10000	NA	0.27	0.41	0.34	NA	NA	NA	veg111	hyaluronidase, catalyse the degradation of hyaluronic acid (HA)
NA	DDB0232429	636596	10000		0.50	0.18	0.34	3.11	3.25	3.18	NA	NA
NA	DDB0232432	2970418	10000		0.44	0.24	0.34	NA	NA	NA	NA	NA
DDB_G0288241	DDB0232432	1242825	10000	NA	0.39	0.29	0.34	3.59	3.87	3.73	DDB_G0288241	NA
DDB_G0287347	DDB0232432	163503	10000	NA	0.41	0.22	0.32	3.17	3.75	3.46	DDB_G0287347	NA
DDB_G0279263	DDB0232430	1859464	10000	NA	0.32	0.29	0.31	NA	NA	NA	DDB_G0279263	NA
NA	DDB0232429	1040513	10000		0.40	0.20	0.30	NA	NA	NA	NA	NA
DDB_G0274019	DDB0232429	3672782	10000	NA	0.26	0.32	0.29	-0.24	-0.05	-0.15	tkt-2	catalyzes the reaction D-ribose-5-phosphate + D-xylulose-5-phosphate <=> D-sedoheptulose-7-phosphate + D-glyceraldehyde-3-phosphate; there is a second copy of this gene, tkt-1
NA	DDB0232430	2774786	10000		-0.06	0.63	0.29	0.96	0.46	0.71	NA	NA

NA	DDB0232432	4104588	10000		0.56	-0.02	0.27	4.22	4.43	4.33	NA	NA
DDB_G0291964	DDB0232433	897280	10000	NA	0.29	0.25	0.27	0.66	0.49	0.57	DDB_G0291964_RTE	partial ORF1 and ORF2 of tRNA-specific non-long terminal repeat retrotransposon TRE3-B;B refer to GenBank AF134170 for full-length consensus element
DDB_G0283037	DDB0232431	193457	10000	NA	0.34	0.19	0.26	NA	NA	NA	esd	very similar to human ESD and to S. cerevisiae S-formylglutathione hydrolase (YJL068C), which seems to be involved in formaldehyde detoxification
NA	DDB0232432	312522	10000		0.26	0.26	0.26	NA	NA	NA	NA	NA
DDB_G0277421	DDB0232429	8052002	10000	NA	0.18	0.35	0.26	0.42	0.13	0.28	DDB_G0277421	conserved hypothetical 278 aa Dictyostelium protein
DDB_G0291277	DDB0232433	44771	10000	NA	0.48	0.01	0.25	NA	NA	NA	DDB_G0291277	NA
DDB_G0281573	DDB0232430	4829972	10000	Yes	0.11	0.38	0.24	NA	NA	NA	gefP	putative Ras guanine nucleotide exchange factor;B promotes the exchange of GDP for GTP on Ras small GTPases thus converting them into the active form
DDB_G0277959	DDB0232430	66698	10000	NA	0.27	0.22	0.24	1.13	0.97	1.05	cupJ	similar to calcium up-regulated genes
DDB_G0271990	DDB0232429	1143710	10000	NA	0.34	0.13	0.24	0.47	0.68	0.57	DDB_G0271990	NA

DDB_G0274597	DDB0232429	3807776	10000	NA	0.26	0.21	0.23	NA	NA	NA	ctnA	component of the counting factor complex, which includes CF60, CF50, CF45-1, and CtnA (countin)
DDB_G0291722	DDB0232433	720839	10000	NA	0.25	0.21	0.23	NA	NA	NA	DDB_G0291722	NA
NA	DDB0232432	604687	10000		0.15	0.30	0.23	NA	NA	NA	NA	NA
DDB_G0292962	DDB0232433	2140723	10000	NA	0.17	0.26	0.22	NA	NA	NA	DDB_G0292962	NA
DDB_G0291079	DDB0232432	4967215	10000	Yes	0.06	0.36	0.21	NA	NA	NA	gbpC	member of the TKL (tyrosine kinase-like) group and ROCO family of protein kinases; belongs to the LRRK family of protein kinases; contains LRR, Roc, COR, RasGEF, protein kinase, DEP, cyclic nucleotide-binding, and GRAM domains; involved in cGMP-mediated chemotaxis; catalyzes GDP to GTP exchange on its own Roc domain; translocates from cytoplasm to cell cortex after cAMP stimulation; GRAM domain binds directly to plasma membrane
DDB_G0278965	DDB0232430	1484823	10000	NA	0.33	0.09	0.21	NA	NA	NA	DG2033	tRNA/rRNA methyltransferase SpoU family protein
NA	DDB0232432	990130	10000		0.06	0.30	0.18	NA	NA	NA	NA	NA

DDB_G0281595	DDB0232430	4685628	10000	NA	0.29	0.05	0.17	NA	NA	NA	rchy	RING finger and CHY zinc finger-containing protein
NA	DDB0232430	235065	10000		0.24	0.08	0.16	NA	NA	NA	NA	NA
DDB_G0284387	DDB0232431	1930479	10000	NA	0.18	0.09	0.13	NA	NA	NA	DDB_G0284387	NA
NA	DDB0232430	6596	10000		0.18	0.08	0.13	NA	NA	NA	NA	NA
NA	DDB0232433	2138274	10000		0.09	0.17	0.13	NA	NA	NA	NA	NA
DDB_G0293498	DDB0232433	2964711	10000	NA	-0.06	0.28	0.11	0.77	1.46	1.12	DDB_G0293498	contains a UBX domain%2C found in ubiquitin-regulatory proteins
DDB_G0268856	DDB0232428	2262588	10000	NA	0.18	0.00	0.09	NA	NA	NA	DDB_G0268856	Putative subtilase-type proteinase YCR045C (Automated)
DDB_G0268344	DDB0232428	798220	10000	NA	0.07	0.09	0.08	NA	NA	NA	DDB_G0268344	NA
DDB_G0283109	DDB0232431	259378	10000	NA	0.04	0.11	0.08	NA	NA	NA	iksA	similar to fungal kinases;B contains an IQ calmodulin-binding region
NA	DDB0232431	2220133	10000		-0.11	0.26	0.07	NA	NA	NA	NA	NA

DDB_G0283967	DDB0232431	1391049	10000	NA	0.05	0.10	0.07	NA	NA	NA	DDB_G0283967	NA
DDB_G0275267	DDB0232429	5120757	10000	NA	0.03	0.11	0.07	NA	NA	NA	wrky1	contains two WRKY DNA-binding domains
NA	DDB0232430	958032	10000		0.16	-0.03	0.06	0.50	0.75	0.62	NA	NA
NA	DDB0232428	3806020	10000	Yes	0.12	-0.04	0.04	NA	NA	NA	NA	NA
DDB_G0295373	DDB0232433	3312784	10000	NA	-0.01	0.09	0.04	-4.09	-4.09	-4.09	tRNA-Ile-UAU-1	transfers an isoleucine residue to a growing polypeptide chain during protein synthesis
NA	DDB0232429	6626359	10000		-0.01	0.07	0.03	-0.18	-0.10	-0.14	NA	NA
NA	DDB0232432	4607922	10000		-0.07	0.13	0.03	0.95	0.63	0.79	NA	NA
DDB_G0268946	DDB0232428	1980965	10000	NA	-0.05	0.04	0.00	NA	NA	NA	DDB_G0268946	NA
NA	DDB0237465	73529	10000		-0.09	0.08	0.00	NA	NA	NA	NA	NA
NA	DDB0232430	5200378	10000		-3.86	-3.86	-3.86	NA	NA	NA	NA	NA

NA	DDB0232431	1906685	10000		-3.87	-3.87	-3.87	NA	NA	NA	NA	NA
DDB_G0276857	DDB0232429	7493548	10000	NA	-3.87	-3.87	-3.87	NA	NA	NA	DDB_G0276857	NA
NA	DDB0232429	5020456	10000		-3.88	-3.88	-3.88	NA	NA	NA	NA	NA
DDB_G0285643	DDB0232431	3523485	10000	NA	-3.89	-3.89	-3.89	NA	NA	NA	mrkB	CAMKL family protein kinase, similar to SNF1 kinases%2C MARK kinases%2C and AMPK kinases
NA	DDB0232432	2531767	10000		-3.91	-3.91	-3.91	NA	NA	NA	NA	NA
DDB_G0276403	DDB0232429	6817178	10000	NA	-3.95	-3.95	-3.95	NA	NA	NA	DDB_G0276403	NA
DDB_G0279159	DDB0232430	1709580	10000	NA	-4.05	-4.05	-4.05	NA	NA	NA	aco1	catalyzes the reaction citrate <=> cis-aconitate + H2O; highly similar to iron responsive element binding protein; expressed in pstAB cells and in upper cup and stalk during culmination
DDB_G0269338	DDB0232428	2565394	10000	Yes	-4.31	-4.31	-4.31	-4.22	-4.22	-4.22	bzpE	putative basic-leucine zipper (bZIP) transcription factor
DDB_G0286967	DDB0232431	5055783	10000	Yes	-4.37	-4.37	-4.37	-4.37	-4.37	-4.37	med25	putative ortholog of the poorly conserved mediator of RNA polymerase II transcription subunit 25;B the mediator complex functions as a bridge to convey

												information from gene-specific regulatory proteins to the basal RNA polymerase II transcription machinery
DDB_G0286967	DDB0232431	5054391	10000	Yes	-4.64	-4.64	-4.64	-4.84	-4.84	-4.84	med25	putative ortholog of the poorly conserved mediator of RNA polymerase II transcription subunit 25;B the mediator complex functions as a bridge to convey information from gene-specific regulatory proteins to the basal RNA polymerase II transcription machinery

Appendix 4

Disrupted Gene(s)	Gene Name	Site	ID	Chromosome	Position	Insert	Mutants in well	Insert Orientation	Disruption
DDB_G0267844	expl6	1	GWDI_473_A_6	DDB0232428	961,864	C4	1	+	intragenic
DDB_G0267844	expl6	2	GWDI_494_H_8	DDB0232428	961,284	G3	1	+	intragenic
DDB_G0270586	DDB_G0270586	1	GWDI_354_D_11	DDB0232428	3,182,265	G2	1	-	intragenic
DDB_G0270586	DDB_G0270586	2	GWDI_446_A_12	DDB0232428	3,183,023	G2	2	+	intragenic
DDB_G0270934	DDB_G0270934	1	GWDI_51_F_11	DDB0232428	3,487,098	G1	1	+	intragenic
DDB_G0270934	DDB_G0270934	2	GWDI_420_E_6	DDB0232428	3,486,126	C4	1	+	intragenic
DDB_G0270964	DDB_G0270964_ps	1	GWDI_441_F_8	DDB0232428	3,615,829	G2	2	-	intergenic_down
DDB_G0270964	DDB_G0270964_ps	2	GWDI_193_H_4	DDB0232428	3,616,586	C4	1	+	intragenic
DDB_G0270452	DDB_G0270452	1	GWDI_508_B_2	DDB0232428	4,908,049	G3	1	-	intragenic
DDB_G0270452	DDB_G0270452	2	GWDI_67_B_6	DDB0232428	4,907,487	G2	1	+	intragenic
DDB_G0269028	DDB_G0269028	1	GWDI_422_C_12	DDB0232428	2,368,271	C4	1	-	intergenic_up
DDB_G0269028	DDB_G0269028	2	GWDI_467_H_9	DDB0232428	2,368,126	C4	1	-	intergenic_up
DDB_G0270640	DDB_G0270640	1	GWDI_496_F_6	DDB0232428	3,582,360	G3	1	+	intragenic
DDB_G0270640	DDB_G0270640	2	GWDI_155_H_8	DDB0232428	3,584,862	G1	1	+	intragenic

Appendix 5

Biological processes

#term ID	term description	observed gene count	background gene count	false discovery rate	matching proteins in your network (IDs)	matching proteins in your network (labels)
GO:0065007	biological regulation	14	1040	0.00031	DDB0185012,DDB0185194,DDB0191289,DDB0191346,DDB0191359,DDB0216398,DDB0219952,DDB0231507,DDB0232001,DDB0233746,DDB0233872,DDB0266469,DDB0266833,DDB0304493	DDB0216398,abcG18,dokA,fhkD,gacE,gbpC,gefE,ku70,med26,nsfl1c,padA,pikD,pldB,upf1
GO:0050789	regulation of biological process	13	951	0.00037	DDB0185194,DDB0191289,DDB0191346,DDB0191359,DDB0216398,DDB0219952,DDB0231507,DDB0232001,DDB0233746,DDB0233872,DDB0266469,DDB0266833,DDB0304493	DDB0216398,dokA,fhkD,gacE,gbpC,gefE,ku70,med26,nsfl1c,padA,pikD,pldB,upf1
GO:0050794	regulation of cellular process	11	885	0.0045	DDB0185194,DDB0191289,DDB0191346,DDB0191359,DDB0216398,DDB0219952,DDB0231507,DDB0232001,DDB0233872,DDB0266833,DDB0304493	DDB0216398,dokA,fhkD,gacE,gbpC,gefE,ku70,med26,nsfl1c,pikD,pldB

GO:0050896	response to stimulus	10	797	0.0077	DDB0185194,DDB0191289,DDB0191346,DDB0191359,DDB0219952,DDB0231507,DDB0232001,DDB0233872,DDB0266362,DDB0266469	cupJ,dokA,fhkD,gacE,gbpC,gefE,ku70,padA,pikD,pldB
GO:0007154	cell communication	7	477	0.0283	DDB0185194,DDB0191289,DDB0191346,DDB0191359,DDB0219952,DDB0233872,DDB0266469	dokA,fhkD,gacE,gbpC,gefE,padA,pikD
GO:0009987	cellular process	16	2299	0.0283	DDB0185012,DDB0185194,DDB0191289,DDB0191346,DDB0191359,DDB0215000,DDB0216398,DDB0219952,DDB0220004,DDB0231507,DDB0232001,DDB0233746,DDB0233872,DDB0266469,DDB0266833,DDB0304493	DDB0216398,DDB0220004,abcG18,dokA,fhkD,forB,gacE,gbpC,gefE,ku70,med26,nsfl1c,padA,pikD,pldB,upf1
GO:0051716	cellular response to stimulus	8	615	0.0283	DDB0185194,DDB0191289,DDB0191346,DDB0191359,DDB0219952,DDB0232001,DDB0233872,DDB0266469	dokA,fhkD,gacE,gbpC,gefE,ku70,padA,pikD
GO:0016310	phosphorylation	6	369	0.0335	DDB0185194,DDB0191346,DDB0191359,DDB0216398,DDB0219952,DDB0220004	DDB0216398,DDB0220004,dokA,fhkD,gbpC,pikD
GO:0006468	protein phosphorylation	5	282	0.043	DDB0185194,DDB0191359,DDB0216398,DDB0219952,DDB0220004	DDB0216398,DDB0220004,dokA,fhkD,gbpC

GO:0006796	phosphate-containing compound metabolic process	7	549	0.043	DDB0185194,DDB0191346,DDB0191359,DDB0216398,DDB0219952,DDB0220004,DDB0231507	DDB0216398,DDB0220004,dokA,fhkD,gbpC,pikD,pldB
GO:0006950	response to stress	6	398	0.043	DDB0185194,DDB0191346,DDB0219952,DDB0232001,DDB0266362,DDB0266469	cupJ,dokA,fhkD,ku70,padA,pikD
GO:0007165	signal transduction	6	397	0.043	DDB0185194,DDB0191289,DDB0191346,DDB0191359,DDB0219952,DDB0233872	dokA,fhkD,gacE,gbpC,gefE,pikD
GO:0033554	cellular response to stress	5	296	0.043	DDB0185194,DDB0191346,DDB0219952,DDB0232001,DDB0266469	dokA,fhkD,ku70,padA,pikD
GO:0035556	intracellular signal transduction	5	267	0.043	DDB0185194,DDB0191289,DDB0191346,DDB0191359,DDB0219952	dokA,fhkD,gbpC,gefE,pikD
GO:0040011	locomotion	4	168	0.043	DDB0185194,DDB0191289,DDB0191346,DDB0231507	dokA,gefE,pikD,pldB
GO:0060255	regulation of macromolecule metabolic process	6	435	0.043	DDB0191359,DDB0232001,DDB0233746,DDB0266469,DDB0266833,DDB0304493	gbpC,ku70,med26,nsfl1c,padA,upf1

Molecular function

#term ID	term description	observed gene count	background gene count	false discovery rate	matching proteins in your network (IDs)	matching proteins in your network (labels)
GO:0000166	nucleotide binding	9	888	0.028	DDB0185012,DDB0191346,DDB0191359,DDB0216398,DDB0219952,DDB0220004,DDB0232001,DDB0233746,DDB0266469	DDB0216398,DDB0220004,abcG18,fhkD,gbpC,ku70,padA,pikD,upf1
GO:0004672	protein kinase activity	5	276	0.028	DDB0185194,DDB0191359,DDB0216398,DDB0219952,DDB0220004	DDB0216398,DDB0220004,dokA,fhkD,gbpC
GO:0005488	binding	14	1989	0.028	DDB0185012,DDB0191289,DDB0191346,DDB0191359,DDB0215000,DDB0216398,DDB0219952,DDB0220004,DDB0231507,DDB0232001,DDB0233746,DDB0266362,DDB0266469,DDB0304493	DDB0216398,DDB0220004,abcG18,cupJ,fhkD,forB,gbpC,gefE,ku70,nsfl1c,padA,pikD,pldB,upf1
GO:0005524	ATP binding	8	641	0.028	DDB0185012,DDB0191346,DDB0191359,DDB0216398,DDB0219952,DDB0220004,DDB0232001,DDB0233746	DDB0216398,DDB0220004,abcG18,fhkD,gbpC,ku70,pikD,upf1
GO:0016301	kinase activity	6	331	0.028	DDB0185194,DDB0191346,DDB0191359,DDB0216398,DDB0219952,DDB0220004	DDB0216398,DDB0220004,dokA,fhkD,gbpC,pikD
GO:0016773	phosphotransferase activity, alcohol group as acceptor	6	300	0.028	DDB0185194,DDB0191346,DDB0191359,DDB0216398,DDB0219952,DDB0220004	DDB0216398,DDB0220004,dokA,fhkD,gbpC,pikD

GO:0043167	ion binding	10	1357	0.028	DDB0185012,DDB0191346,DDB0191359,DDB0216398,DDB0219952,DDB0220004,DDB0231507,DDB0232001,DDB0233746,DDB0266469	DDB0216398,DDB0220004,abcG18,fhkD,gbpC,ku70,padA,pikD,pldB,upf1
GO:0043168	anion binding	9	917	0.028	DDB0185012,DDB0191346,DDB0191359,DDB0216398,DDB0219952,DDB0220004,DDB0232001,DDB0233746,DDB0266469	DDB0216398,DDB0220004,abcG18,fhkD,gbpC,ku70,padA,pikD,upf1
GO:0051020	GTPase binding	3	91	0.028	DDB0191289,DDB0191359,DDB0215000	forB,gbpC,gefE
GO:0098772	molecular function regulator	4	145	0.028	DDB0191289,DDB0191359,DDB0233872,DDB0304493	gacE,gbpC,gefE,nsfl1c
GO:0004674	protein serine/threonine kinase activity	4	240	0.0286	DDB0191359,DDB0216398,DDB0219952,DDB0220004	DDB0216398,DDB0220004,fhkD,gbpC
GO:0004386	helicase activity	2	45	0.0395	DDB0232001,DDB0233746	ku70,upf1
GO:0005085	guanyl-nucleotide exchange factor activity	2	45	0.0395	DDB0191289,DDB0191359	gbpC,gefE
GO:0008289	lipid binding	2	50	0.0444	DDB0191359,DDB0304493	gbpC,nsfl1c

Reactome pathway

#term ID	term description	observed gene count	background gene count	false discovery rate	matching proteins in your network (IDs)	matching proteins in your network (labels)
DDI-156711	Polo-like kinase mediated events	2	4	0.0043	DDB0216398,DDB0220004	DDB0216398,DDB0220004